

2003 54241447

LIPPARY
Michigan State
University

This is to certify that the

thesis entitled

CONSTRUCTION, CALIBRATION, AND APPLICATION OF A SPLIT HOPKINSON PRESSURE BAR

presented by Guojing Li

has been accepted towards fulfillment of the requirements for

MS degree in Mechanical Engineering

Major professor

Date \_\_\_\_12/16/02

MSU is an Affirmative Action/Equal Opportunity Institution

# PLACE IN RETURN BOX to remove this checkout from your record. TO AVOID FINES return on or before date due. MAY BE RECALLED with earlier due date if requested.

DATE DUE	DATE DUE	DATE DUE

6/01 c:/CIRC/DateDue.p65-p.15

# CONSTRUCTION, CALIBRATION AND APPLICATION OF A SPLIT HOPKINSON PRESSURE BAR

By

**Guojing Li** 

# **A THESIS**

Submitted to
Michigan State University
In partial fulfillment of the requirements
for the degree of

**MASTER OF SCIENCE** 

**Department of Mechanical Engineering** 

2002

#### **ABSTRACT**

# CONSTRUCTION, CALIBRATION AND APPLICATION OF A SPLIT HOPKINSON PRESSURE BAR

By

# Guojing Li

The behavior of materials at high strain rates is different from that under quasi-static loading. Among the experimental techniques for dynamic behavior of materials, Split Hopkinson Pressure Bar (SHPB) is the most common technique for dynamic stress-strain characterizations due to its capability of producing a large range of nearly uniform strain rates. Although many SHPBs have been constructed, there is no step-by-step guidelines for SHPB construction, neither is there a standard design. It is the primary goal of this research to construct an SHPB for characterizations of materials, especially thick laminated composites. Thick laminated composites have different material properties from thin counterparts because the thermal cycle for curing polymer matrix is not necessarily uniform through the thickness of thick laminated composites. Consequently, when subjected to dynamic loading, thick laminated composites behave differently from thin counterparts. Experimental results based on SHPB have verified the difference of the properties close to the surface and those close to the midplane of laminated composites. In addition, it has been found from this research that stress-strain curves are strongly affected by the specimen dimensions.

#### **ACKNOWLEDGEMENTS**

This thesis represents a culmination of hundreds of hours work by its author, Dr. Dahsin Liu from Michigan State University and many previous investigators. I would like to thank Dr. Liu for his insight and directions. Dr. Liu directed my thesis research step by step from the very beginning and helped me to rewrite the thesis. I would like to thank Dr. Gary Cloud and Mr. Brian Wright for the directions on the circuit designs. I would like to thank the tutors in the writing center of Michigan State University for taking time to review my thesis. I would also like to thank Sen Li, my wife, and Xinui Li, my daughter, for all of their love and understanding, though they probably don't know it. Thanks to all of you, I appreciate everything you have done for me.

# **TABLE OF CONTENTS**

LIST OF TABLESvii	į
LIST OF FIGURESvii	i
CHAPTER 1 INTRODUCTION1	I
1. Background1	l
2. Statement of the Problem and Objectives	3
3. Organization of the Thesis	ļ
CHAPTER 2 CONSTRUCTION OF A SPLIT HOPKINSON PRESSURE BAR	6
The Pressure Source System	3
2. The Split Bar System	8
3. The Data Acquisition System1	0
3.1 Wheatstone Bridge Circuit10	)
3.2 Differential Amplifier12	2
3.3 Computer-Aided Data Processing12	2
4. Overall Operation of the SHPB1	4
5. Detailed Operation Procedures1	6
5.1 Starting Up Procedures16	;
5.2 Shutting Down Procedures1	В
CHAPTER 3 CALIBRAIONS OF COMPONENTS AND SHPB	Ę
1. Calibration of Differential Amplifiers1	9

2.	Calibration of Wheatstone Bridge Circuits (with Differential Amplifier)22
3.	Calibration of the Whole SHPB25
	3.1 Calibration with Load Cell25
	3.2 Calibration with Instrumented Striker Bar28
	3.3 Calibration by Testing 6061-T6 Aluminum34
	PTER 4 RACTERIZATIONS OF THICK LAMINATED COMPOSITES46
1.	Specimen Preparation46
2.	Experimental Results49
	2.1 Strain-Rate Effect
	2.2 Laminated and Assembled Specimens49
	2.3 Effect due to L/D Ratio53
	2.4 Effect due to Specimen Inhomogeneity53
	2.5 Young's Modulus and Yielding Point54
	PTER 5 USSIONS
1.	Dimensions of Bars61
	1.1 Bar Diameter D <sub>bar</sub> 61
	1.2 Bar Length L <sub>bar</sub> 62
2.	Dimensions of Specimens63
	2.1 Specimen Diameter D63
	2.2 Specimen Length L63
3.	Constant Strain Rate64

CHAPTER 6 CONCLUSIONS AND RECOMMENDATIONS	67
1. Conclusions	67
2. Recommendations	68
APPENDICES	70
APPENDIX A OTHER FIGURES AND WAVE SIGNALS	71
APPENDIX B SPLIT HOPKINSON PRESSURE BAR THEORY	104
REFERENCES	<b>11</b> 1

# **LIST OF TABLES**

Table 1	Density, wave speed and Young's modulus of split bars	.31
Table 2	Dimensions and dimensional ratios of aluminum specimens	42
Table 3	Comparison of Yielding Points	45
Table 4	Dimensions and dimensional ratios of Glass/Epoxy specimens	47
Table 5	Parameters of SHPB and L/D of specimen used by various researchers	.65

# **LIST OF FIGURES**

Figure 1	Schematic diagram of a split Hopkinson pressure bar	7
Figure 2	Teflon bearing and associated frame and rail	.9
Figure 3	Detailed design of a Wheatstone bridge circuit	11
Figure 4	Detailed design of a differential amplifier	13
	Overall operation and data acquisition and processing of the split Hopkinson pressure bar	.15
Figure 6	Output wave (below) of an initially sqaure wave (top) with a frequency of 3500 Hz from a differential amplifier	.20
Figure 7	Frequency response function of amplifier	.21
Figure 8	Gain of amplifier based on square waves at 3500 Hz	.21
Figure 9	Wheatstone bridge circuit and shunt calibration resistors	23
Figure 10	(a), (b) Comparisons between experimental measurements and theoretical calculations	.24
Figure 11	Schematic diagram of striker bar impacting on load cell	27
Figure 12	Comparison between the signals from load cell and those from strain gages in striker bar	.29
Figure 13	(a-c) Schematic diagram of the striker bar impacting the incident bar, the transmitter bar and the combination of the two bars	30
Figure 14	The discrepancies of strain measurements between the incident bar and the striker bar and that between the transmitter bar and the striker bar	32
Figure 15	<ul> <li>Wave speed as a function of gas pressure.</li> <li>(a) Striker bar impacting the combination of incident and transmitter bars.</li> <li>(b) Striker bar impacting the incident bar.</li> <li>(c) Striker bar impacting the transmitter bars</li></ul>	33

Figure 16	(a), (b) Strain waves showed on oscilloscope during 500 ms (c), (d) Time durations for the strain waves with 50% of amplitude reduction	.35
Figure 17	Typical incidence, reflection and transmission waves from SHPB for Aluminum 6061-T6	.36
Figure 18	Schematic diagram of time-positon relation of the strain waves in the incident bar, specimen and transmitter bar	.37
Figure 19	Input and output force histories of four aluminum specimens with the same impact gas pressure	41
Figure 20	The stress-strain curves of aluminum 6061-T6 under different strain rates	. 44
Figure 21	Bi-metal hole saw	.48
Figure 22	Typical incidence, reflection and transmission waves from SHPB for glass-epoxy composite	.50
Figure 23	Stress-strain curves for glass-epoxy composites with similar dimensions and L/D ratios (1.6)	.51
Figure 24	Stress-strain curves for two groups of glass-epoxy composites with similar strain rates and total dimensions.  Group one—from thick glass-epoxy composite plates, Group two—from thin glass-epoxy composite plates and assembled	.52
Figure 25	Stress-strain curves for glass-epoxy composites with similar strain rates but different L/D ratios	.55
Figure 26	Stress-strain curves for glass-epoxy composites with different strain rates and different L/D ratios	.56
Figure 27	Stress-strain curves for glass-epoxy composites with similar strain rates but different L/D ratios	.57
Figure 28	Stress-strain curves for three groups of glass-epoxy composites with similar dimensions and L/D ratio (0.8)	.58
Figure 29	Young's Modulus vs. strain rates at different L/D ratios	.60
Figure 30	Yielding points vs. strain rates at different L/D ratios	60

Figure 31	Stress-strain curves at constant strain rates for the composte specimens with D=15.8 mm, L=25.4 mm. (based on various levels of constant incident strain wave tests66
APPENDI	CES
Figure A-1	Other stress-strain curves of aluminum 6061-T6 with different strain rates71
Figure A-2	Stress-strain curves of glass-epoxy composite specimens cutting from the same plate72
Figure A-3	Stress-strain curves of assembled glass-epoxy composite with different layers73
Figure A-4	Stress-strain curves of glass-epoxy composite with different L/D ratios
Figure A-5	5 Calculation of wave speed in bars75
Figure A-6	Wave shapes and forces comparison of Aluminum 6061-Y6 with shaping technique. (from Dr. W. Chen [5])76
Figure A-7	to Figure A-12 Incident, reflected and transmitted waves for the aluminum 6061-T6 specimen with various diameters and lengths77
Figure A-1	3 to Figure A-33 Incident, reflected and transmitted waves for the glass-epoxy composite specimen with various diameters and lengths83
Figure A-3	34 Pressure bar shown with differential element104
Figure A-3	35 Parameters of cylindrical specimen and bars107

#### **CHAPTER 1**

#### INTRODUCTION

# 1. Background

The behavior of materials at high strain rates is different from that under quasi-static loading. As many materials are used for high-performance stuctures and are subjected to dynamic loading, the dynamic behavior of the materials has become a primary concern in structural designs. A few experimental techniques have been developed for characterizations of dynamic behavior of materials, e.g. drop-weight tower, plate impact, split Hopkinson pressure bar (SHPB) and high-speed photography.

Based on a force transducer, the drop-weight tower is a relatively simple testing technique. However, the strain rate produced by the technique of drop-weight tower is limited by the dropping height of the weight. In contrast, the plate impact technique is able to produce strain rates as high as  $10^6 \, \text{s}^{-1}$  and  $10^7 \, \text{s}^{-1}$ . It uses very thin specimens, such as coating a thin film of specimen onto a plate, for impact. Different from direct impacts on specimens like those occur in the drop-weight tower and plate impact techniques, SHPB uses two bars to convey impulsive waves into specimens and to measure the wave signals input into (incident) and output from (reflected and transmitted) the specimens. SHPB is useful for testing specimens at intermediate strain rates, i.e. between  $100 \, \text{s}^{-1}$  and  $10^4 \, \text{s}^{-1}$ . Almost all experiments utilizing the drop-weight tower, plate impact and SHPB use electrical-based devices for signal sensoring. With the

advancements in high-speed cameras and optical methods, such as holographic interferometry and cautics, high-speed photography has also been developed for characterization of dynamic behavior of materials.

Among the four techniques mentioned above, SHPB is the most common technique for dynamic stress-strain characterizations due to its capability of producing a large range of nearly uniform strain rates. The Pressure Bar technique was initiated by Hopkinson in the early 1900's [1]. He used a long rod to convey a force pulse to a force transducer. However, it was not until 1949 that Split Pressure Bar was proposed by Kolsky. He used two Hopkinson's pressure bars to measure the dynamic signals of materials in compression. From then on, Split Hopkinson Pressure Bar has become a standard technique for determining dynamic properties of materials, verifying the constitutive models of materials, identifying the propagation of plastic waves in materials, etc. Since 1949, the SHPB technique has advanced in many aspects. However, the following fundamental assumptions remain [2]. They should be carefully observed to obtain meaningful results from SHPB tests.

- (1) The split bars should remain within elastic range during operations.
- (2) The waves propagated in the bars should be one-dimensional longitudinal type.
- (3) The deformation in the specimen should be uniform through the length of the specimen.

During the past five decades, the advancements of the SHPB technique include the development of instrumentations to detect, process and display the

signals with minimum distortion, the refinement of basic SHPB theories and the extensions of SHPB in characterizing various material properties, such as tensional, torsional, shear and fracture properties, at high strain rates and as effected by temperature. Some issues concerning the basic SHPB theories have been revisited again and again by many researchers and are worth extra attention in the construction and application of SHPB [1-3], e.g.

- (1) the uniformity of stress in the specimen,
- (2) the effect of strain-rate history on the microstructure of the specimen material.
- (3) the effect of  $D/D_{bar}$  ratio (D is the diameter of the specimen) on the assumption of one-dimensional wave propagation,
- (4) the effect of wave dispersion and distortion on the stress-strain curve,
- (5) the effects of friction and radial inertia on the one-dimensional assumption.

Although SHPB has become a standard testing technique and many SHPBs have been constructed over the years, there is neither step-by-step guideline for SHPB construction nor a standard design. As the electronic instrumentation has experienced rapid advancement in recent years, the data acquisition, processing and presentation have become easier, more efficient and more accurate. It is the primary goal of this thesis research to construct a SHPB for material characterization.

# 2. Statement of the Problem and Objectives of the Thesis

Owing to their high stiffness and high strength with low density, fiber-reinforced polymer matrix composite materials are excellent candidate materials for high-performance structures. With increasing number of applications using composite materials, more and more thick composite plates are used for structural applications. However, thick composite plates may have different material properties from thin counterparts as the thermal cycle for curing polymer matrix is not necessarily uniform throught the thickenss of thick composite plates. Consequently, when subjected to dynamic loading, the thick composite plates may behave differently from the thin counterparts. The primary goal of this thesis research is to characterize the compressive behavior of thick laminated composites at high strain rates. In order to achieve the goal, the following efforts are identified:

- (1) to construct a Split Hopkinson Pressure Bar,
- (2) to calibrate the Split Hopkinson Pressure Bar,
- (3) to use the Split Hopkinson Pressure Bar to characterize thick laminated composites,
- (4) to analyze the experimental results.

# 3. Organization of the Thesis

In addition to the introductory chapter, Chapter 1, the thesis is divided into five chapters. Chapter 2 describes the construction of a Split Hopkinson Pressure Bar. Overall setting-up procedures and operation procedures are also given. Chapter 3 presents the calibration procedures in validating the Split Hopkinson

Pressure Bar. Calibrations for both individual components and the whole SHPB are included. Chapter 4 presents the application of the SHPB in the characterization of thick laminated composites. Specimens with different dimensions and dimensional ratios are investigated. Chapter 5 presents discussions on the effects of dimensions and dimensional ratios of bars and specimens. The conclusions from the thesis research are summarized in Chapter 6. Some recommendations for future research are also identified.

#### **CHAPTER 2**

### CONSTRUCTION OF A SPLIT HOPKINSON PRESSURE BAR

Split Hopkinson Pressure Bars (SHPBs) have been commonly used for characterizations of material behavior at high strain rates. An SHPB usually consists of three major component systems: a pressure source system, split bar system and data acquisition system. The schematic diagram of the Split Hopkinson Pressure Bar constructed in the thesis research is given in Figure 1. The three component systems can be clearly identified in the diagram.

# 1. The Pressure Source System

The pressure source system provides required pressure for accelerating the striker bar. A gas source system, originally used for a gas gun, was used as the pressure source system in the Split Hopkinson Pressure Bar. It includes a cylindrical tank for storing nitrogen gas, a small gas chamber for storing the required amount of gas in each operation, a piping-and-valve system for controlling the pressure of the operating gas and an electro-magnetic valve for controlling the gas releasing. The gun barrel of the original gas gun was retained for gas releasing.

In the piping-and-valve system, there are two pressure gauges; one is used for measuring gas pressures up to 3000 psi (21 MPa) and the other is used for measuring gas pressures lower than 100 psi (700 kPa). The former is for large-scale adjustment while the latter fine adjustment. Due to the strength of the

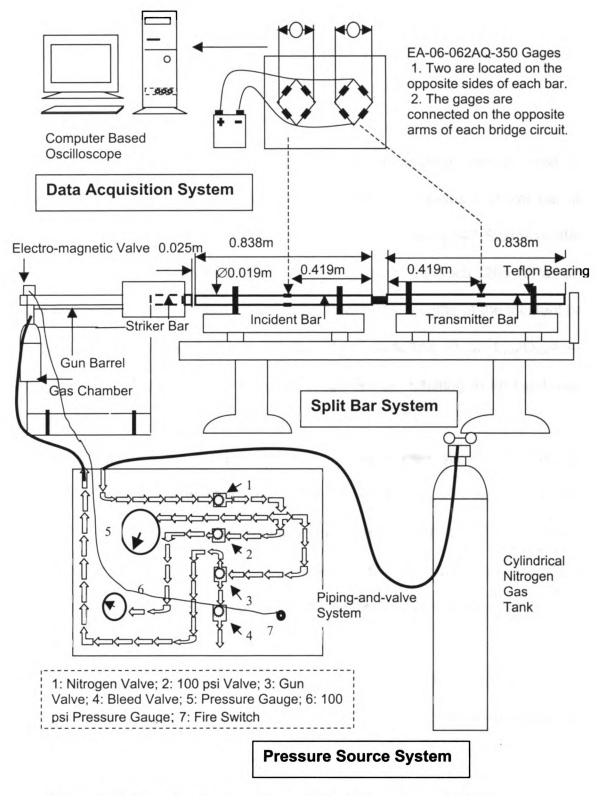


Figure 1 Schematic diagram of a split Hopkinson pressure bar.

pipes, the maximum operating pressure of the piping-and-valve system is set at 400 psi (2.8 MPa).

# 2. The Split Bar System

The split bar system is the loading and measuring device used for characterizations of specimens at high strain rates. It includes a striker bar, an incident bar and a transmitter bar. All three bars are made of 347 Stainless Steel with high stiffness 27.6 Msi (193 GPa), high strength 29.3 ksi (205 MPa) and have an identical diameter D<sub>bar</sub> of 0.75" (0.019 m). The lengths of the incident bar and the transmitter bar L<sub>bar</sub> are 33" (0.838 m), resulting in an L<sub>bar</sub>/D<sub>bar</sub>= 44, whereas that of the striker bar L<sub>striker</sub> is 7" (0.178 m), resulting in an L<sub>bar</sub>/L<sub>striker</sub>= 4.7.

In order to hold the incident bar and the transmitter bar horizontally with minimum friction and deflection and to achieve excellent alignment of the bars, two Teflon bearings were built for each bar. The Teflon bearings were framed and fixed on an aluminum rail, which was joined to a solid steel foundation. Details of the Teflon bearing and associated frame and rail are depicted in Figure 2.

Since the gun barrel (for gas releasing) has a diameter of 0.5" (12.5 mm), which is different from the diameter of the striker bar (0.75"), a joining component was built and attached to the end of the gun barrel to accommodate the striker bar. A small clearance around 0.04" (1 mm) was maintained between the striker bar and the joining component. A gap of 1" (0.025 m) was also kept between the

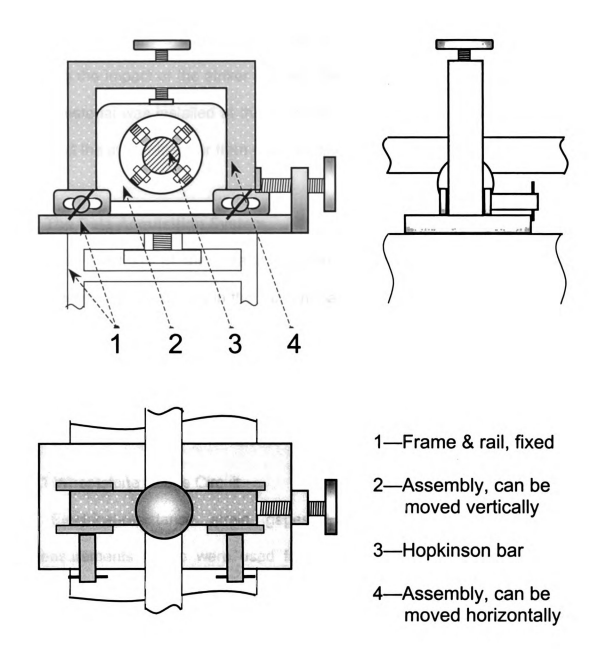


Figure 2 Teflon bearing and associated frame and rail

striker bar and the incident bar. Both the clearance and the gap were required to warrant a complete separation of the striker bar from the joining component during the impact of the striker bar onto the incident bar. In addition, a relatively soft material was installed at the very end of the transmitter bar as a stopper to protect the transmitter bar from overshooting.

# 3. The Data Acquisition System

The functions of the data acquisition system are to detect, process and present the strain signals in the incident bar and the transmitter bar. The system consists of a Wheatstone bridge circuit and an amplifier for each bar. The signals output from the amplifier are then input into a computer-based oscilloscope for data processing and display.

# 3.1 Wheatstone Bridge Circuit

Electrical-resistance strain gages EA-06-062AQ-350 manufactured by Measurements Group were used for strain wave measurements. Two strain gages were mounted on the mid-span of each bar at opposite sides to measure the strain waves. They were called active gages. Two strain gages of the same type, so-called dummy gages, were added to form a four-arm Wheatstone bridge circuit. Figure 3 shows the details of a Wheatstone bridge circuit. An adjustable resistor ranging from 0 to 25  $\Omega$  was used for initial circuit balancing. A resistor of 510  $\Omega$  was also inserted in the circuit for circuit stability. Since the two active gages are located on the opposite side of each bar and on the opposite arm of

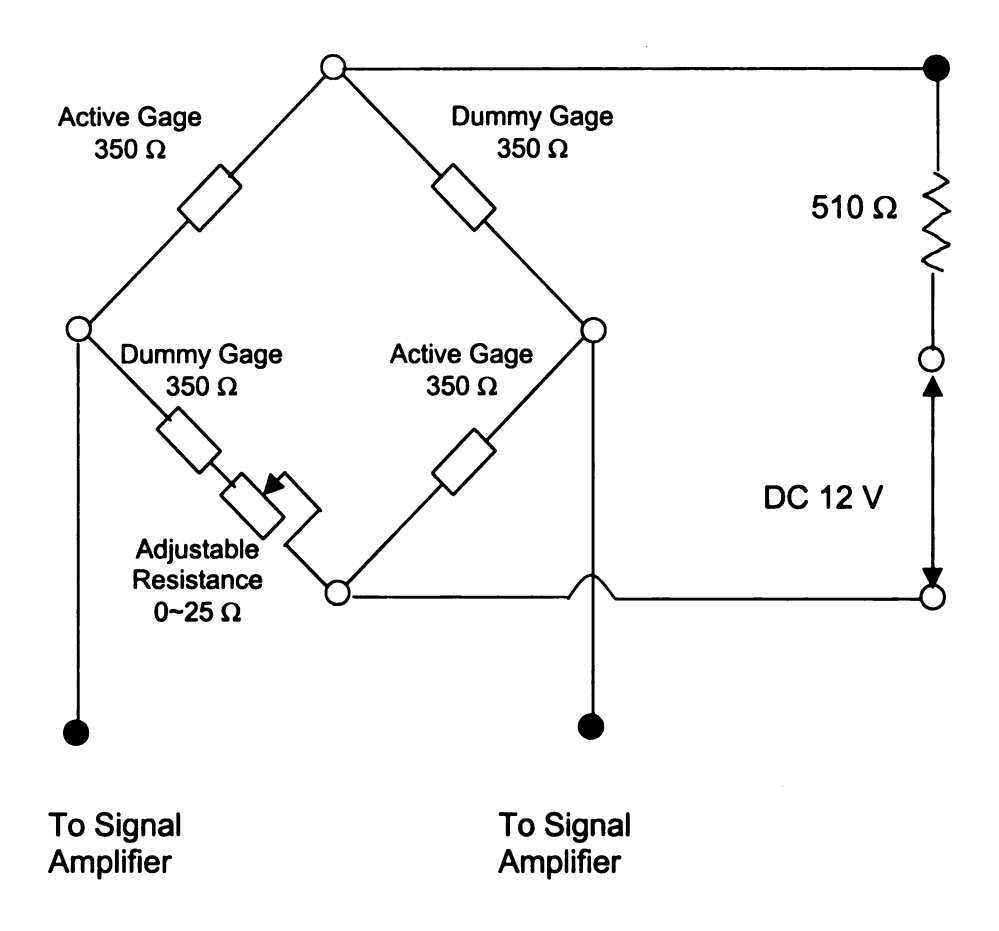


Figure 3 Detailed design of a Wheatstone bridge circuit.

each circuit, signals caused by bar bending can be automatically eliminated in the signal processing. Besides, the use of two active gauges has sensitivity twice that of one active gauge.

# 3.2 Differential Amplifier

Since the signals from the Wheatstone bridge circuits are usually very small, a differential amplifier was designed to magnify the signals output from each Wheatstone bridge circuit. Figure 4 shows the design details of a differential amplifier. A TL084CN amplifier chip (outlined by the dotted lines) is the core of the design. A resistor of 47 k $\Omega$  and a resistor of 1 M $\Omega$  were used to produce a magnification factor around 20 (1 M $\Omega$ /47 k $\Omega$ ), which was determined based on the signal output from the Wheatstone bridge circuit and required by the digital oscilloscope. Besides, a DC power supply capable of providing  $\pm 15$  V was used due to the possibility of having positive and negative strains during experimental measurements.

# 3.3 Computer-Aided Data Processing

Triggering technique is an important issue in dynamic measurements. Since an electrical disturbance with a voltage around 100 mV was usually generated from switching the electro-magnetic valve used, the electrical disturbance was used as a triggering source to initiate the recording of the wave signals. In signal acquisition, a commercial circuit product 5112 Digital Oscilloscope manufactured by National Instrument was used. The Digital Oscilloscope has two channels and

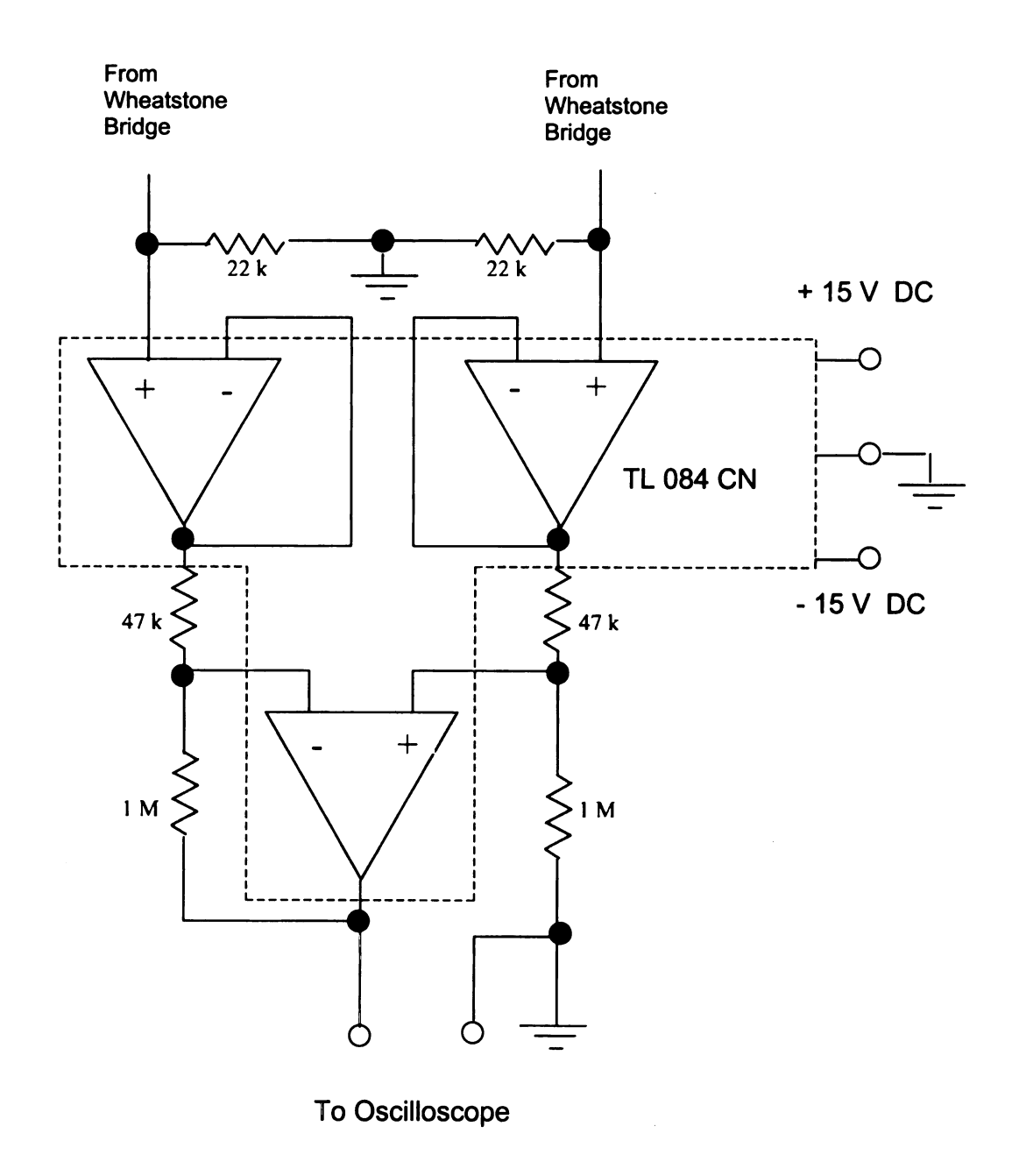


Figure 4 Detailed design of a differential amplifier.

a total sampling rate of 100 million samples per second. With a measuring duration of 0.5 ms, each channel can acquire as many as 25,000 samples, which is sufficient for subsequent data manipulation. For example, Microsoft Excel was used for data integration. Once the signals were processed, they were displayed on a computer monitor. The digitized data was also stored in the computer for later applications

# 4. Overall Operation of the SHPB

Figure 5 gives a flow chart of overall operation procedures for the split Hopkinson pressure bar. Initially, all mechanical components should be adjusted and electronic components should be engaged, e.g. aligning the split bars, installing a specimen between the incident bar and the transmitter bar, adjusting the needed gas pressure, setting up the striker bar, and turning on the computer and power supplies for the Wheatstone bridge circuits and the amplifiers. In setting up the SHPB, the alignment and leveling of the individual bars were perhaps the most important step. In this procedure, a laser beam was used for the alignment while a level rule was used to adjust the level of the bars. In specimen installation, both specimen ends were carefully polished to ensure that they were parallel to each other. A lubricant was applied to both surfaces to ensure low friction (caused by the transverse enlargement due to Poisson's effect) and close contact between the specimen and the bars, hence the one-dimensional wave propagation through the aligned bars and specimen.

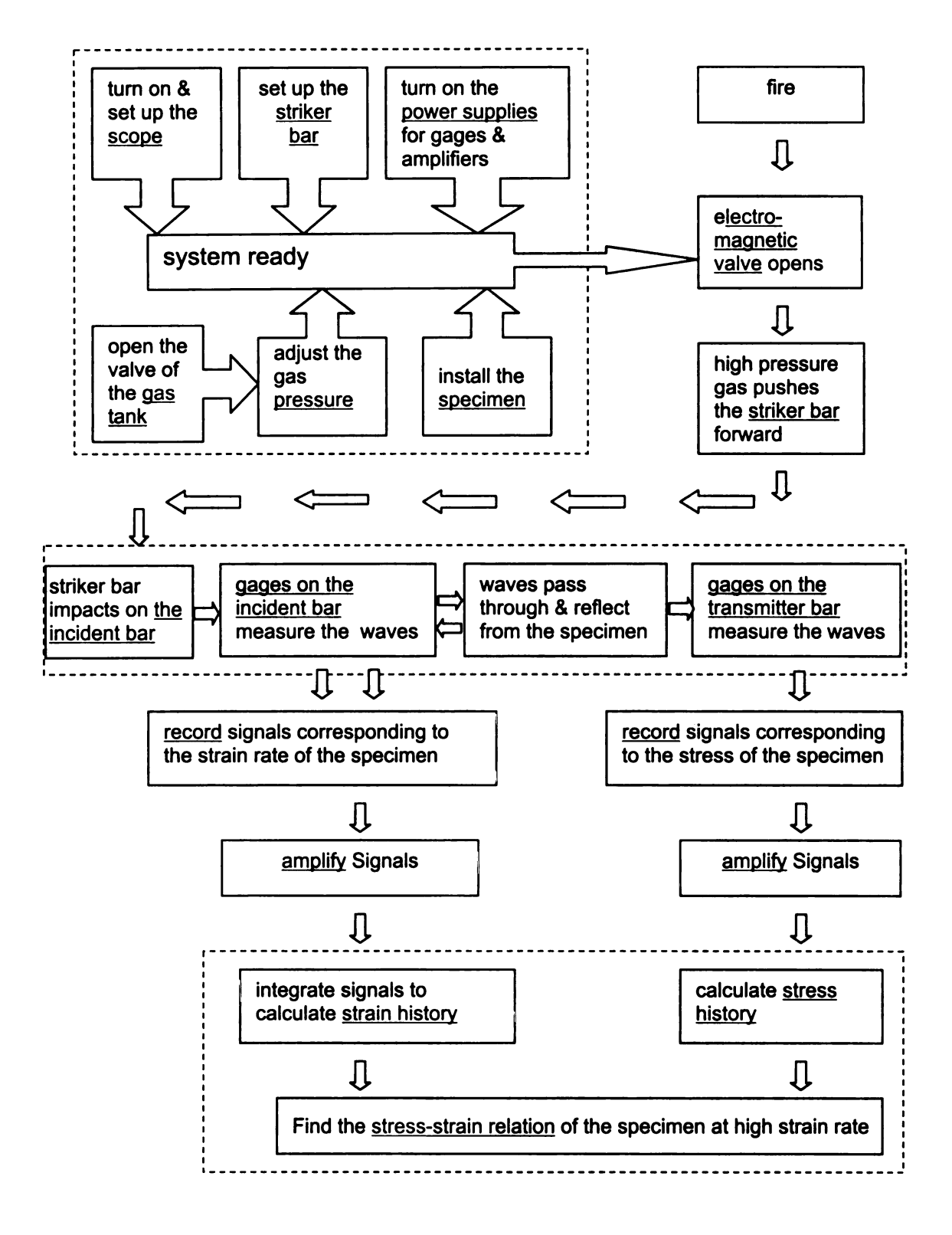


Figure 5 Overall operation and data acquisition and processing of the split Hopkinson pressure bar.

Once the impact between the striker bar and the incident bar takes place, a strain wave will be generated and propagate through the strain gages mounted on the incident bar. A part of the wave will subsequently pass through the specimen and reach the strain gages mounted on the transmitter bar while another part of the wave will be reflected from the front end of the specimen and again be recorded by the strain gages mounted on the incident bar. The strain waves detected by the strain gages will be amplified and input to the computer for data processing. Since the strain wave recorded by the strain gages mounted on the incident bar is associated with the strain history and since that recorded by the strain gages mounted on the transmitter bar is associated with the stress history, a stress-strain relation can be established for the specimen under the investigation of the strain rate, which is also associated with the strain wave recorded by the strain gages mounted on the incident bar.

# 5. Detailed Operating Procedures

# 5.1 Starting Up Procedures

# A. Computer-based Oscilloscope

- a. Turn on the computer. Run the NI 5112 program.
- b. Adjust the voltage range (e.g. 50 mV) and the time range (e.g. 500 ms) for each channel (two channels, one for the incident bar and the other for the transmitter bar).
- c. Set up 100 mV for system triggering.

#### B. Power and Circuits

- a. Turn on the power supplies for the Wheatstone bridge circuits and the amplifiers.
- b. Check all connections from the gages up to the computer.

# C. Split Bars

- Adjust the gap between the striker bar and the incident bar. Do not use
   a gap more than one inch on the first try.
- b. Adjust the gap between the transmitter bar and the bar stopper.
- c. Install the specimen with the lubricant.
- d. Close the protection cover case.

#### D. Gas Pressure

- a. Close all valves.
- b. Close the firing switch.
- c. Open the tank valve.
- d. Open the 100 psi valve (if used).
- e. Open the gun valve.
- f. Open the Nitrogen valve to a pressure above the firing pressure.
- g. Bleed to set the pressure.
- h. Close the gun valve.

# E. Safety Caution

- a. Clear the area surrounding the bar launching mechanism.
- b. Notify personnel in the testing area of test.

#### F. Execution

- a. Record test date and time, specimen material and dimensions, operating gas pressure and the gap between the striker bar and the incident bar.
- b. Fire the gas gun.
- c. Check the figures in the screen and save the data.

# 5.2 Shutting Down Procedures

- A. Close the tank valve.
- B. Close the 100 psi valve.
- C. Open the gun valve, bleed valve, nitrogen valve and 100 psi valve.
- D. Close all valves.
- E. Turn off the switches of the power supplies.
- F. Rest striker bar on a nylon pad.
- G. Exit from the computer program and turn off the computer.

#### **CHAPTER 3**

#### CALIBRATIONS OF COMPONENTS AND SHPB

Once the Split Hopkinson Pressure Bar (SHPB) is constructed, calibrations should be performed before the bar can be used for any material characterization. The calibrations of the SHPB must be conducted on individual components as well as the whole SHPB.

# 1. Calibration of Differential Amplifiers

During the operation of the Split Hopkinson Pressure Bar, elastic strain waves are expected to travel through the strain gages mounted on the incident bar and the transmitter bar. The shape of the elastic waves is usually close to square due to the blunt impact between the striker bar and the incident bar. The frequency of the waves should be around 3,500 Hz because the bars are made of 347 stainless steel. Hence, a square wave with a frequency of 3,500 Hz was created by a function generator and used in the calibration of differential amplifiers. Figure 6 shows the input and output waves on the oscilloscope. Although the square corners of the waves are slightly smoothed out, the overall quality of the output waves seems to remain very close to the input waves.

Figure 7 shows the gain (i.e. the magnification factor) as a function of frequency. Apparently, an almost constant gain exists for frequencies up to 10,000 Hz. For a frequency of 3,500 Hz, a linear relationship between the input and the output voltages is identified and given in Figure 8. The linear relation has

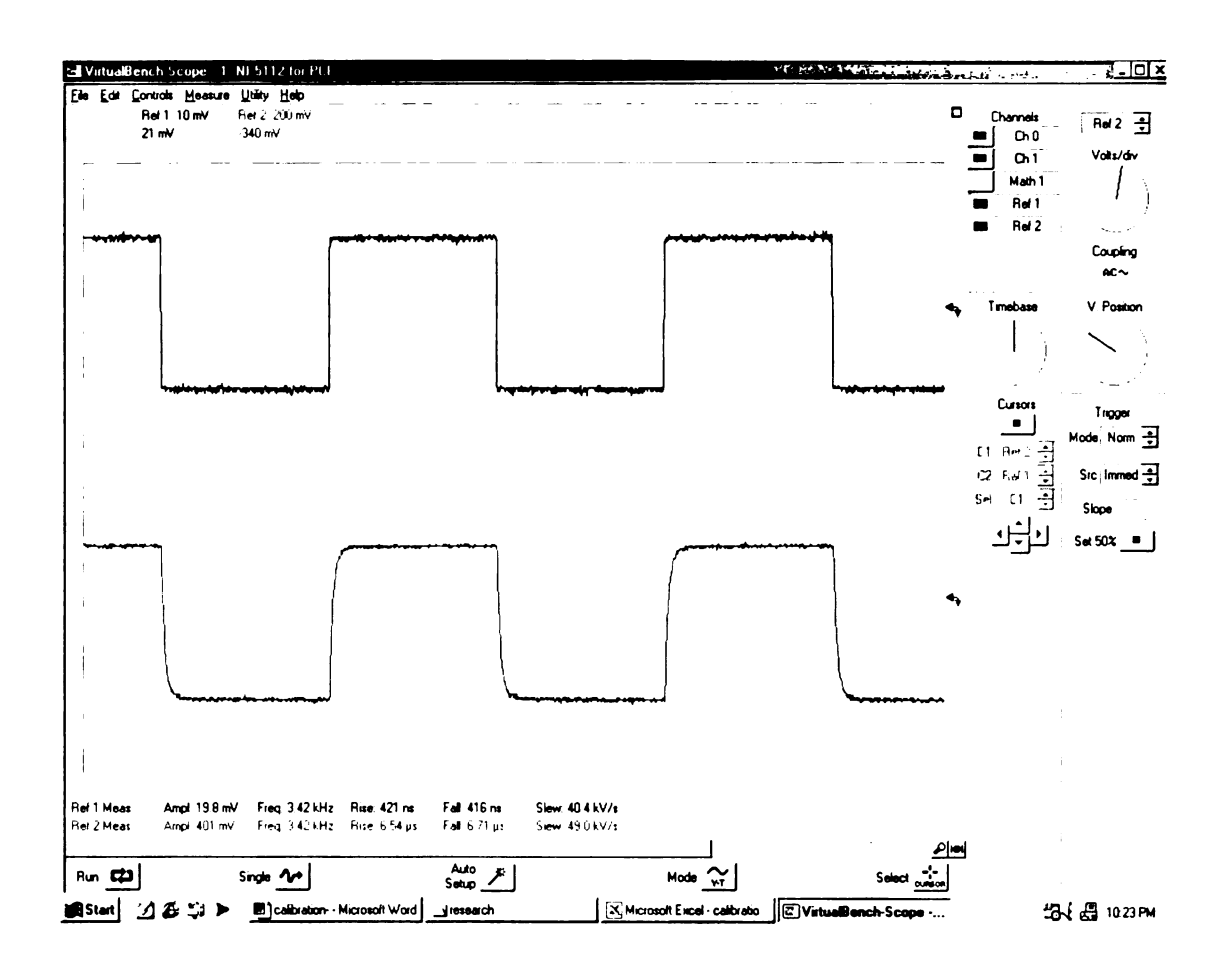


Figure 6 Output wave (below) of an initially sqaure wave (top) with a frequency of 3500 Hz from a differential amplifier.

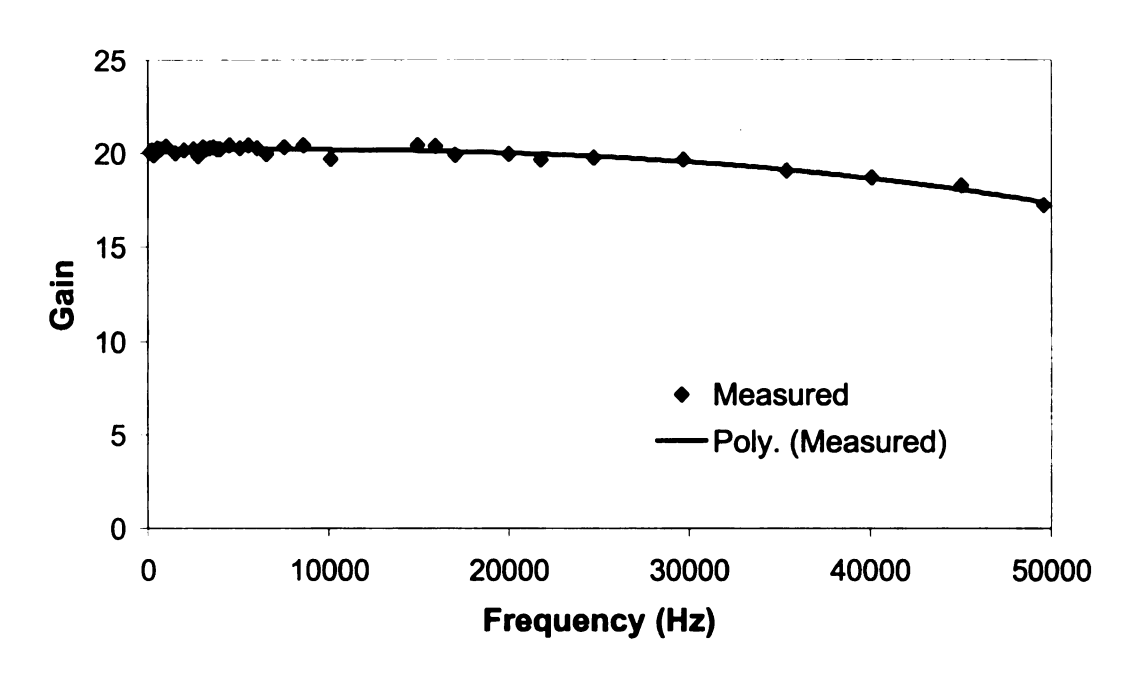


Figure 7 Frequency response function of amplifier

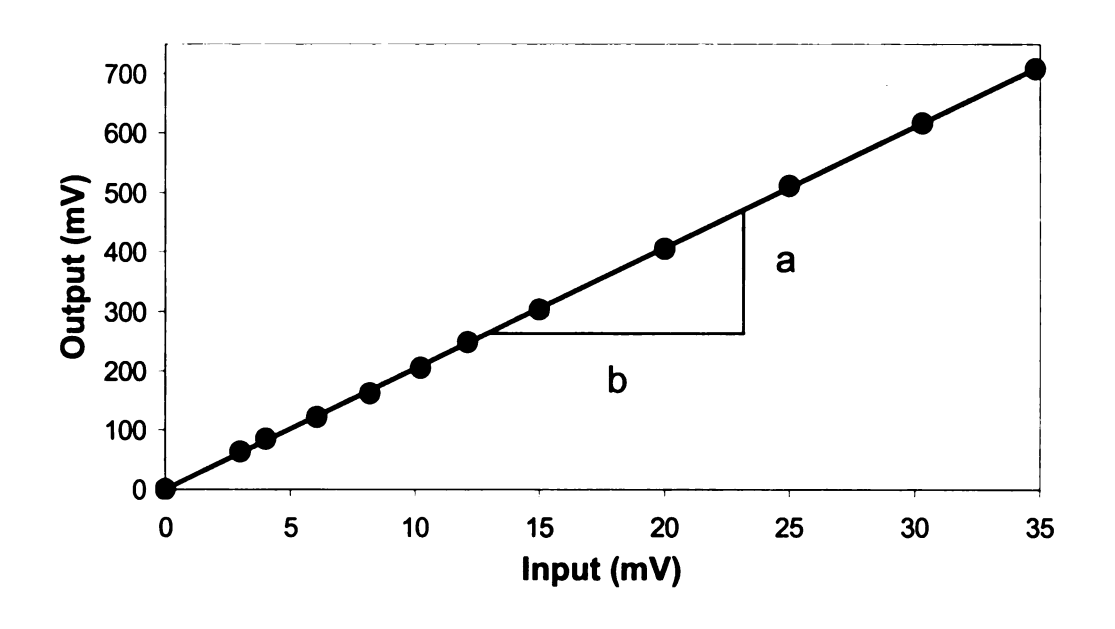


Figure 8 Gain of amplifier based on square waves at 3500 Hz

a slope, i.e. the gain, of 20.38. This value is very close to what was mentioned in section 3.2 of Chapter 2. Results from both Figures 7 and 8 seem to validate the accuracy of the differential amplifiers in the measurement of strain waves.

# 2. Calibration of Wheatstone Bridge Circuits (with Differential Amplifier)

Shunt calibration is the common technique for calibrating Wheatstone bridge circuits. It was also used in this thesis research. As shown in Figure 9, each Wheatstone bridge circuit consists of two active gages and two dummy gages with nominal electrical resistance of  $350\,\Omega$ . An adjustable resistor as shown in Figure 9 is also used for initial circuit balancing.

The resistance of the calibration resistor  $R_c$  should be at least:

$$R_c = \frac{R_g}{F_\sigma \varepsilon_s} - R_g \tag{3.1}$$

where  $R_g$  is the gage resistance, i.e.  $350\,\Omega$ ,  $F_g$  is the gage factor and  $\mathcal{E}_s$  is the strain limit of the gage. If the gage deformation limit is 3% and the gage factor is 2.105, the resistance of the calibration resistor should be at least 5.192 k $\Omega$  according to Equation (3.1). Resistors of 4.67 k $\Omega$ , 6.78 k $\Omega$ , 9.95 k $\Omega$ , 21.8 k $\Omega$ , 46.6 k $\Omega$  and 996 k $\Omega$  were also selected and used to evaluate the linearity of the output from the Wheatstone bridge circuit.

A DC power supply with a constant voltage of 4.88V was used in each Wheatstone bridge circuit. In calibrating the circuits, the resistors were shunt one by one and the corresponding voltage from the oscilloscope was recorded. The simulated strains can then be calculated from:

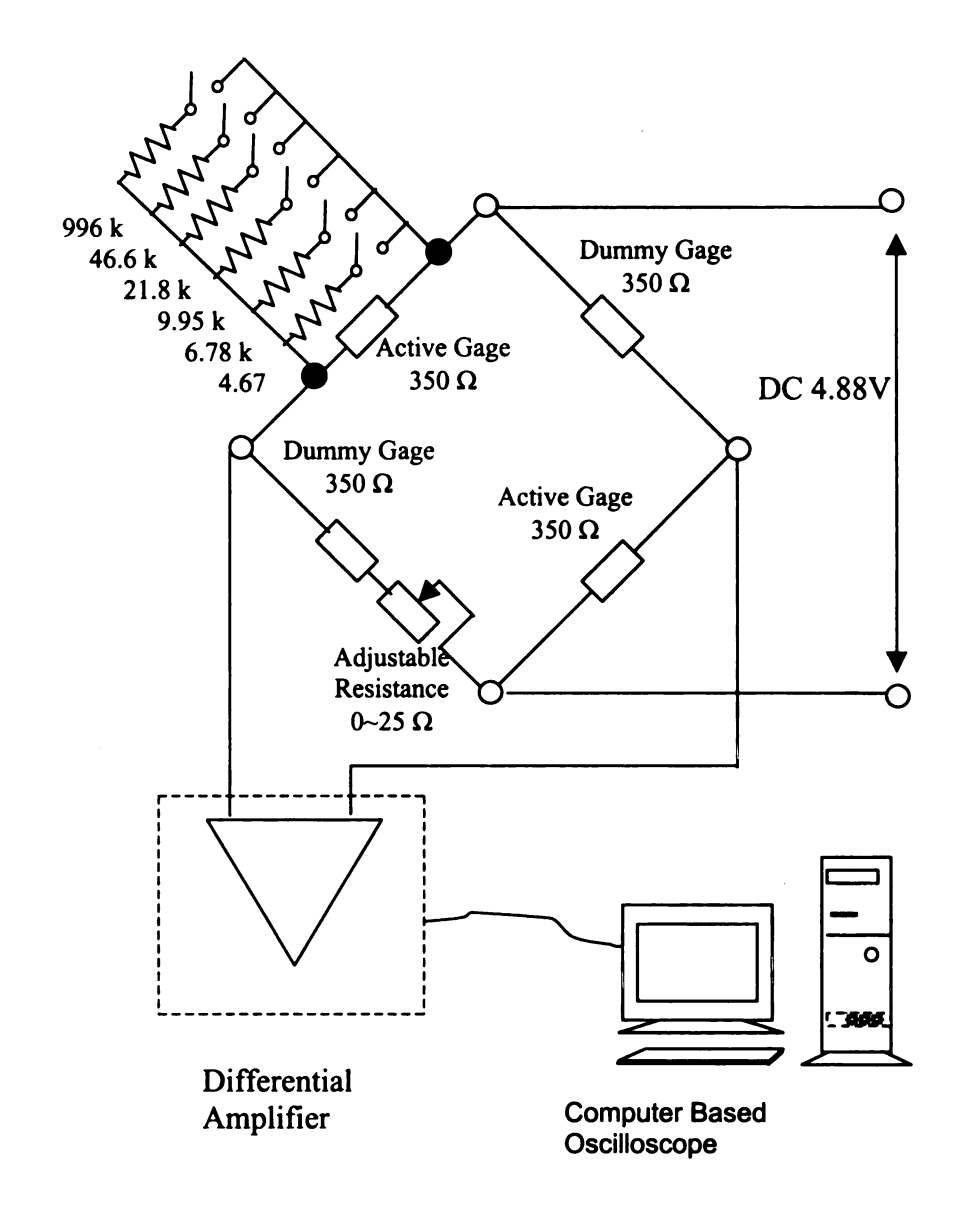
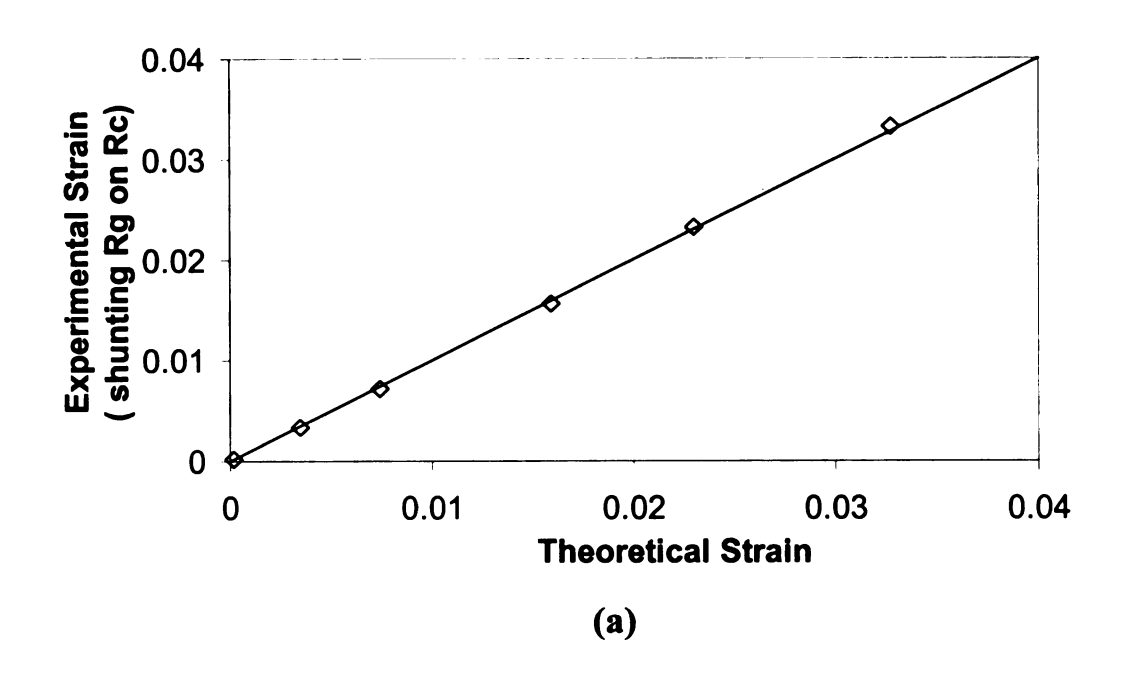


Figure 9 Wheatstone bridge circuit and shunt calibration resistors.



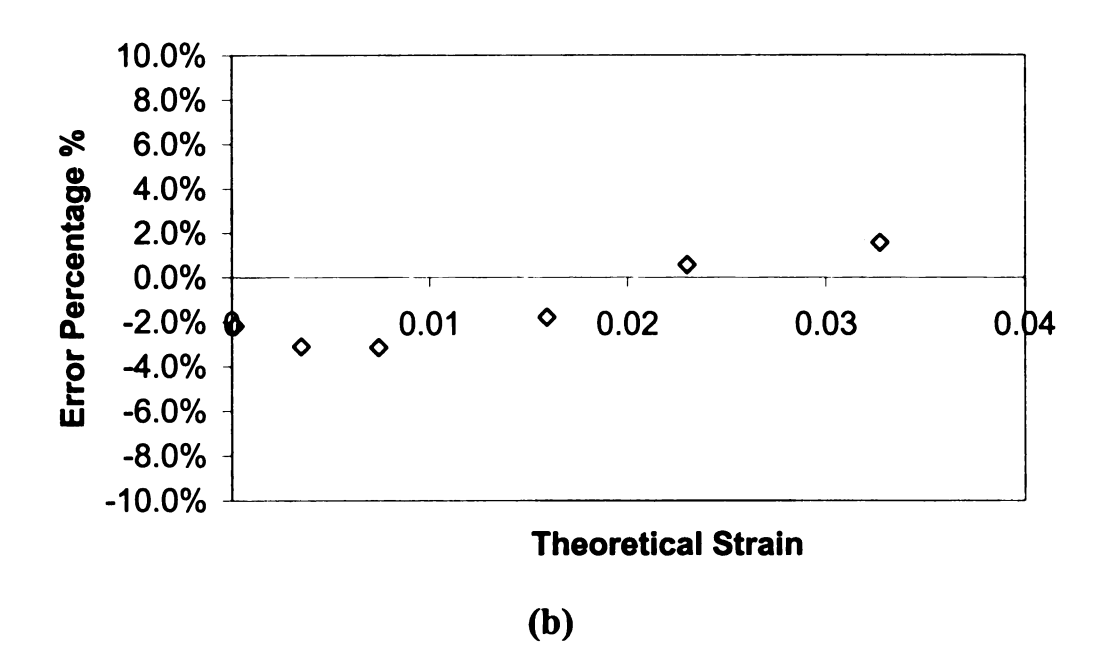


Figure 10 (a), (b) Comparisons between experimental measurements and theoretical calculations.

$$\varepsilon s = \frac{R_g}{F_g (R_g + R_c)} \tag{3.2}$$

The direct measurements and the simulated strains were compared and are shown in Figure 10. They seem to agree with each other very well, validating the accuracy of the Wheatstone bridge circuits.

#### 3. Calibration of the Whole SHPB

Based on the theory of wave propagation, the wave speed in a material  $C_o$ , the dynamic Young's modulus of the material E and the density of the material  $\rho$  have the following relation:

$$C_o = \sqrt{\frac{E}{\rho}} \tag{3.3}$$

The wave speed can also be identified from the wave pattern based on the following formula:

$$C_o = \frac{2l}{T} \tag{3.4}$$

where 2l is the total length of wave propagation and T is the traveling time of the wave within the distance 2l. Both Equations 3.3 and 3.4 are useful for the calibration of the whole SHPB. In this thesis research, the following three tests were designed and performed for the calibration of the whole SHPB.

## 3.1 Calibration with Load Cell

In this calibration study, two strain gages were mounted on the striker bar close to the impacting end. The installation of the strain gages and the

subsequent circuits design were identical to those used for the incident bar and the transmitter bar. In addition, a calibrated load cell, usually used for impact testing, was placed in front of the striker bar as shown in Figure 11. When the striker bar impacts the load cell, the history of the contact force can be detected by the load cell and recorded in a computer. Similarly, the history of the strain waves can be detected by the strain gages on the striker bar and recorded in a computer.

Based on the recorded strain wave, the wave speed in the striker bar can be calculated with the use of Equation 3.4. Subsequently, the dynamic Young's modulus E of the striker bar can be determined by using Equation 3.3, the calculated wave speed and the density of the striker bar  $\rho$ , i.e. 489.6 lb/ft<sup>3</sup> (7,859.1 kg/m<sup>3</sup>). For example, if the wave speed is 16,188 ft/s (4,934.2 m/s), the dynamic Young's modulus of the striker bar E will be 27.3 Msi (191.4 GPa). This value is not very much different from the static Young's modulus – 27.6 Msi (193 GPa).

The stresses in the striker bar can be identified from two independent methods: the load cell and the strain gages on the striker bar. Based on the load cell, the stresses can be obtained by dividing the contact forces with the cross-sectional area of the striker bar. Based on the strain gages, the stresses can be obtained from the multiplication of Young's modulus with the strains. The procedure to determine the Young's modulus has been mentioned earlier. The procedure to determine the strains is given below.

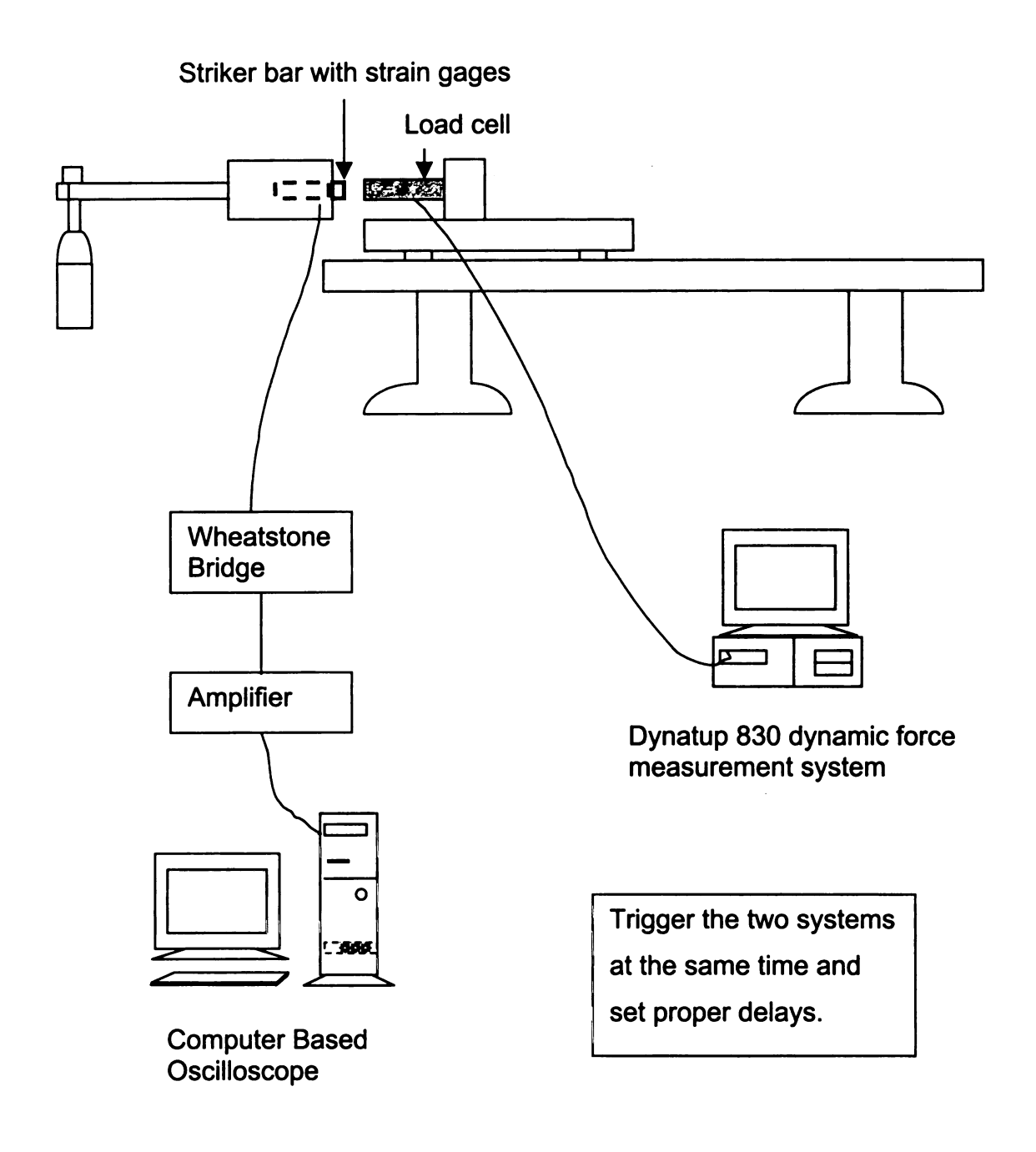


Figure 11 Schematic diagram of striker bar impacting on load cell.

The change of voltage in a Wheatstone bridge circuit due to the changes in strain gages can be expressed as

$$\Delta E = \frac{E_c * F_g}{4} (-\varepsilon_1 + \varepsilon_2 - \varepsilon_3 + \varepsilon_4)$$
 (3.5)

where  $\Delta E$  is the change of voltage,  $E_c$  is the circuit voltage (4.88 V) and  $F_g$  is the gage factor (2.105). Since  $\Delta E$  is a reading from the amplifier, it should be divided by the gain (20.38) before being substituted into the above equation. Equation 3.5 can be further simplified as

$$\varepsilon = \frac{2 * \Delta E}{E_c * F_g} \tag{3.6}$$

if there are no strains in the dummy gages.

Figure 12 shows the comparison of stresses from the load cell and the strain gages on the striker bar. The results from the strain gages seem to be constantly lower than those from the load cell. The offset is around 286 psi (2 MPa). A calibration for the load cell may be required.

#### 3.2 Calibration with Instrumented Striker Bar

In this calibration study, the instrumented striker bar used in the previous section was also used to impact the incident bar, the transmitter bar and the combination of the two bars, shown in Figures 13 (a-c), respectively. As mentioned earlier, the dynamic Young's modulus of the striker bar can be determined from the wave propagation equation, Equation 3.4. Similarly, the Young's moduli of the incident bar and the transmitter bar can be characterized

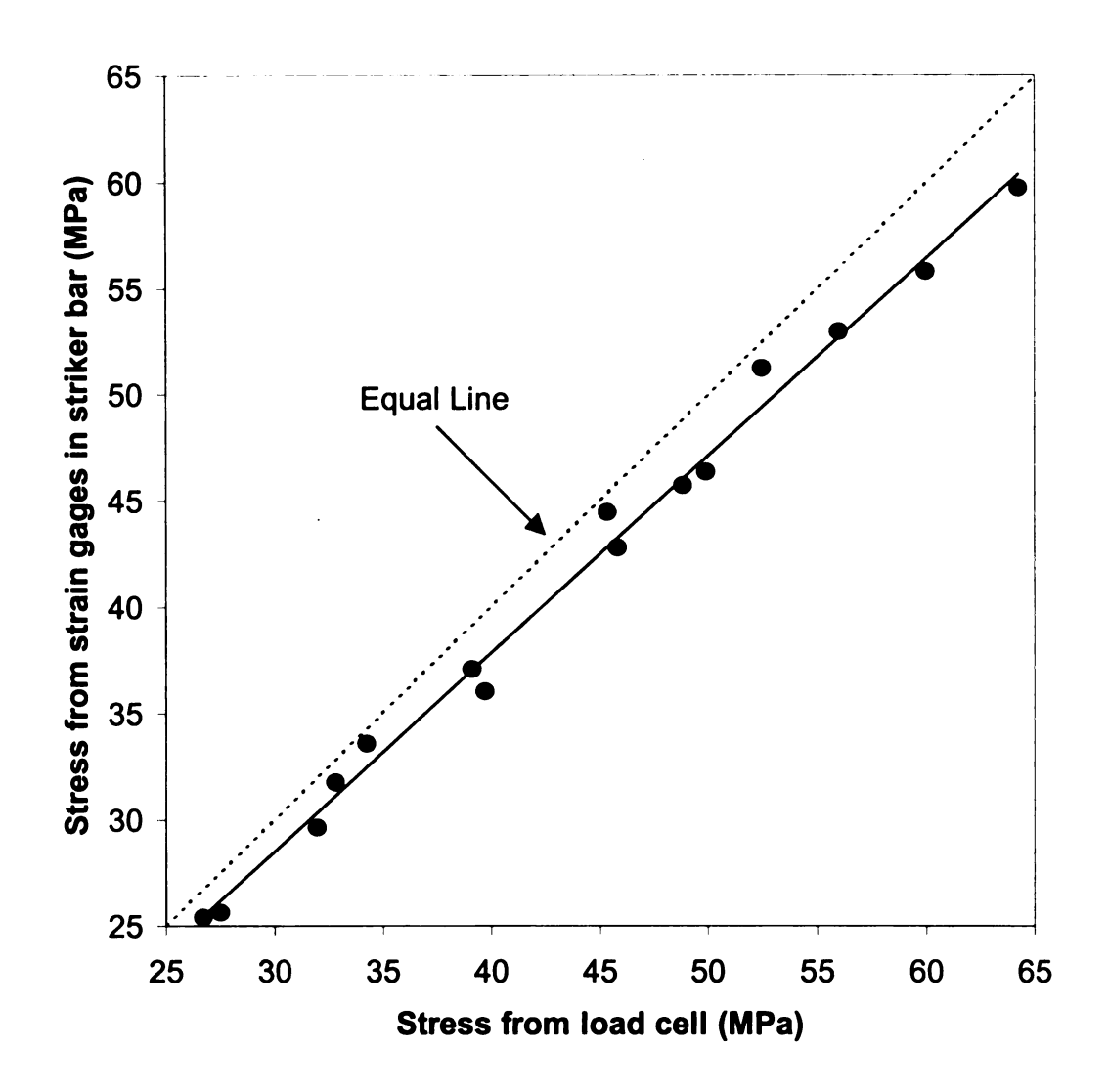


Figure 12 Comparison between the signals from load cell and those from strain gages in striker bar.

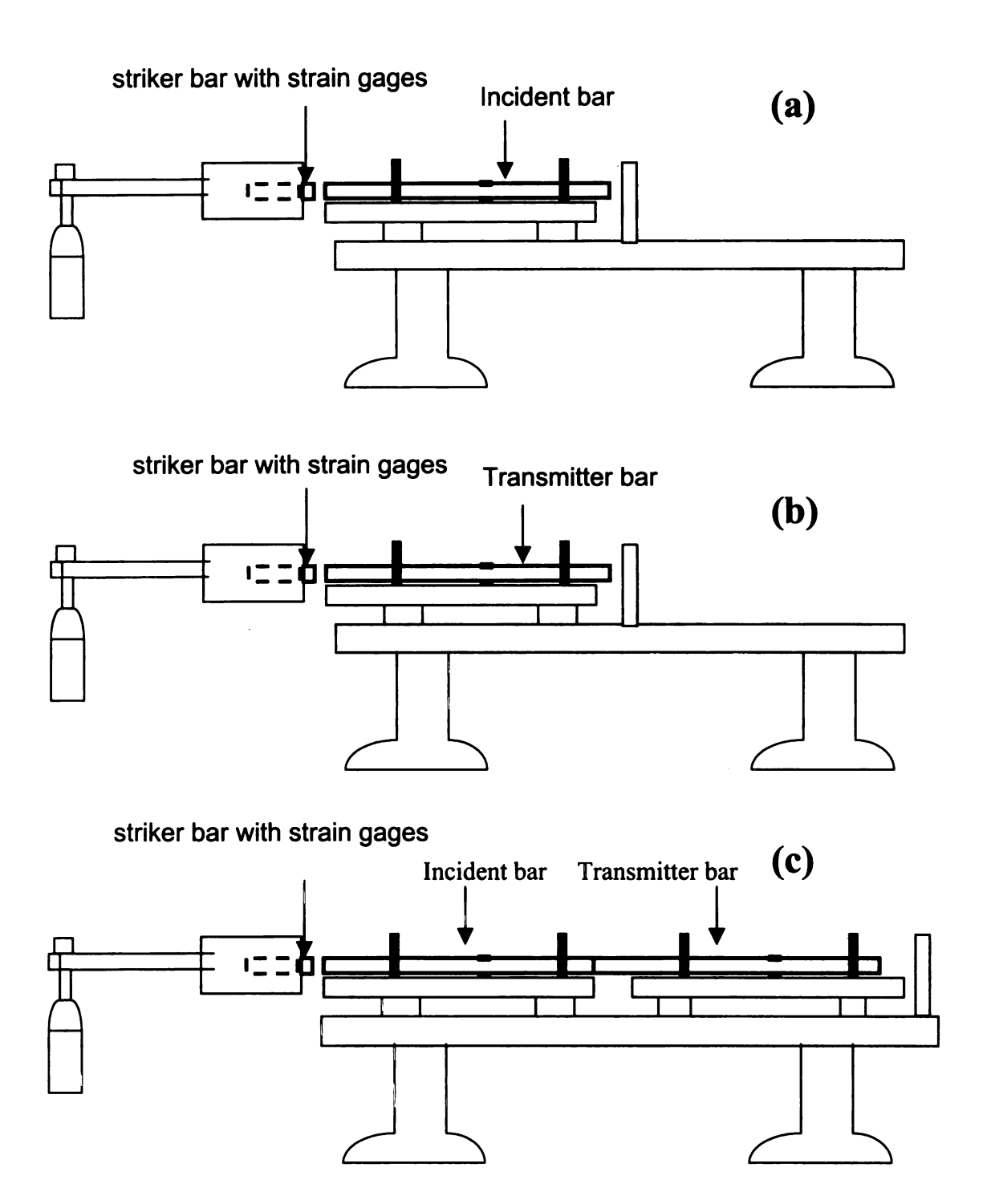


Figure 13 (a-c) Schematic diagram of the striker bar impacting the incident bar, the transmitter bar and the combination of the two bars.

with the same method. The density, wave speed and Young's modulus of each bar are summarized in Table 1. They are all very close.

In order to further compare the discrepancy of measurements between the bars, measurements of strains due to the impact between the striker bar and the incident bar, and that between the striker bar and the transmitter bar, were performed. The experimental results are given in Figure 14 for comparison. The strains in the incident bar and those in the transmitter bar are normalized with the strain in the striker bar. The discrepancies of strain measurements between the incident bar and the striker bar (45° line) and that between the transmitter bar and the striker bar (45° line) are around 8% and 6%, respectively. Misalignments of bars and strain gages are believed to be responsible for the discrepancies.

Table 1: Density, wave speed and Young's modulus of split bars.

	Density (kg/m <sup>3</sup> )	Wave Speed (m/s)	Young's Modulus (GPa)
Striker Bar	7855.03	4935	191.245
Incident Bar	7858.03	4935	191.376
Transmitter Bar	7855.85	4946	192.180

Besides the accuracy, the range of application is also an important concern in the calibration of SHPB because SHPB will be used at various levels of high strain rate. In this calibration study, the wave speeds of the individual bars subjected to various levels of impact pressure were investigated. Figure 15 shows the experimental results. They seem to indicate that the wave speeds,

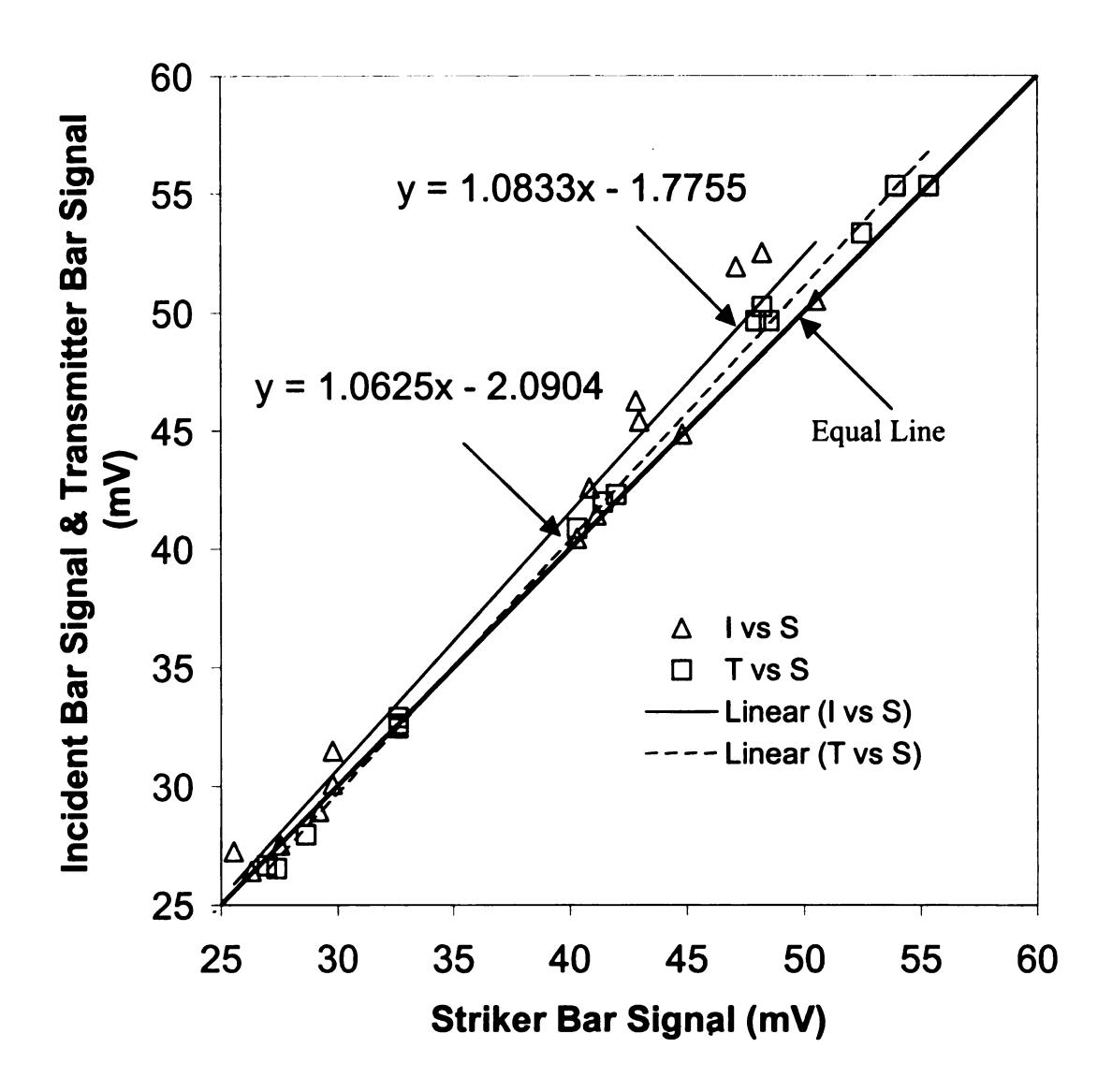


Figure 14 The discrepancies of strain measurements between the incident bar and the striker bar and that between the transmitter bar and the striker bar.

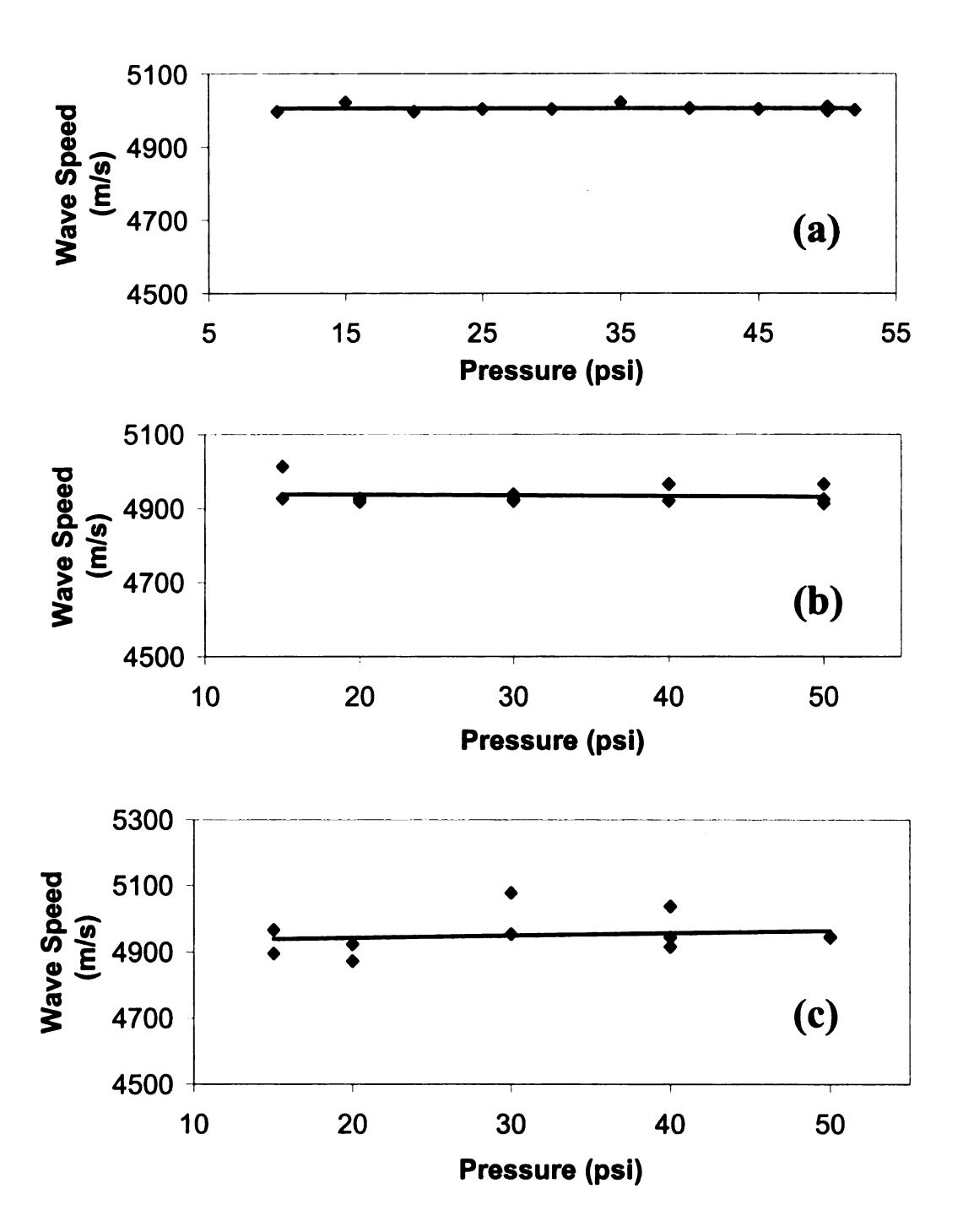


Figure 15 Wave speed as a function of gas pressure.

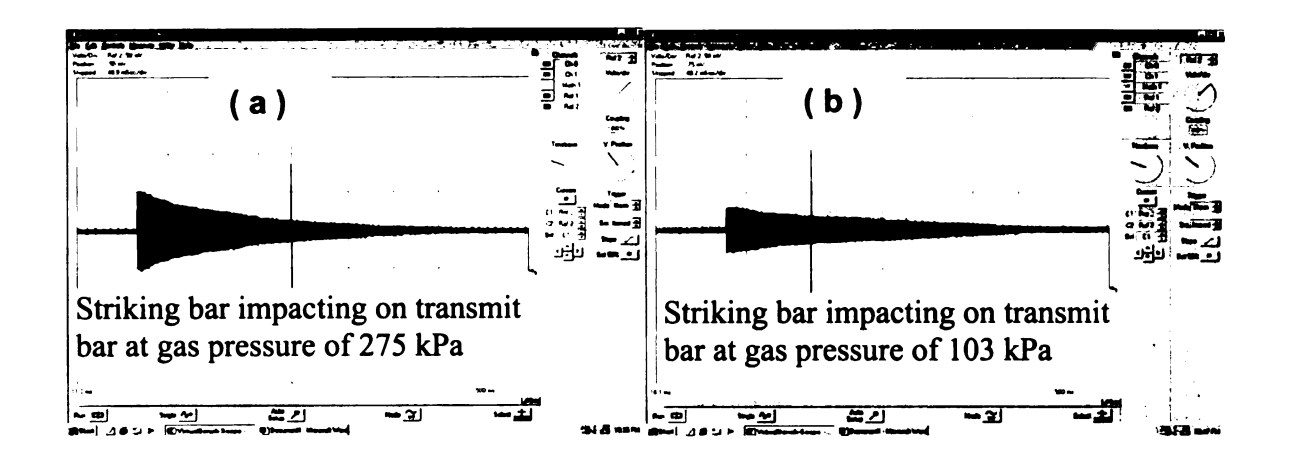
- (a) Striker bar impacting the combination of incident and transmitter bars.
- (b) Striker bar impacting the incident bar.
- (c) Striker bar impacting the transmitter bars.

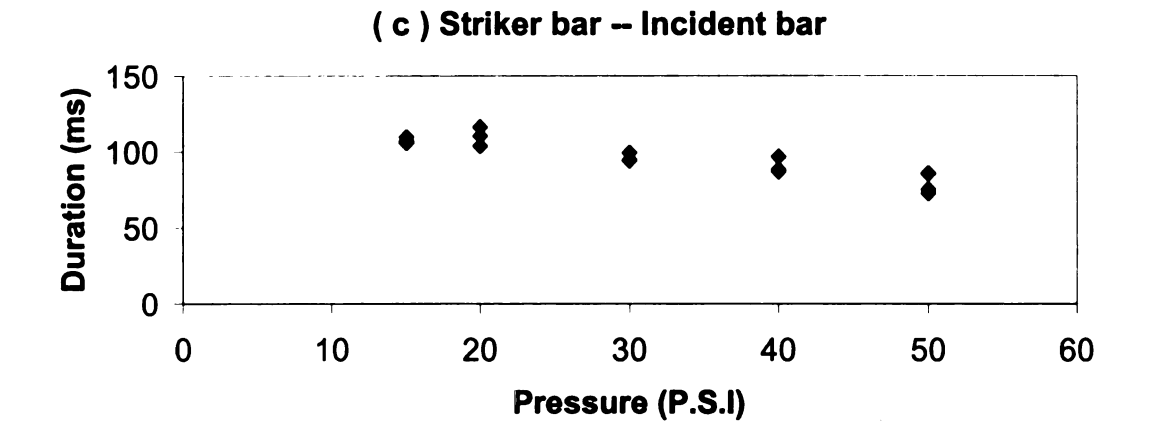
and hence the Young's moduli, of the bars are not sensitive to the impacting pressure up to 360 psi (2.52 MPa). The attenuations of the strain waves in the incident bar and the transmitter bar were also investigated. Figure 16 shows the results displayed on the oscilloscope. The time durations for the strain waves with 50% of amplitude reduction are given in Figure 16 for comparison. A noticeable difference between the incident bar and the transmitter bar seems to exist.

## 3.3 Calibration by Testing 6061-T6 Aluminum

The most common approach to calibrate an SHPB is to characterize a well-known material. Results from the characterization can be used to evaluate the SHPB when compared with the existing knowledge. In this study, 6061-T6 aluminum was used for the calibration of the SHPB. Cylindrical specimens were prepared. Although suggestions on the specimen dimensions and dimensional ratios are available in the literature, there is no conclusive suggestion. In fact, the dimensions and dimensional ratios used by different researchers vary a great deal. Hence, specimens with various dimensions and dimensional ratios were investigated. Figure 17 shows the typical incidence, reflection and transmission waves recorded by the bars.

In order to understand the wave propagation measured from the SHPB, it is useful to examine a schematic diagram of time-positon relation of the strain waves in the incident bar, specimen and transmitter bar, as shown in Figure 18. The waves in the striker bar and the incident bar are generated right after the





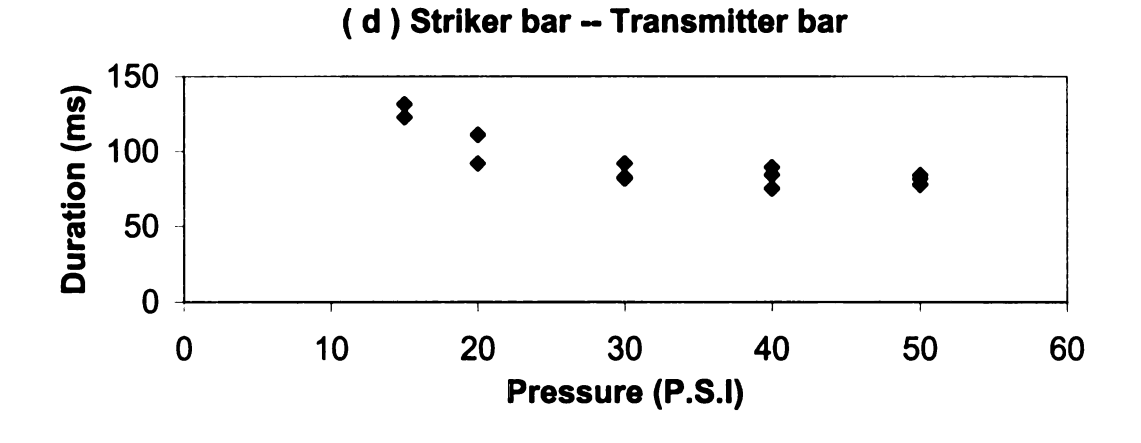


Figure 16 (a), (b) Strain waves showed on oscilloscope during 500 ms (c), (d) Time durations for the strain waves with 50% of amplitude reduction

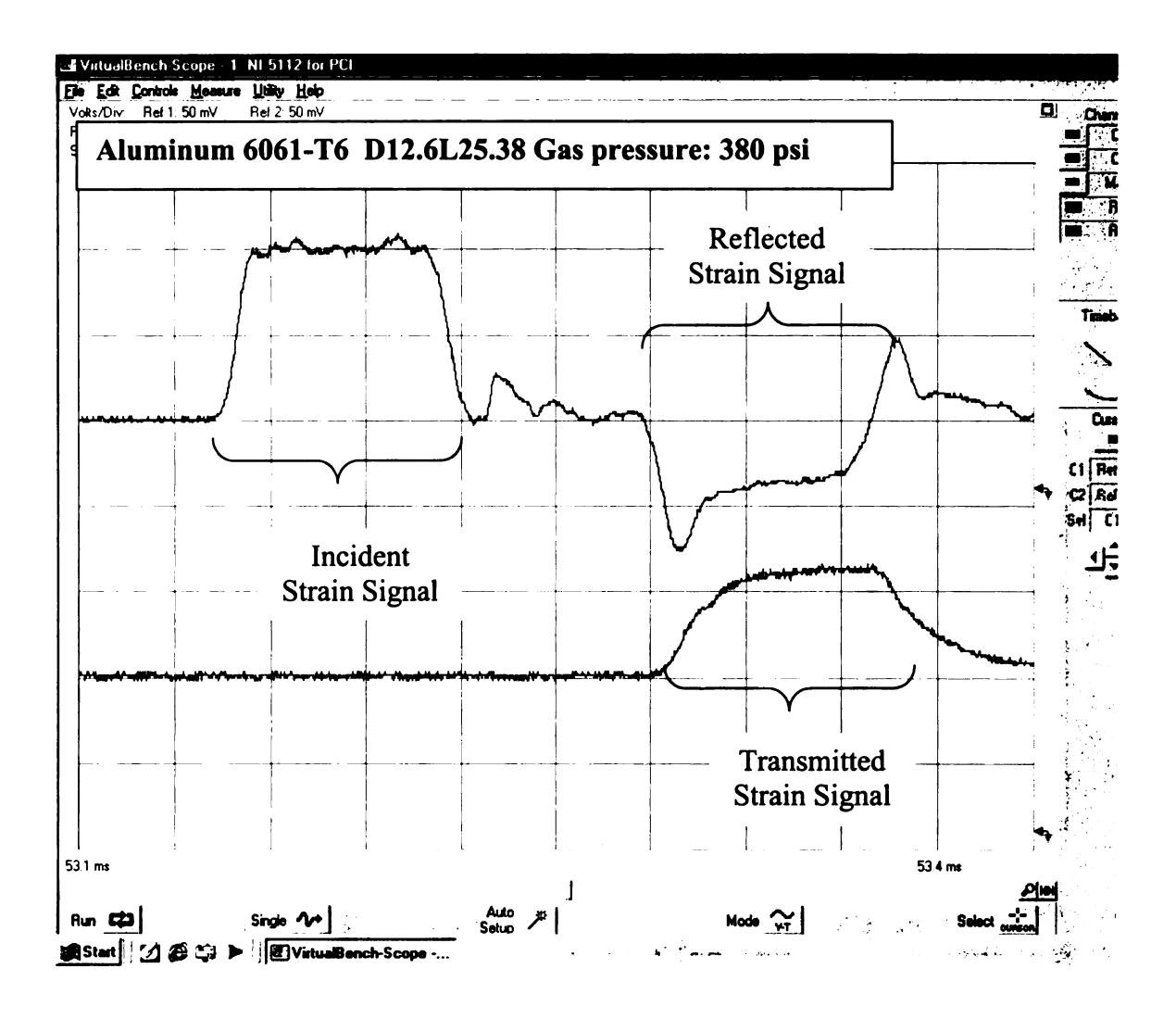


Figure 17 Typical incidence, reflection and transmission waves from SHPB for Aluminum 6061-T6.

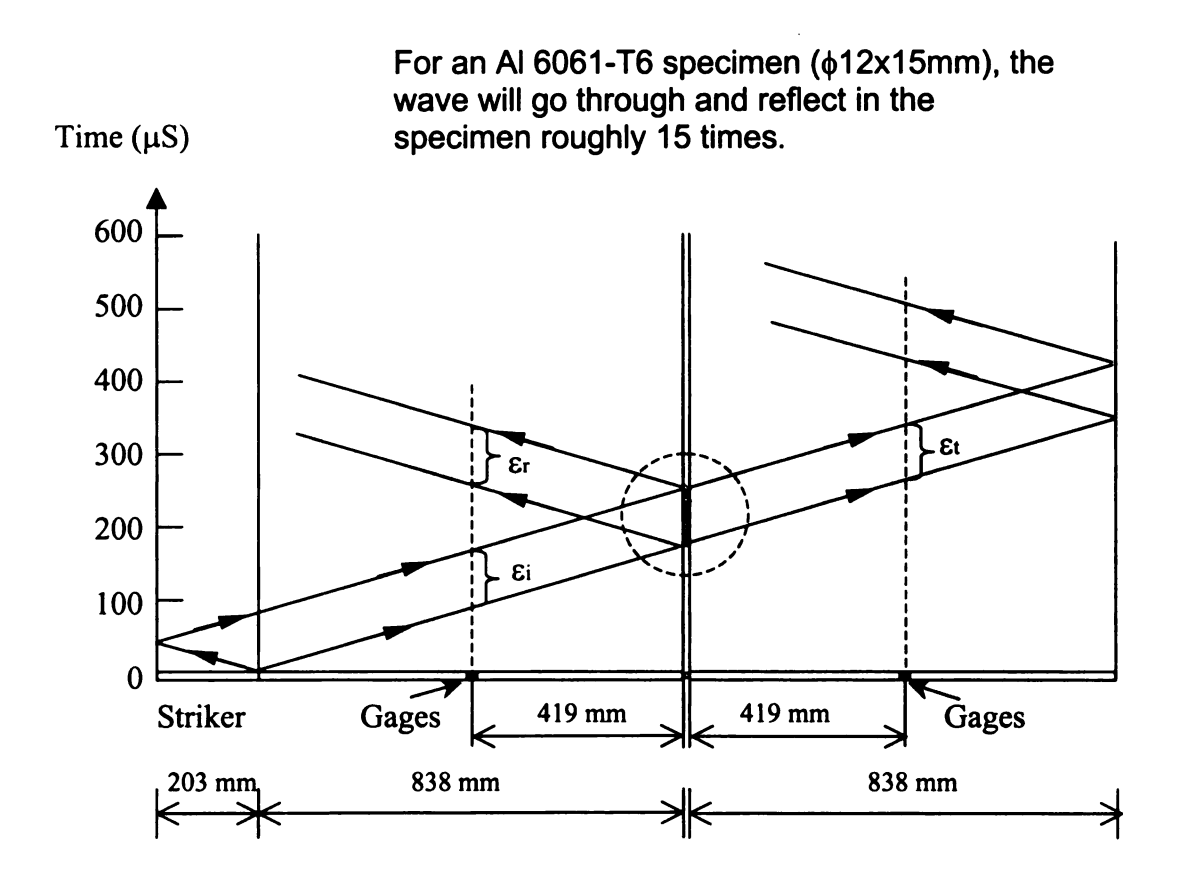


Figure 18 Schematic diagram of time-positon relation of the strain waves in the incident bar, specimen and transmitter bar

impact between the striker bar and the incident bar. The wave in the striker bar propagates to the free end of the bar while the wave in the incident bar, the so-called incident wave, i.e.  $\varepsilon_I$ , propagates to the interface between the incident bar and the specimen. The length of the incident wave is proportional to the duration of the imapet-contact. It ends when the striker bar separates from the incident bar. Based on the theory of wave propagation, the separation is due to the arrival of the tensile wave on the contact surface between the two bars. This happens when the impact-induce compressive wave in the striker bar returns from the free end of the striker bar. Accordingly, the incident wave is an input wave for material characterizations at high strain rates. It is noted that the incident wave is only based on the impact-contact relation between the striker bar and the incident bar.

Once the incident wave arrives at the interface between the incident bar and the specimen, one part of the strain wave continues to propagate into the specimen while the other part is reflected from the interface. The reflection part will again be dectected by the strain gages mounted on the incident bar and is called reflection wave, i.e.  $\mathcal{E}_R$ . The division of the incident wave into a propagation part and a reflection part is essentially based on the mechanical impedances, i.e. the Young's moduli, of the specimen and the bar. If the specimen has a higher mechanical impedance than the bar, the strain wave will experience larger propagation than reflection. On the contrary, if the specimen has a lower mechanical impedance than the bar, the strain wave will experience higher reflection than propagation. The difference between the propagation part and the reflection part should not be too great if an accurate measurement is

desired. For example, a significant error may arise when using a high-modulus SHPB to characterize a low-modulus polymer.

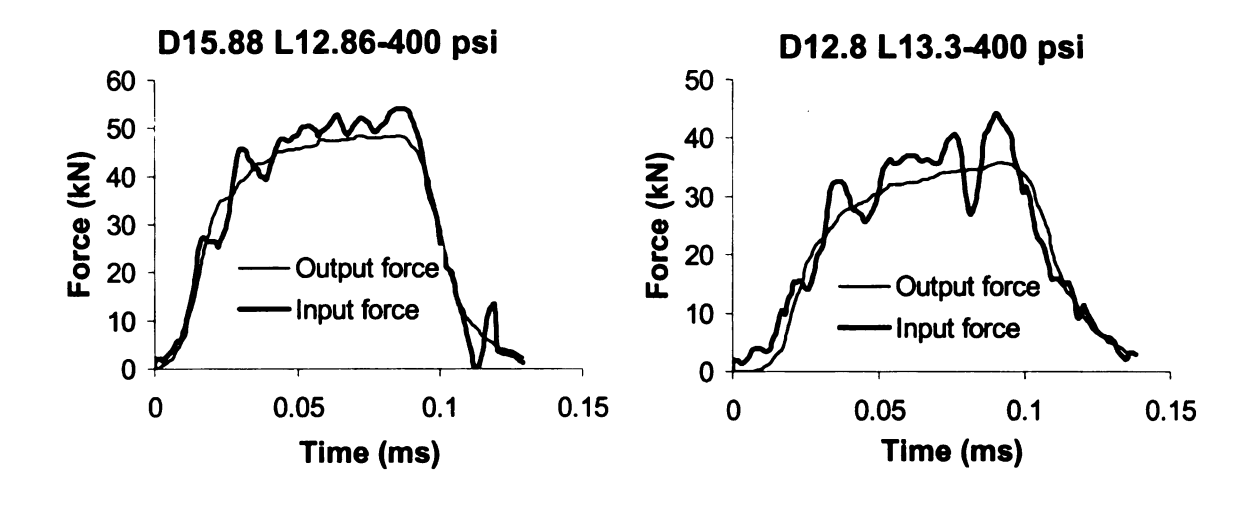
As the wave in the specimen continues to propagate, it will soon hit another specimen-bar interface. Another wave division into propagation and reflection will take place on the interface between the specimen and the transmitter bar. The part that propagates into the transmitter bar will be recorded by the strain gages mounted on it and is usually called transmission wave, i.e.  $\mathcal{E}_T$ . The part that reflected from the interface will propagate through the specimen before it is again divided into propagation and reflection parts at the interface between the specimen and the incident bar.

As mentioned earlier, the duration of the incident wave is proportional to the double-length of the striker bar. Since the thickness of the specimen is much shorter than the double-length of the striker bar, many wave divisions may take place on both interfaces within the duration of the incident wave, also shown in Figure 18. As a consequence, both the reflection wave  $\mathcal{E}_R$  and the transmission wave  $\mathcal{E}_T$  will be continuously modified with the addition of the wave components propagating through the specimen. Apparently, the higher the number of times the wave bounces between the two ends of the specimen, the greater the influence of the specimen properties on the waves. In other words, the many wave bouncings between the two ends of the specimen will impose a more uniform wave propagation to the specimen, and hence a more uniform deformation, which is an important assumption of the SHPB technique.

The incidence, reflection and transmission strains shown in Figure 17, i.e.  $\mathcal{E}_I$ ,  $\mathcal{E}_R$  and  $\mathcal{E}_T$ , respectively, are required for establishing the stress-strain curve of the specimen under investigation. Because these waves do not take place at the same time, it is important to carefully match the initial points of the waves to establish accurate results. In this calibration study and subsequent studies, details of the strain histories were examined. Artificial judgements were made to determine the starting point of each strain wave.

## A. Input and Output Force History

An important step to validate the strain waves is to compare the input force history and output force history at the two ends of the specimen [3]. The former is the multiplication of the difference of strain history between the incidence wave and the reflection wave, recorded by the incident bar, with the Young's modulus while the latter is the multiplicaiton of the strain history of the transmission wave, recorded by the transmitter bar, with the Young's modulus. Figure 19 shows the results from four specimens with different diameters and lengths and subjected to a gas pressure of 400 psi. The dimensions and dimensional ratios of the specimens are summarized in Table 2. Apparently, the discrepancy increases as the ratio between the specimen diameter and the bar diameter increases. The result seems to suggest the diameter of the specimen should not be too small.



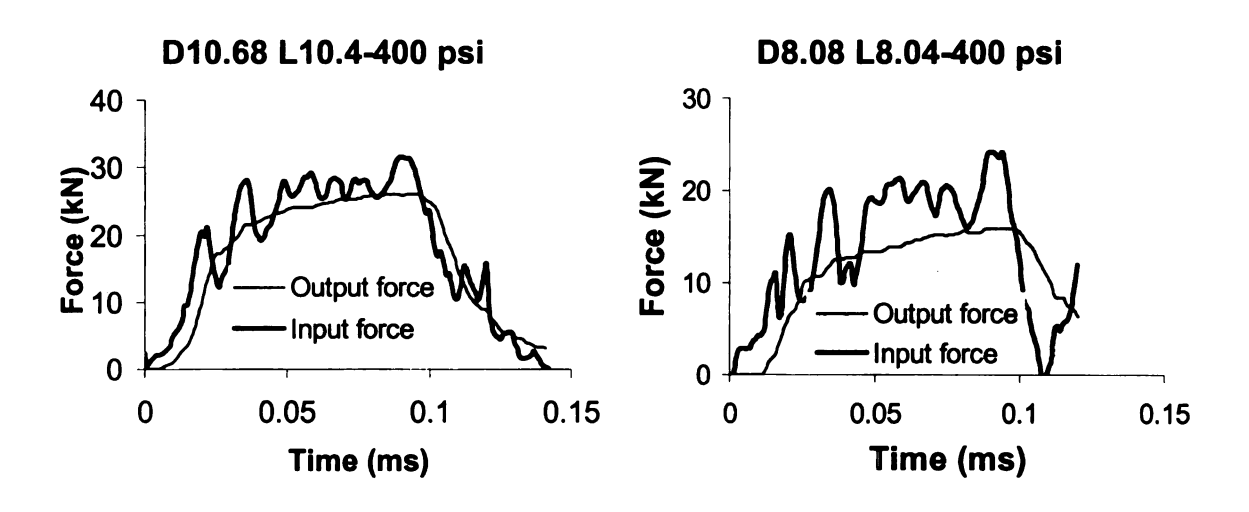


Figure 19 Input and output force histories of four aluminum specimens with the same impact gas pressure.

Table 2: Dimensions and dimensional ratios of aluminum specimens.

	D: Diameter	L: Length	L/D	D/D <sub>bar</sub>
	(mm)	(mm)	Ratio	Ratio
Specimen A	15.80	12.86	0.81	0.84
Specimen B	12.80	13.30	1.04	0.67
Specimen C	10.68	10.40	0.97	0.56
Specimen D	8.08	8.04	1.00	0.43

 $D_{bar} = 19 \text{ mm}$ 

D= specimen diameter

### B. Stress-strain Curve

Since SHPB is a one-dimensional technique for material characterizations, it is ideal that uniform stress, strain and strain rate take place in the specimen during the testing. In order to establish the stress-strain curve for the specimen material, it is necessary to investigate the displacements and forces at both ends of the specimen. If the forces, and hence the stresses, on the two ends are approximately equal to each other, the stress in the specimen could be considered to be uniform in the specimen and the stress and strain histories can be determined by using the following equations based on the transmission and reflection waves, i.e.  $\mathcal{E}_T$  and  $\mathcal{E}_R$ , respectively,

$$\sigma = \frac{EA_B}{A_S} \varepsilon_T \tag{3.7}$$

$$\varepsilon = -2 \int_0^t \frac{C_o}{L_o} \varepsilon_R(t') dt'$$
 (3.8)

where E is the Young's modulus of the transmitter bar,  $A_B$  and  $A_S$  are the cross-sectional areas of the bar and the specimen, respectively,  $C_o$  is the wave speed in the bar, and  $L_o$  is initial length of the specimen.

In presenting a stress-strain curve, it is useful that the stress-strain relation is based on a constant strain rate. The strain rate can be obtained from taking the time derivative of the above strain equation, i.e.

$$\dot{\varepsilon} = -2\frac{C_o}{L_o} \,\varepsilon_R \tag{3.9}$$

Since the reflection strain  $\mathcal{E}_R$  is generally a function of time, it is imperative that constant strain rate is achieved during the test. Otherwise, special techniques, such as shaping technique for incident wave, are required to obtain stress-strain curves at various strain rates.

Figure 20 shows the stress-strain curves from six tests. They were obtained from specimens with different dimensions and strain rates. The notation used in the diagram represents the diameter D and the length L of the specimens. For example, D12.6L35.38 denotes a cylindrical specimen with a diameter of 12.6 mm and a length of 35.38 mm. The value given behind the hypen denotes the strain rate in terms of s<sup>-1</sup>. The result from Chen [5] is also given for comparison. Table 3 shows the yielding points obtained from all tests. The discrepancies between Chen's study and this calibration study are likely caused by differences in both dimensions and strain rate. Chen's result was obtained from a relatively uniform strain rate after using a shaping technique to impose the relatively uniform reflection wave while this calibration study was based on relatively

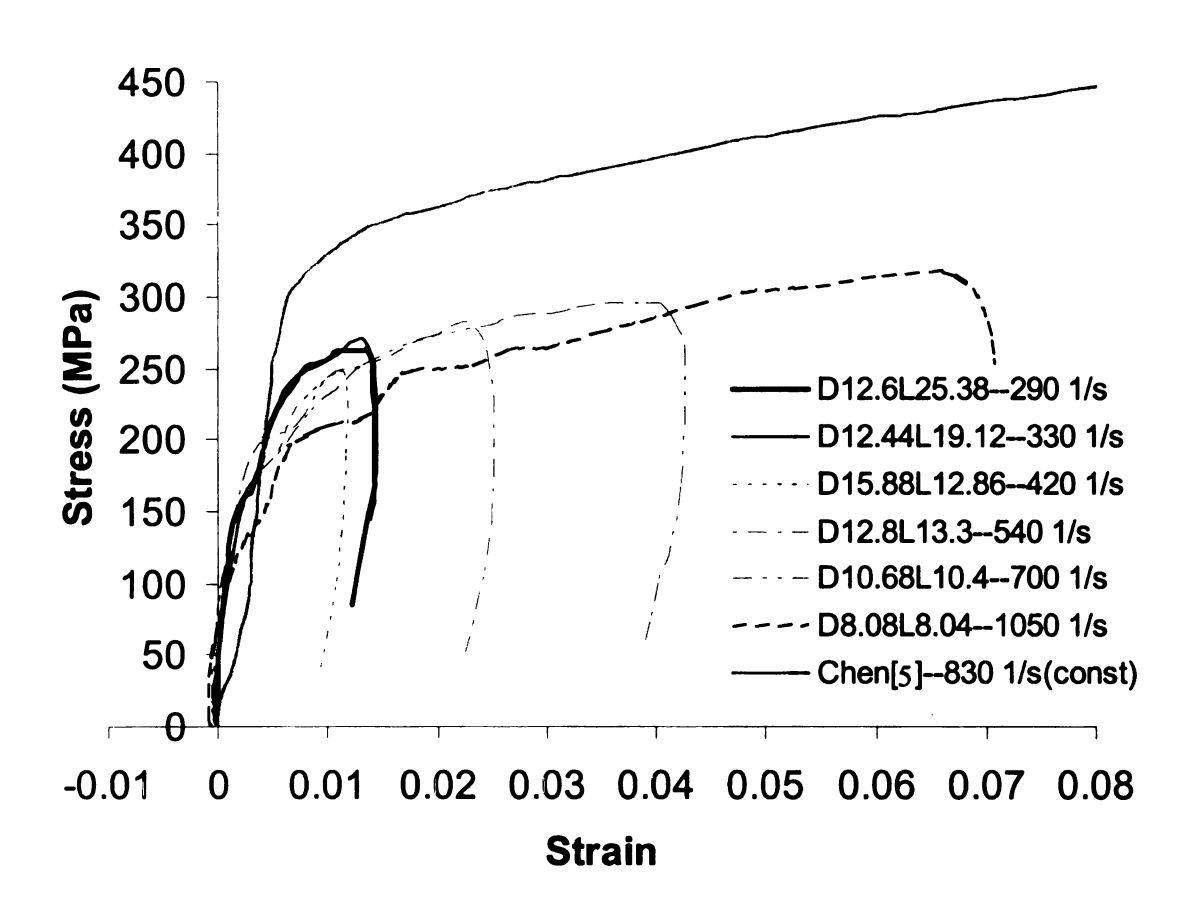


Figure 20 The stress-strain curves of aluminum 6061-T6 under different strain rates.

constant stresses, i.e. relatively uniform incident waves. The maximum strain rate at each calibration test was defined as the strain rate.

Table 3: Comparison of Yielding Points

Specimen	Yielding Point		
	ksi	MPa	
D12.6L25.38	32.1	225	
D12.44L19.12	32.9	230	
D15.88L12.86	30.0	210	
D12.8L13.3	30.7	215	
D10.68L10.4	30.7	215	
D8.08L8.04	30.0	210	
Chen's[5]	47.9	335	

#### **CHAPTER 4**

### CHARACTERIZATION OF THICK LAMINATED COMPOSITES

As more laminated composites are used for structures subjected to high strain rates, such as ballistic impact and crashworthiness, the behavior of laminated composites at high strain rates is becoming a primary concern in composite structural designs. Since SHPB has been used as the standard method for characterizing homogeneous materials, such as conventional metals, at high strain rates, the feasibility of using SHPB for characterizing inhomogeneous laminated composites has become a primary interest in composite research. Besides the inhomogeneity, the use of the SHPB-based characterization technique for laminated composites is becoming more sophisticated, if not more controversial, as the laminated composites for structural designs are becoming thicker. This thesis research explores the application of SHPB in thick laminated composites subjected to high strain rates.

### 1. Speceimen Preparation

In this thesis research, laminated composites made of glass fibers and an epoxy matrix were of interest. All composite plates were cross-ply laminates and had the following stacking sequence: [0/90/0...]<sub>17</sub>, [0/90/0...]<sub>33</sub> and [0/90/0...]<sub>67</sub>. They had the following thickness: 6.25mm, 12.5mm and 25 mm, respectively. Since specimen dimensions and dimensional ratios had strong effects on the

behavior of composite plates, several specimen dimensions and dimensional ratios, as shown in Table 4, were used in the study.

Table 4: Dimensions and dimensional ratios of Glass/Epoxy specimens.

	D: Diameter (mm)	L: Length (mm)	L/D Ratio	D/D <sub>bar</sub> Ratio
Specimen A	15.80	25.50	1.61	0.83
Specimen B	15.80	12.95	0.82	0.83
Specimen C	15.80	11.50	0.73	0.83
Specimen D	12.40	12.80	1.03	0.65

The preparation of the specimens for SHPB characterizations required extra care. In order to prepare cylindrical specimens, a bi-metal hole saw, as depicted in Figure 21, with different diameters were used. Because of the inhomogeneity of the laminated composites, surface chipping and interfacial delamination can easily take place during the machining of specimens. Hence, a proper drilling speed and a well clamping for specimens were critically important to prepare damage-free specimens. A drilling speed of 1000 rpm with water cooling was found to be suitable for the glass/epoxy composite plates. Since bi-metal hole saws with inner diameters of 15.8 mm, 12.8 mm, 10.68 mm and 8.08 mm were available, only limited specimen dimensions and dimensional ratios were possible. Among the combinations of specimen diameter D (based on the size of bi-metal hole saws) and specimen length L (based on the thickness of laminated composites), the selected dimensions and dimensional ratios are summarized in





Figure 21 Bi-metal hole saw

Table 4. The selection was based on the guidelines that the  $D/D_{bar}$  ratio should be higher than 0.65 and the L/D ratio should be higher than 0.7.

## 2. Experimental Results

Figure 22 shows the typical incidence, reflection and transmission waves for a laminated composite specimen. They resemble those for an aluminum specimen up to some extent. The stress-strain curves of all tests are summarized in Figures 23-28.

### 2.1 Strain-Rate Effect

Figure 23 shows the stress-strain curves for specimens with a diameter around 15.8 mm and a length around 25.5 mm, resulting in a L/D ratio of approximately 1.6. The strain rates vary between 190 s<sup>-1</sup> and 310 s<sup>-1</sup>. Generally speaking, the stress-strain curves have similar shapes. At constant strain level, the stress rises as the strain rate increases.

## 2.2 Laminated and Assembled Composites

Figure 24 shows the stress-strain curves for specimens subjected to the same level of strain rate. Although all specimens have about the same dimensions and dimensional ratios, they can be divided into two groups; one group of specimens is made of laminated composites while the other group is made of assembled composites. The laminated composites were virgin composites with thickness around 25.5 mm while the assembled composites

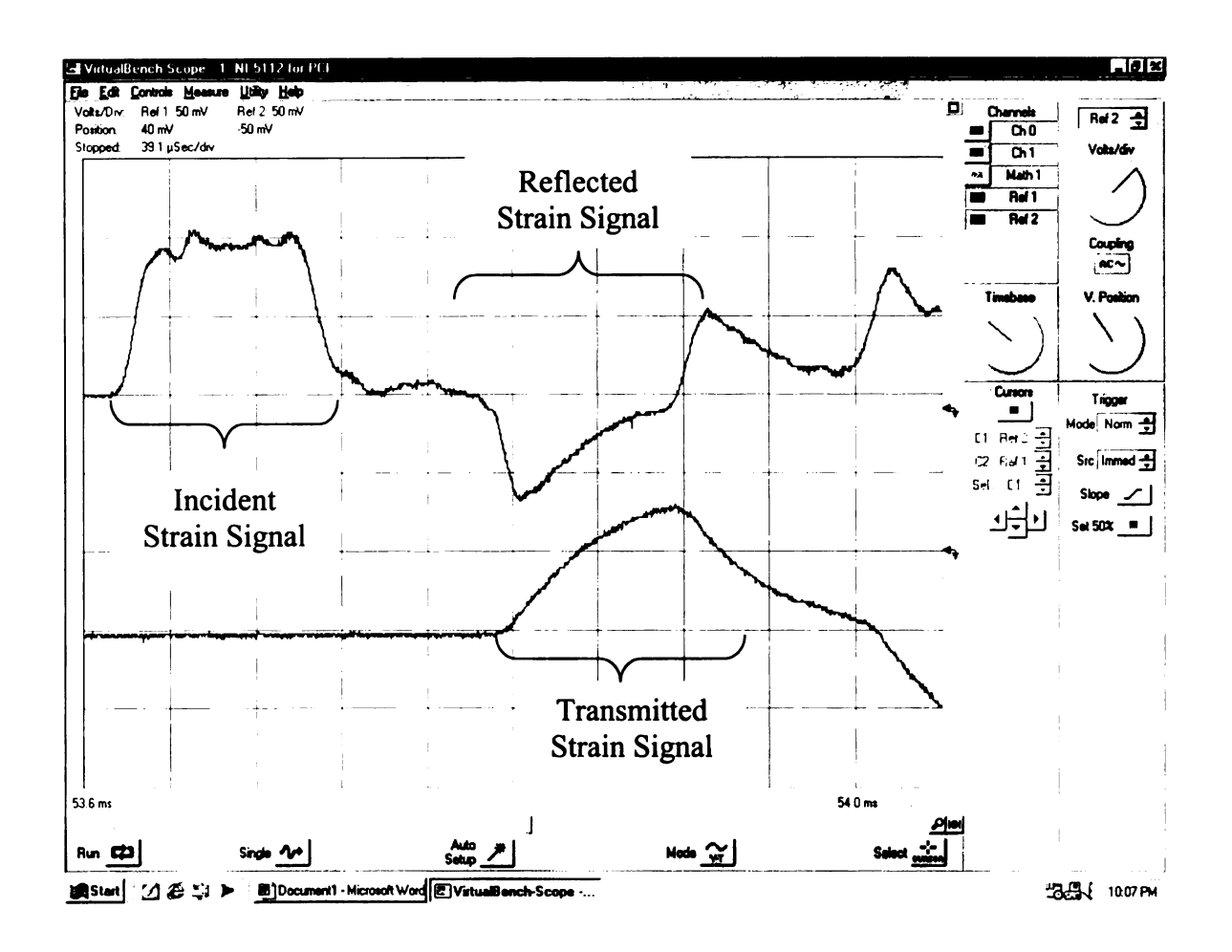


Figure 22 Typical incidence, reflection and transmission waves from SHPB for glass-epoxy composite

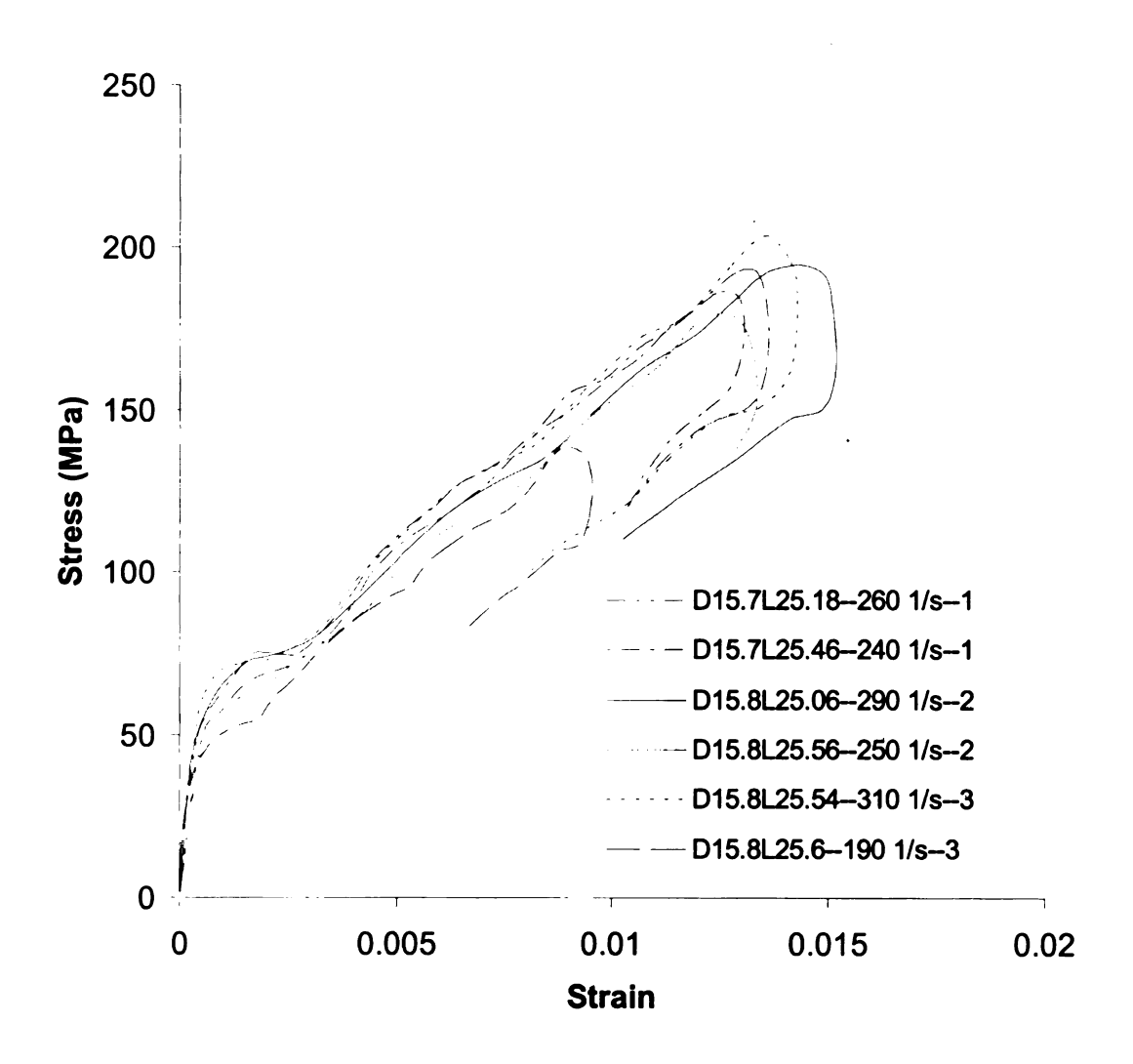


Figure 23 Stress-strain curves for glass-epoxy composites with similar dimensions and L/D ratios (1.6).

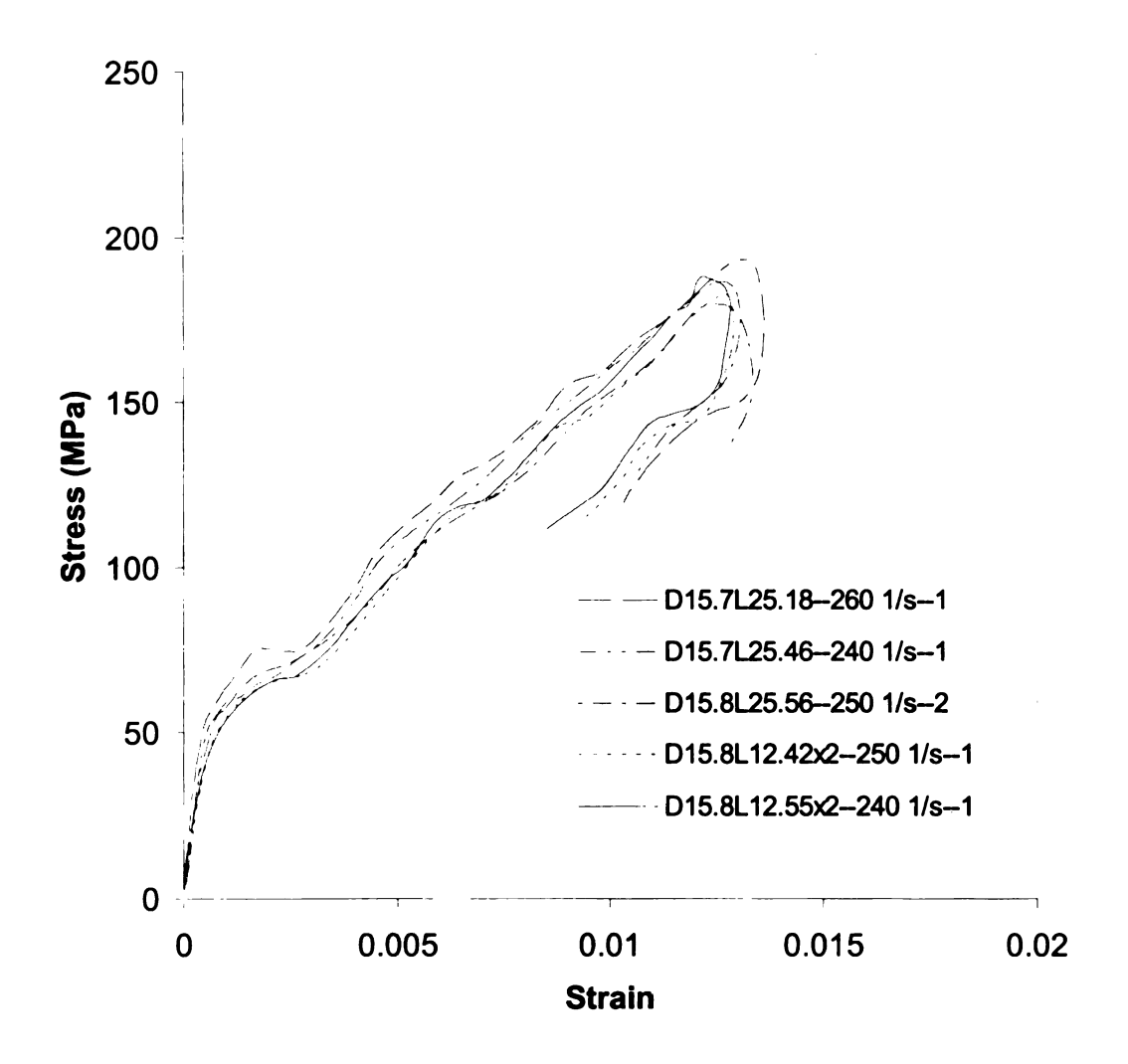


Figure 24 Stress-strain curves for two groups of glass-epoxy composites with similar strain rates and total dimensions.

Group one—from thick glass-epoxy composite plates,
Group two—from thin glass-epoxy composite plates and assembled

were made from placing together two thin laminated composites, each had a thickness around 12.5 mm. The lubricant applied to the interfaces between the ends of specimens and bars was also applied to the interfaces between the thin laminated composites for the ensurance of continuity of wave propagation. From Figure 24, it can be seen that the laminated composites have slightly higher stresses than those assembled at the same strain level.

### 2.3 Effect due to L/D Ratio

Figure 25 shows the stress-strain curves of specimens subjected to about the same strain rates. However, the L/D ratio of the specimens are not the same; two specimens have the L/D ratio greater than 1.0 while the third one has the L/D ratio around 0.8. The difference of stress-strain curve caused by the difference of L/D ratio is very significant. With the same strain level, the specimens with larger L/D ratios have higher stress than the specimen with a lower L/D ratio. A similar result can also be found from Figure 26 for another study.

## 2.4 Effect due to Specimen Inhomogeneity

Figure 27 shows a study similar to the previous section. Once again, there are two L/D ratios; one is 1.62 and the other is 0.82. The specimen with the higher L/D ratio has higher stress than those with the lower L/D ratio when the specimens are compared at the same strain level. It should be pointed out that the specimens with the lower L/D ratio were prepared from the material with the higher L/D ratio by removing half the layers from one side, namely the edge

specimens. This exercise is based on the fundamental understanding that the material properties in a thick laminated composite are not uniform through the laminate thickness due to the nonuniform thermal curing cycle throught the laminate thickness. It is believed that the composite layers close to the laminate surface have higher material properties than those close to the midplane due to the imposition of a more accurate curing cycle on the layers close to the laminate surface. Figure 27 seems to indicate that the effect due to L/D ratio outplays the effect due to the difference in material properties.

In order to further verify the effect due to the property difference, more tests were performed and the results are given in Figure 28. All specimens have about the same level of L/D ratio. Three types of specimen were used in the study. Those designated with "edge" and "middle" were prepared from laminated composites with 67 layers, i.e. the [0/90/0...]<sub>67</sub> compsoite plates. The "edge" specimens were prepared from removing about 33 layers from one side of the laminated composites while the "middle" specimens were prepared from removing about 27 layers, from each side of the laminated composites. The specimens "without" any designation were virgin laminated composites, which had 34 layers, i.e. [0/90/0...]<sub>34</sub> compsoite plates. Experimental results clearly shows the rising trend of the stress-strain curves from "middle" to "without", then to "edge" under constant strains

# 2.5 Young's Modulus and Yielding Point

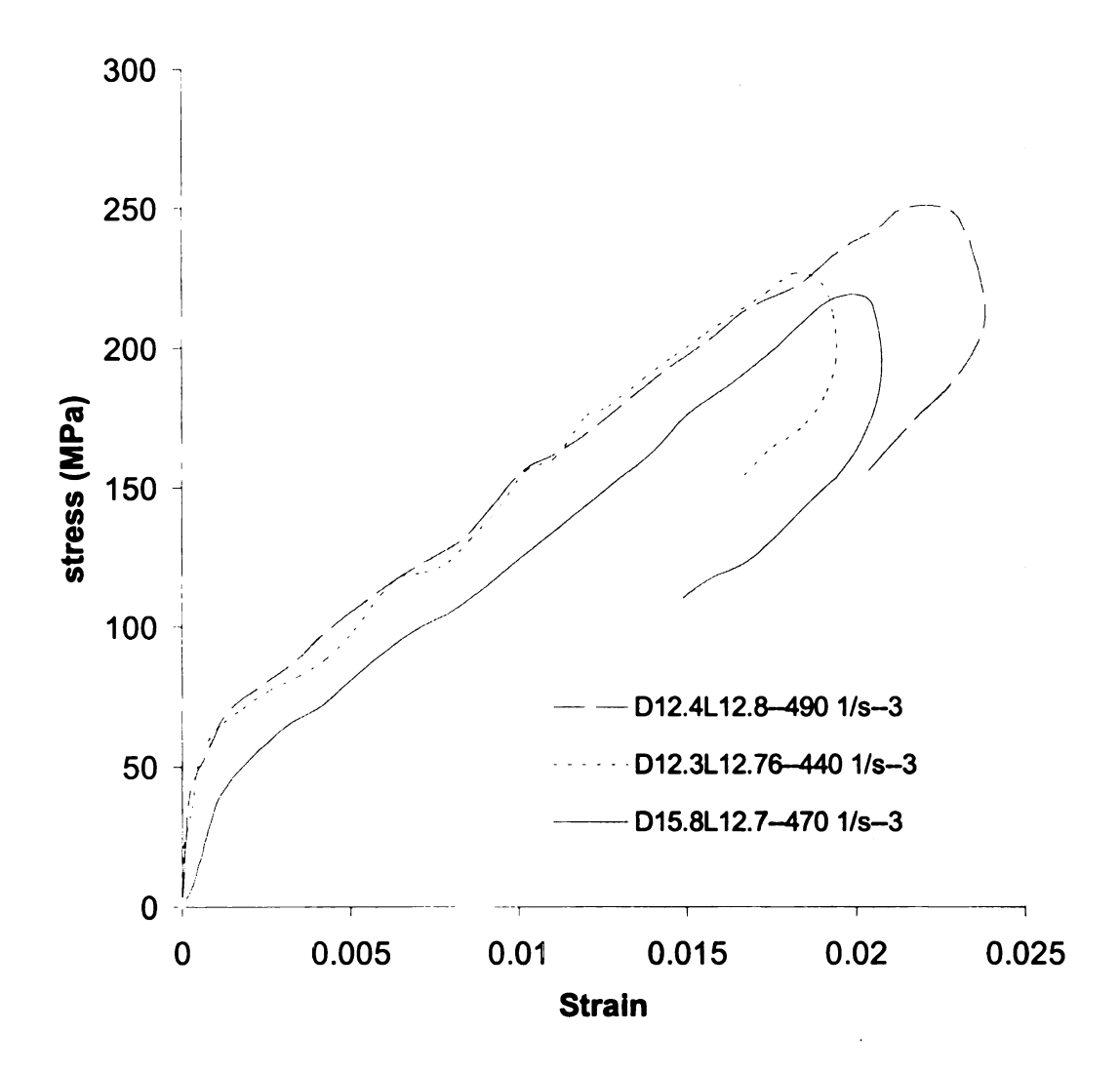


Figure 25 Stress-strain curves for glass-epoxy composites with similar strain rates but different L/D ratios.

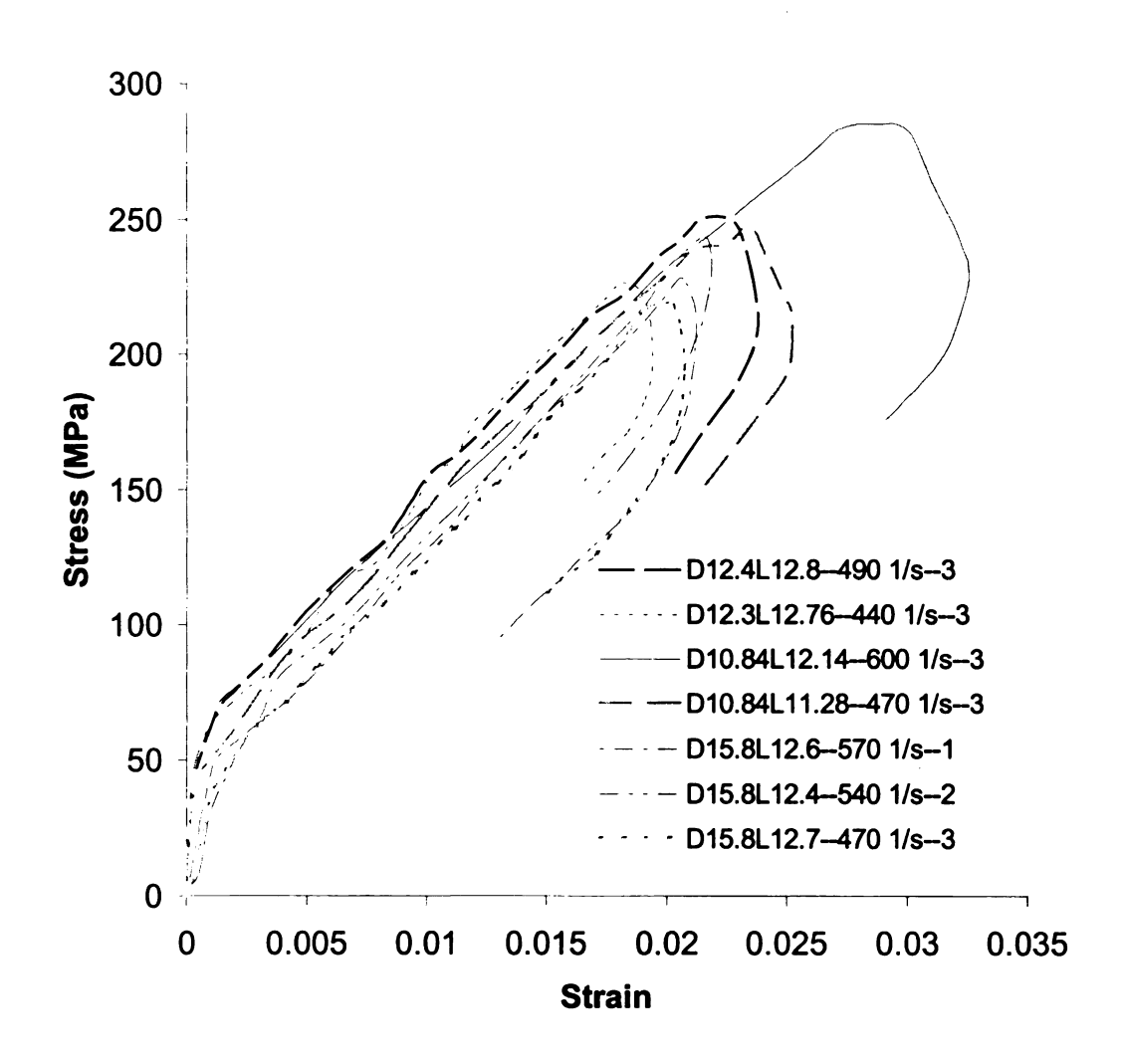


Figure 26 Stress-strain curves for glass-epoxy composites with different strain rates and different L/D ratios

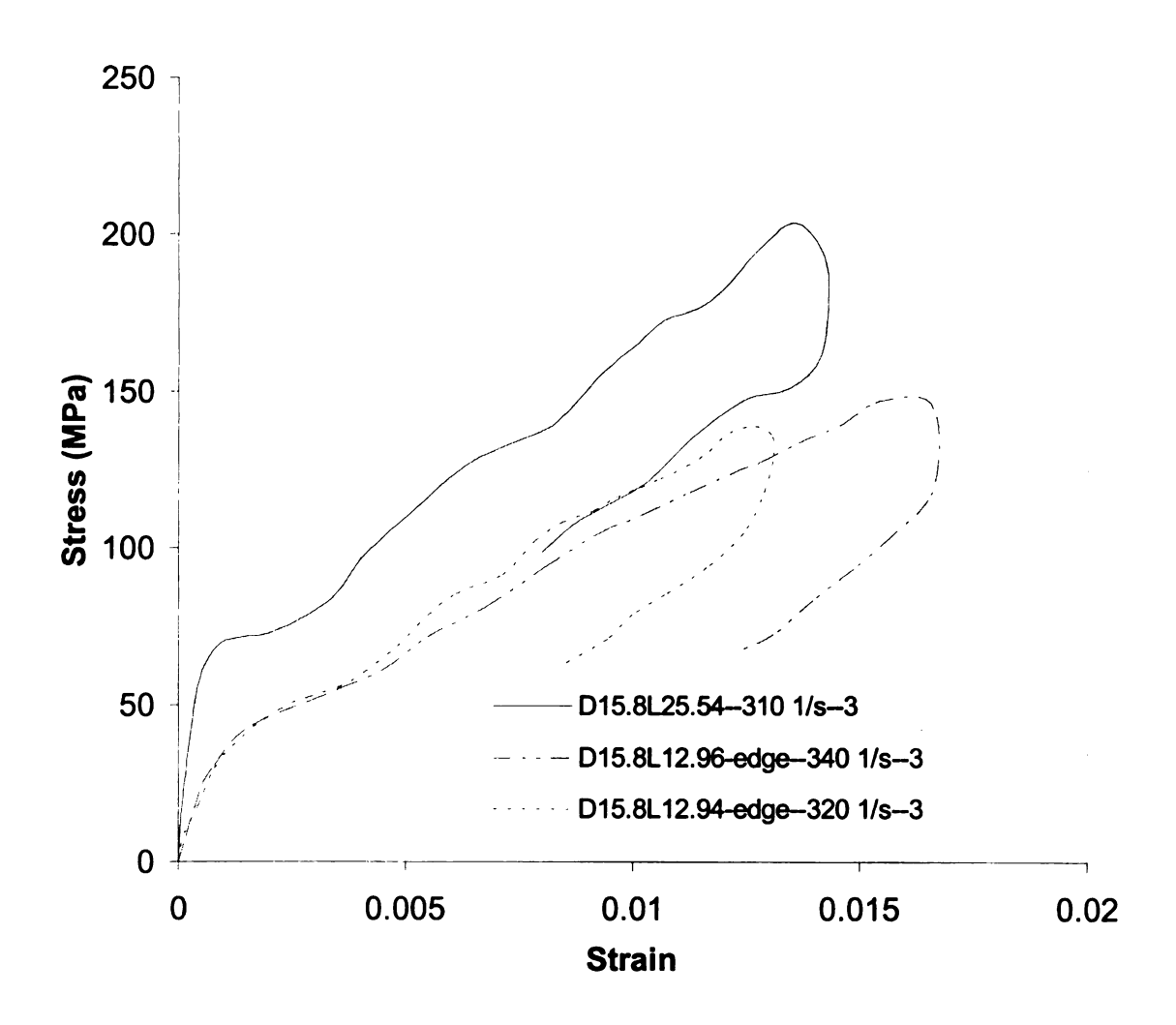
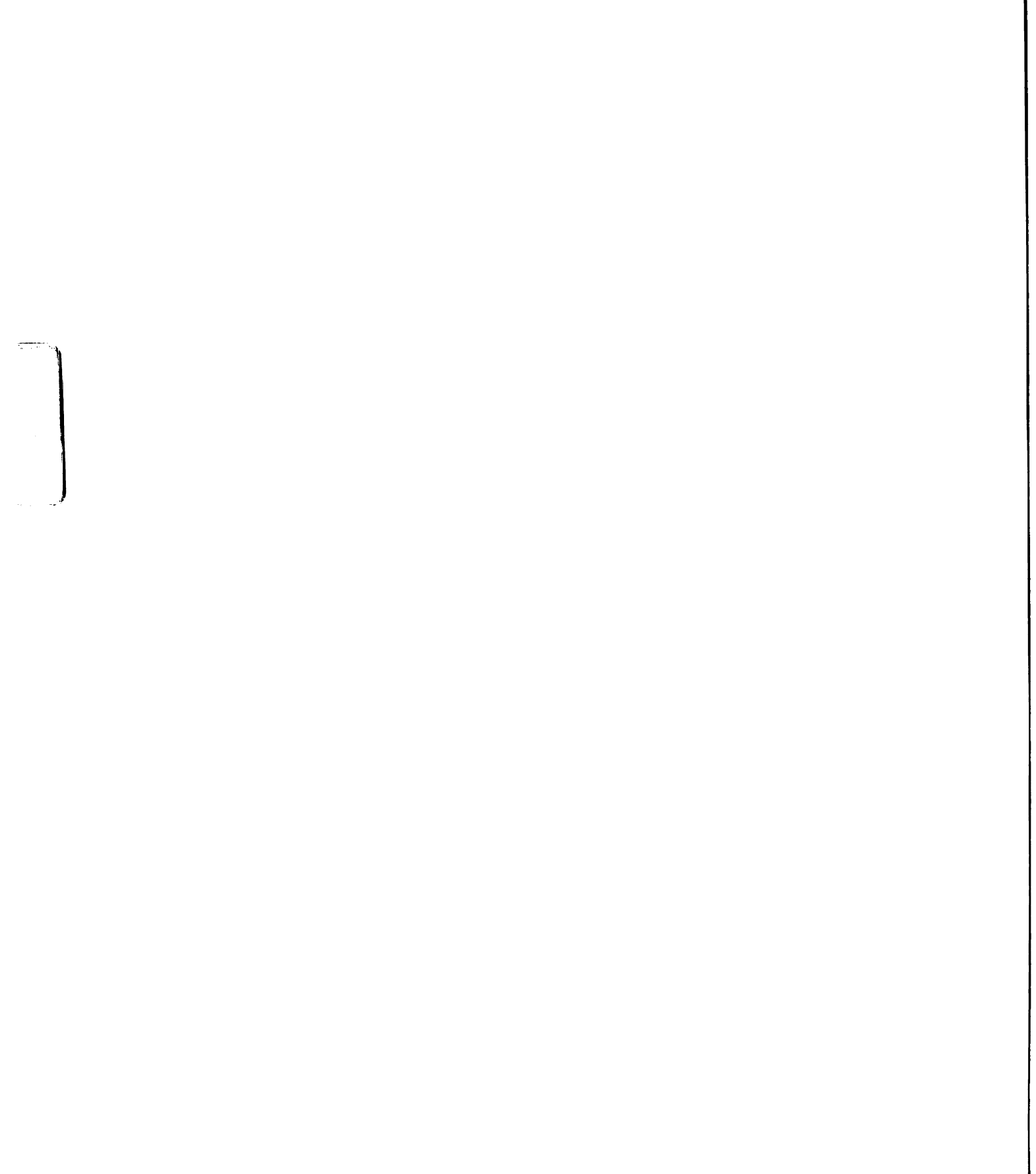


Figure 27 Stress-strain curves for glass-epoxy composites with similar strain rates but different L/D ratios.



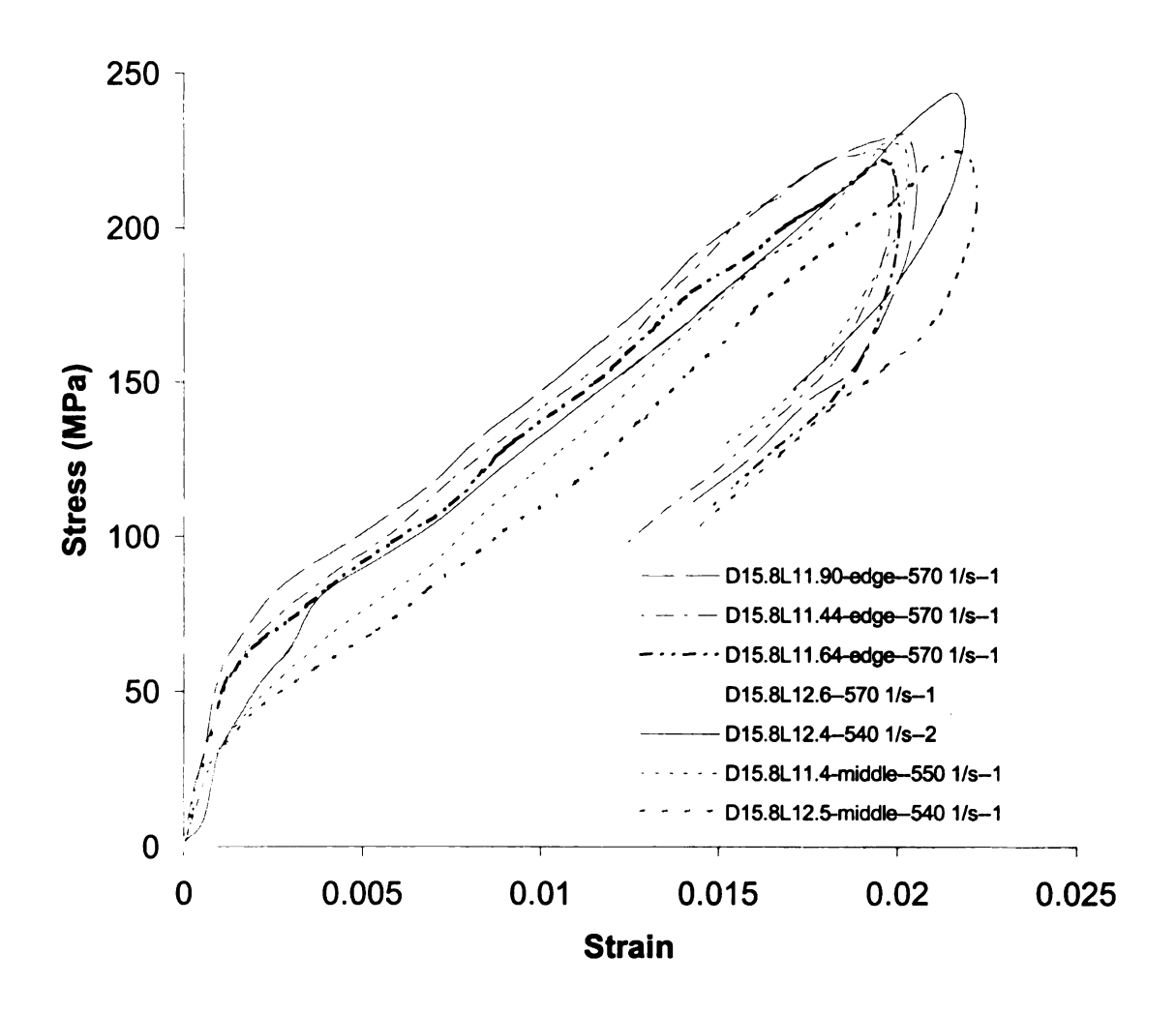


Figure 28 Stress-strain curves for three groups of glass-epoxy composites with similar dimensions and L/D ratio (0.8)

In addition to the stress-strain curves, Young's moduli and yielding points of all cases presented earlier were also carefully examined. The results are shown in Figures 29 and 30. From both figures, Young's modulus and yielding point increase as the strain rate increases. They also increase as the L/D ratio increases.

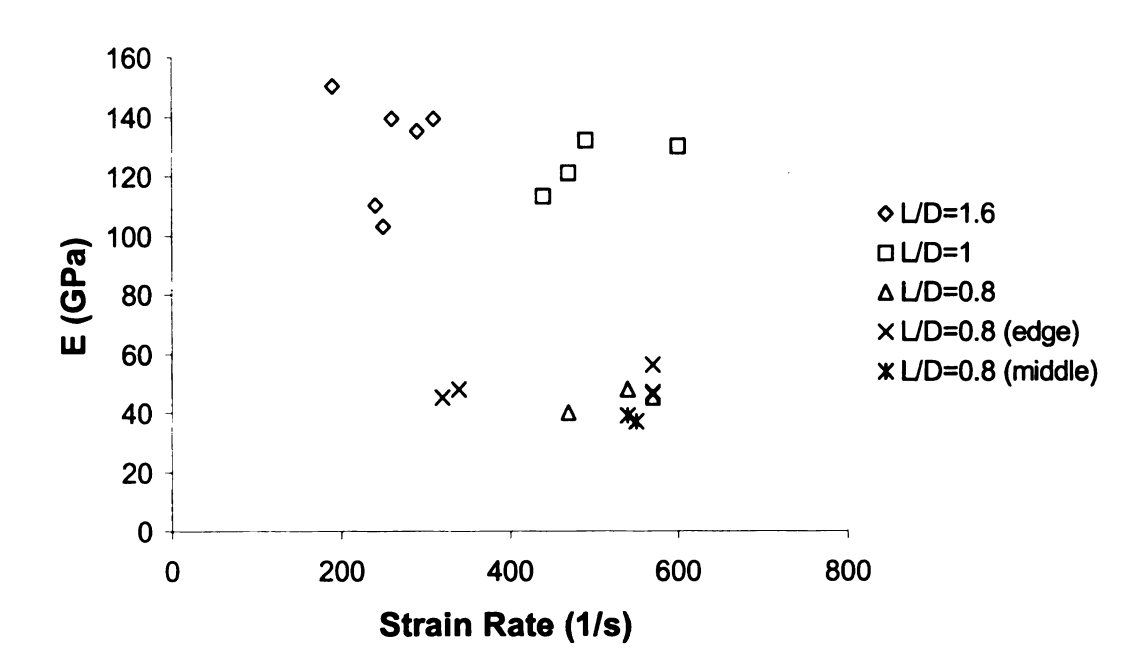


Figure 29 Young's Modulus vs. strain rates at different L/D ratios.

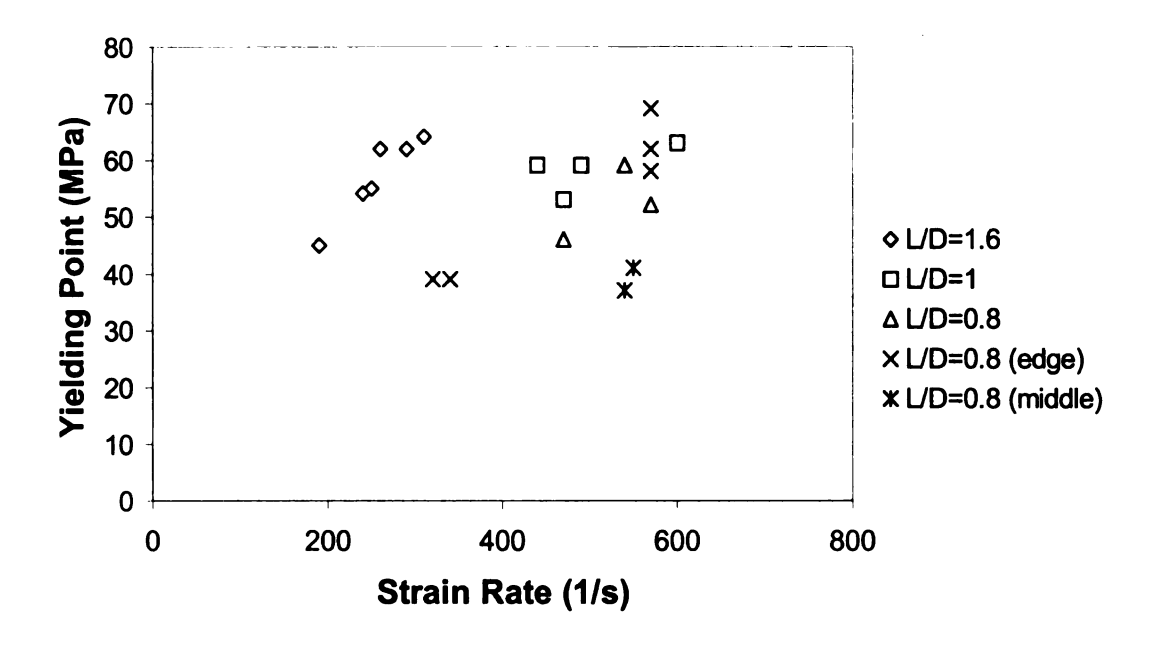


Figure 30 Yielding points vs. strain rates at different L/D ratios.

### **CHAPTER 5**

#### **DISCUSSIONS**

The application of SHPB to material characterization is constrained by the material properties and dimensions of the bars and the specimen. As a general rule, the material properties of the specimen should be softer but not too much softer than those of the bars to warrant relatively equal measurement between the reflection and transmission waves, which is necessary for establishing an accurate stress-strain curve [1, 3]. In addition, from the above studies for laminated composites and the calibration studies for aluminum, it can be found that the dimensions and dimensional ratios of a specimen have strong effects on the stress-strain relations based on SHPB. Hence, they can not be ignored.

#### 1. Dimensions of Bars

### 1.1 Bar Diameter Dbar

SHPB is a one-dimensional wave technique for material characterization. When testing materials are homogeneous, specimens with small diameters will be adequate. Consequently, incident and transmitter bars with small diameters will be sufficient. The determination of the bar diameter will then be dependent on the desired strain rate since it can be increased by reducing the specimen diameter. In contrast, when testing materials are not homogeneous, specimens with large diameters will be required. If the specimen is not uniform, it will not reflect the whole structure when the specimen is very small. Therefore, the bars

for characterizing inhomogeneous materials, such as concretes, usually have a diameter of 3" (75 mm) or greater.

### 1.2 Bar Length Lbar

The first rule to determine the length of the incident and transmitter bars requires that the bars should be long enough to warrant one-dimensional wave propagations. In other words, the transverse inertia should be negligible when compared with the longitudinal counterpart. An aspect ratio, L<sub>bar</sub>/D<sub>bar</sub>, around 10 is usually agreed by researchers [2] as a minimum requirement for a one-dimensional bar.

As the striker bar impacts the incident bar, the wave generated in the latter is usually highly complex due to the nonuniform contact between the striker bar and the incident bar, and the non-longitudinal waves, such as spherical dilatational wave, generated from the impact. Although Saint Venant's principle states that nonuniform contact force can be quickly dampened out in a distance approximately equal to bar diameter into the bars if the bar are made of isotropic materials, the non-longitudinal waves may take 10 times the bar diameter to vanish. Moreover, if electrical-resistance strain gages are to be installed in the bars for wave measurements, the reflection waves from each bar end should be considered in determining the bar length. A bar length more than 20 times the bar diameter (10 times from each bar end) may be required to avoid the overlap of propagation waves with reflection waves.



Although longer bars seem to be excellent for one-dimensional wave measurements and can help to reduce the end effect and transverse effect, they also pose serious challenges on the straightness of the bars. As a bar becomes longer, it sags due to its own weight. The curvature of the bar, accompanied by a low critical buckling load, will have a negative impact on one-dimensional wave propagation.

# 2. Dimensions of Specimens

## 2.1 Specimen Diameter D

The diameter of specimens, D, should always be smaller than the diameter of bars,  $D_{bar}$ , to warrant complete wave propagations into and from the specimens. This is especially true for specimen materials with positive Poisson's ratios. They expand transversely when subjected to longitudinal compression. A  $D/D_{bar}$  ratio around 0.75 is commonly accepted by SHPB researchers [1, 2]. The calibration studies for aluminum specimens in this research have also confirmed that the discrepancy between the input and output force histories increases as the  $D/D_{bar}$  ratio decreases. In other words, the wave patterns seem to be distorted more when the  $D/D_{bar}$  ratio decreases.

# 2.2 Specimen Length L

Many researchers have investigated the effects of the L/D ratio. No definitely idea ratio has been concluded from their studies. The selection of an L/D ratio, however, may be based on the following arguments.

- (1) One of the fundamental assumptions of the SHPB technique is the uniform deformation of the specimen during characterization; however, it is more difficult for a longer specimen to meet the uniformity requirement than a shorter specimen.
- (2) In fact, a longer specimen also suffers lower stability when subjected to compressive loading.
- (3) The stability requirement, however, cannot be satisfied by simply using a very short specimen because of the following considerations: (a) one-dimensional assumption (transverse inertia), (b) Saint Venant's end effect (impact-induced contact), and (c) the frictional effect due to Poisson's effect.

Table 5 shows the suggested L/D ratios from various researchers. Follansbee [2] suggests that the optimum L/D ratio to minimize errors due to inertia is 0.5. ASTM standard E9 specifies that L/D ratio should be from 1.5 to 2.0. Dowling [1] has suggested choosing an L/D ratio of 3 for ductile materials and from 1.5 to 2 for brittle materials. Apparently, there is no conclusive suggestion.

#### 3. Constant Strain Rate

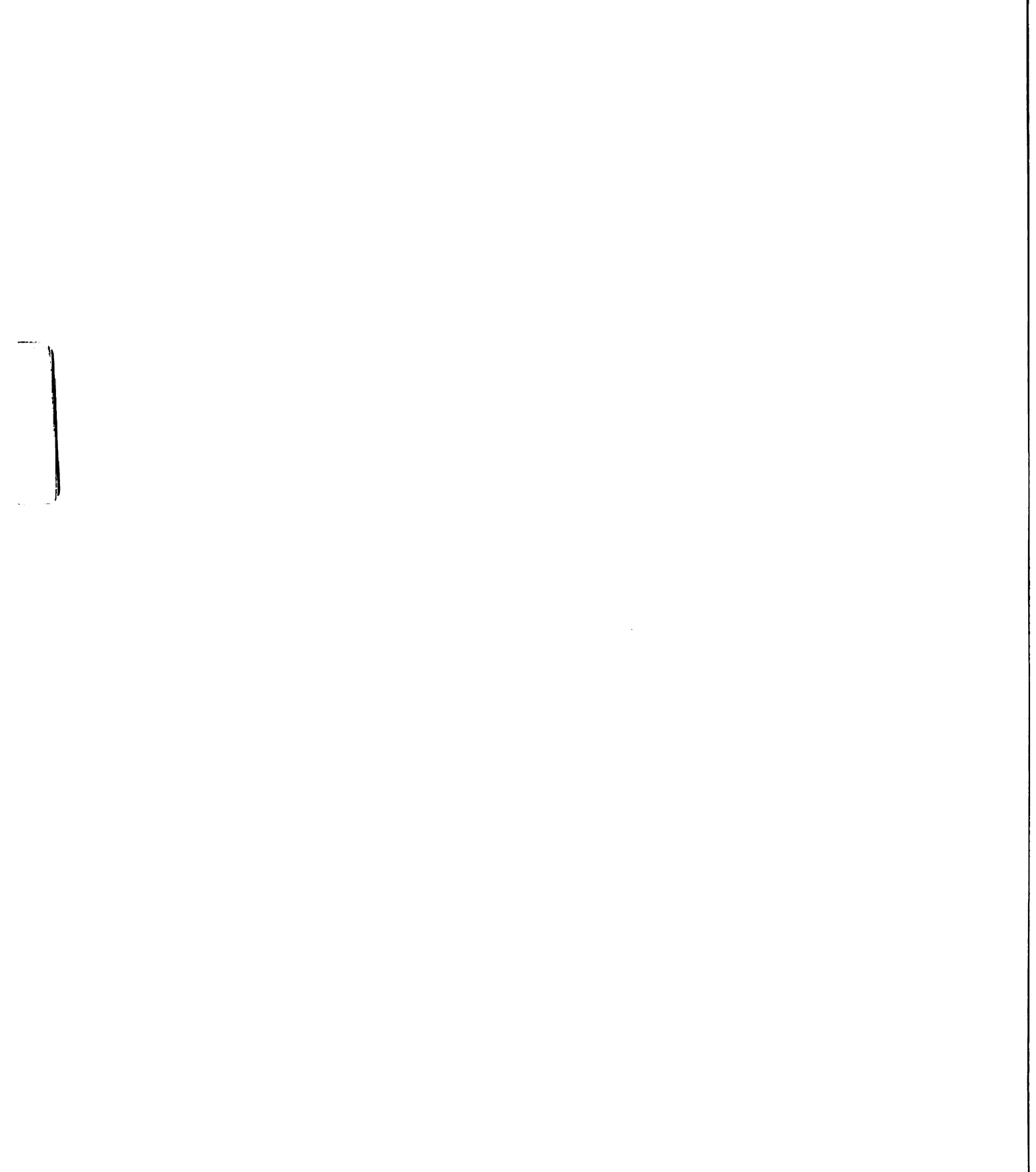
The strain rates based on constant incident strain wave for the calibration and characterization studies are not constant. In order to obtain stress-strain curves based on constant strain rate, a few tests based on various levels of constant incident strain wave were performed. Figure 31 shows the results of stress-strain curves at constant strain rate. The shapes of the stress-strain curves are also similar to those based on constant incident strain waves.

Table 5 Parameters of SHPB and L/D of specimen used by various researchers.

Owner	Hopkinson bars					I /D of	
		Diameter (mm)	Length (mm)			L/D of	Dof
	Material		Striker Bar	Incident Bar	Transmitter Bar	Specimen	Ref.
I.M. Daniel	17-4PH stainless steel	12.7	76~152	914	914	1.5	[9]
O. Sawas N. S. Brar	Cast Acrylic	25.4	890	2500	2500		[10]
Michael Kaiser	MIL-S- 46850D	19		1524	1524	1	[1]
W. Chen	VM350 Steel	12.7	152	2130	915		[7]
C.T. Sun	Hardened steel bars	12.7	100	760	550		[4]
Paul S. Follansbee	SAE-340 maraging steel	9.2		1220	1220	0.5	[2]

----: No data found

Ref.: See the Reference section



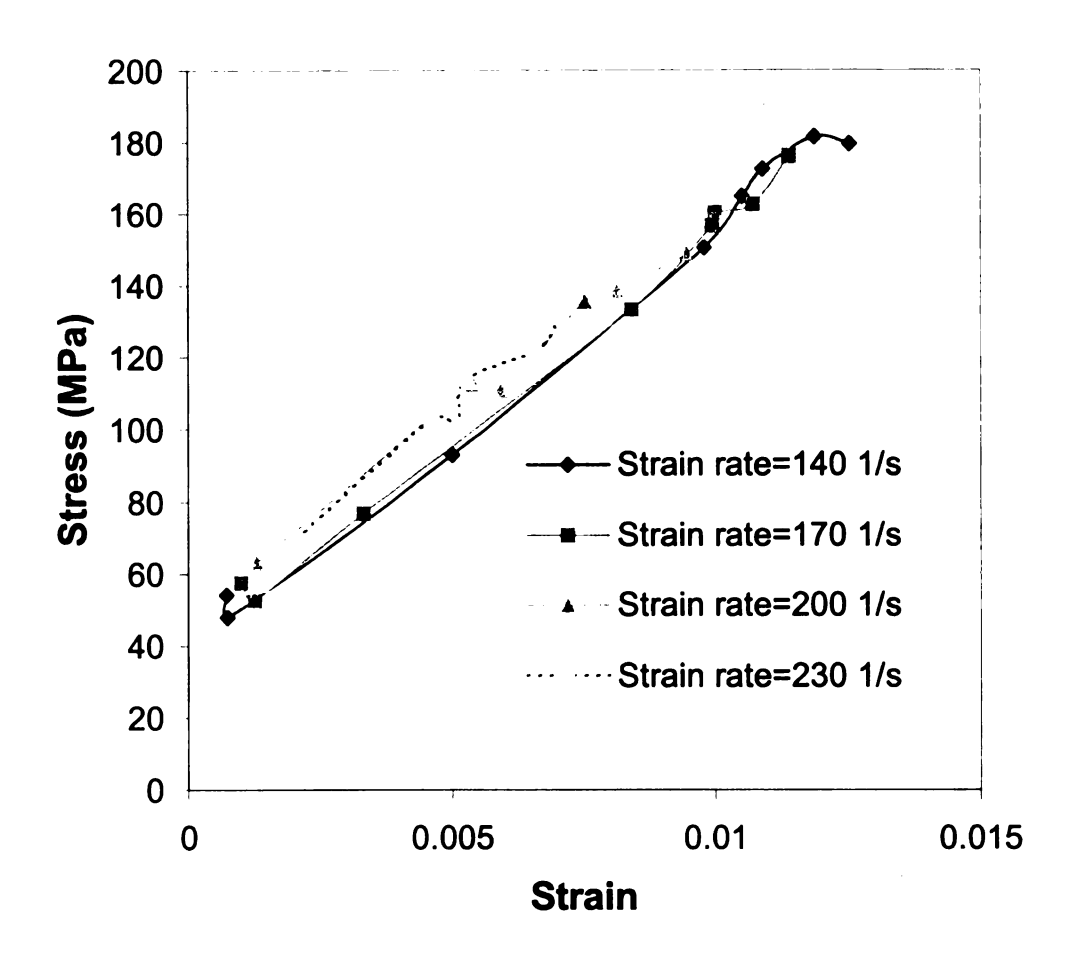


Figure 31 Stress-strain curves at constant strain rates for the composte specimens with D=15.8 mm, L=25.4 mm. (based on various levels of constant incident strain wave tests)

#### **CHAPTER 6**

### **CONCLUSIONS AND RECOMMENDATIONS**

#### 1. Conclusions

Some conclusions concerning the calibraiton of the SHPB and the characterizations for aluminum and thick laminated composites can be drawn as follows:

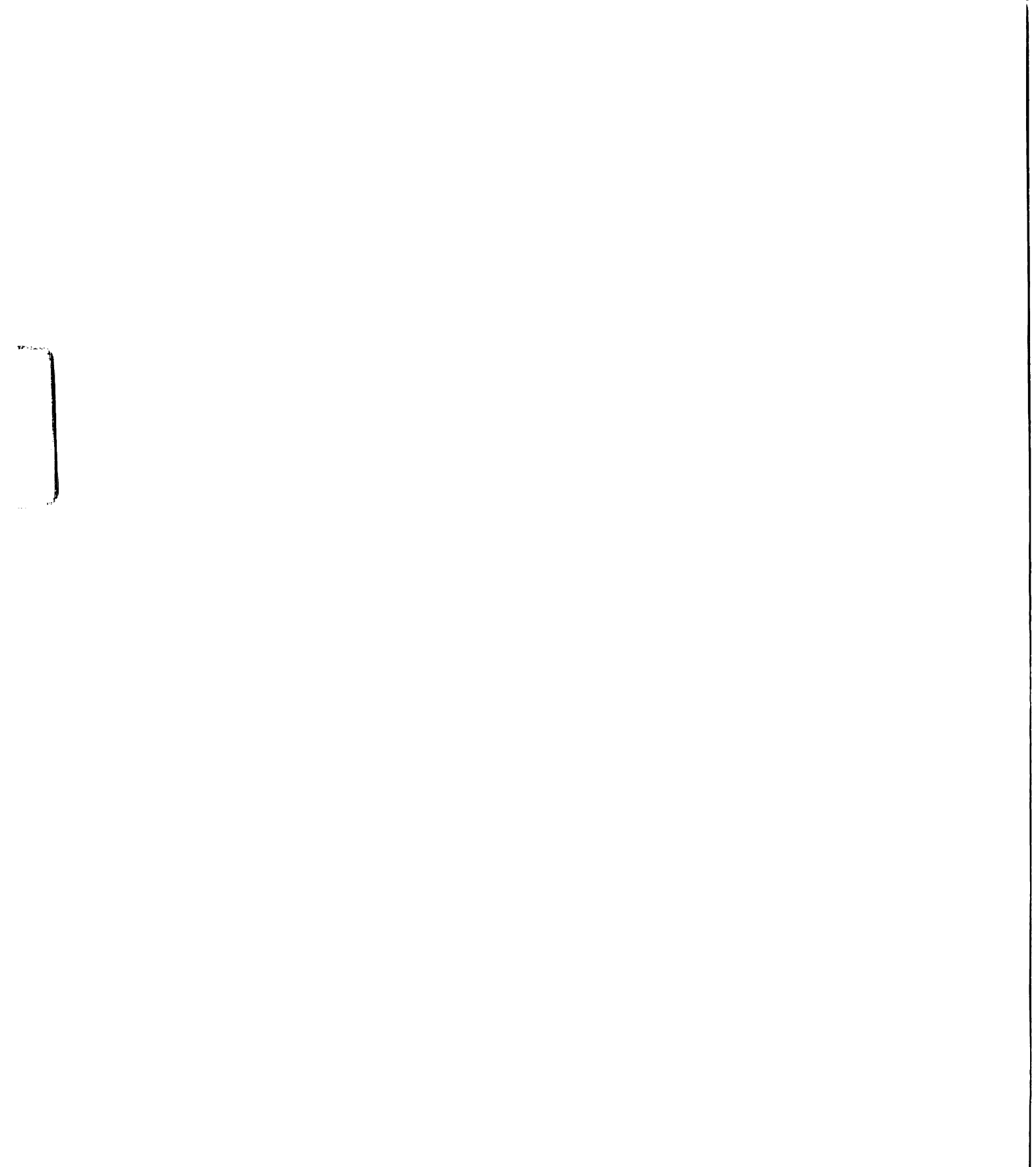
- A. Results from the calibrations for amplifiers and Wheatstone bridge circuits seem to indicate that the electronic components of the SHPB perform as accurate as expected.
- B. Results from the calibration for 6061-T6 aluminum seem to be reasonable when compared with the existing results, such as those obtained by Chen [5]. The accuracy of the SHPB is then verified.
- C. Under constant strains, the stresses in the stress-strain curves rise as the strain rates rise in all cases.
- D. The dimensions and dimensional ratios of specimens seem to affect the stress-strain relations significantly.
- E. There is a noticeable difference between specimens prepared from the surface of thick laminated composites and those from the center of thick laminated composites, implying the nonuniformity of the thick laminated composites.
- F. The difference due to material differences from the same composite is not as significant as that due to geometrical difference.

#### 2. Recommendations

A wave-shaping technique may be required for future studies based on the following discussion.

A. A Split Hopkinson Pressure Bar (SHPB) is a material testing device. Instead of applying quasi-static forces to specimens, an SHPB can apply dynamic waves to specimens for characterizations of dynamic properties. When the impact between the striker bar and the incident bar takes place, a constant strain wave will be generated on the impact surface. Although high strain rates are usually desired in dynamic material characterizations, they may cause damage or yielding to the part of specimen close to the impact surface and result in nonuniform deformation in the specimen and violate the fundamental assumption of SHPB. Hence, a wave-shaping technique to provide non-constant strain waves with a moderate rise in the beginning of the wave pattern is desired.

B. It is true that a high rise in the incident strain gives a high strain rate. However, the incident strain is only an input wave. What really occurs in the specimen is dependent on the material properties and can be represented by the reflection wave. In this thesis study, nearly-constant strain waves were used in the tests. However, the strain rates during the tests did not remain constant. Although a postprocessing technique may be used to convert the stress-strain curves for non-constant strain rates into those for constant strain rates, the microscopic behavior of the materials under non-constant strain rates is believed



to be different from that under constant strain rate. Hence, a wave-shaping technique may be desired.

Since the specimen dimensions and dimensional ratios have great effects on the stress-strain curves, a more comprehensive study on ideal specimen dimensions and dimensional ratios should be performed. **APPENDICES** 

### **APPENDIX A**

# **OTHER FIGURES AND WAVE SIGNALS**

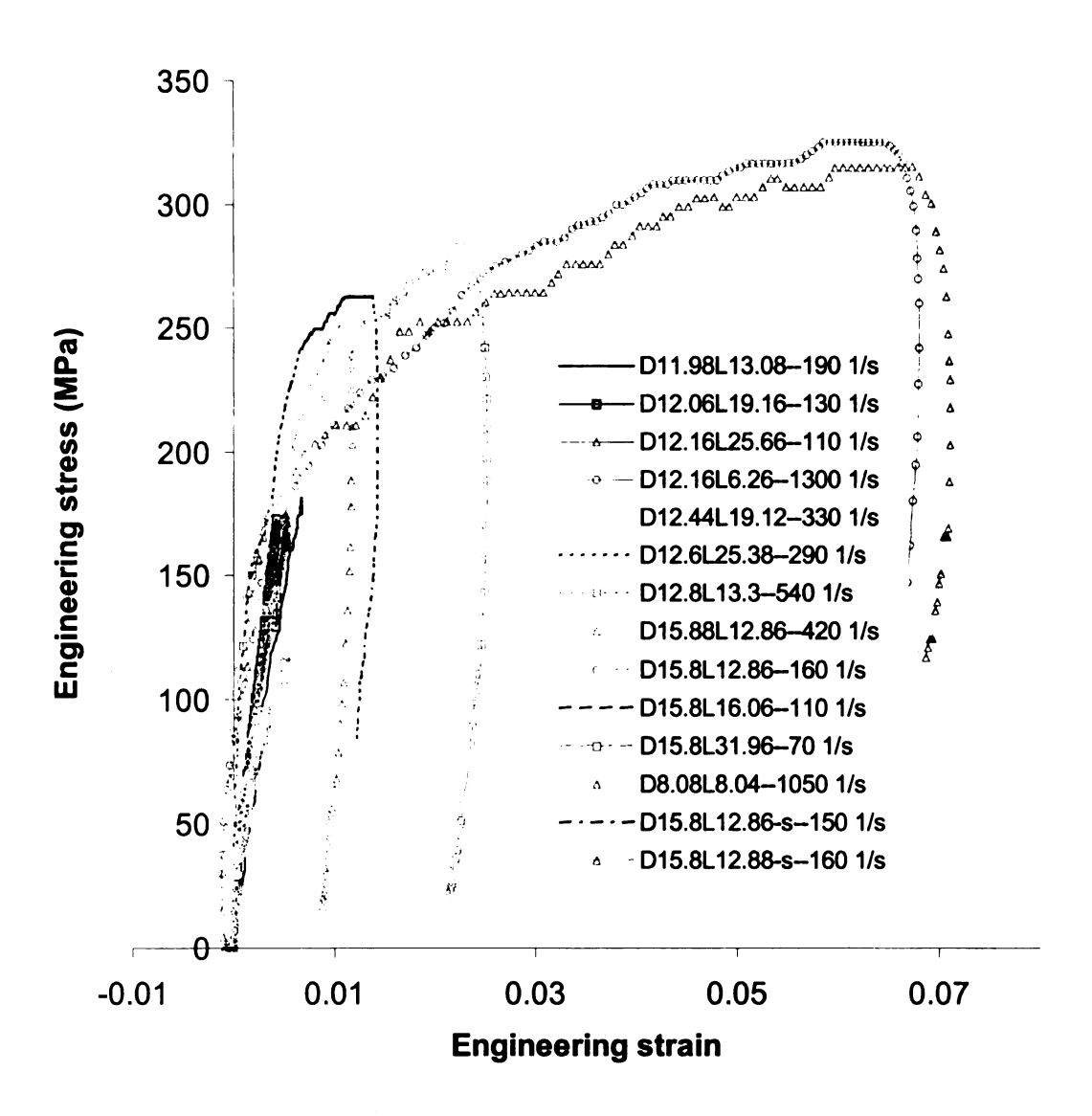


Figure A-1 Other stress-strain curves of aluminum 6061-T6 with different strain rates.

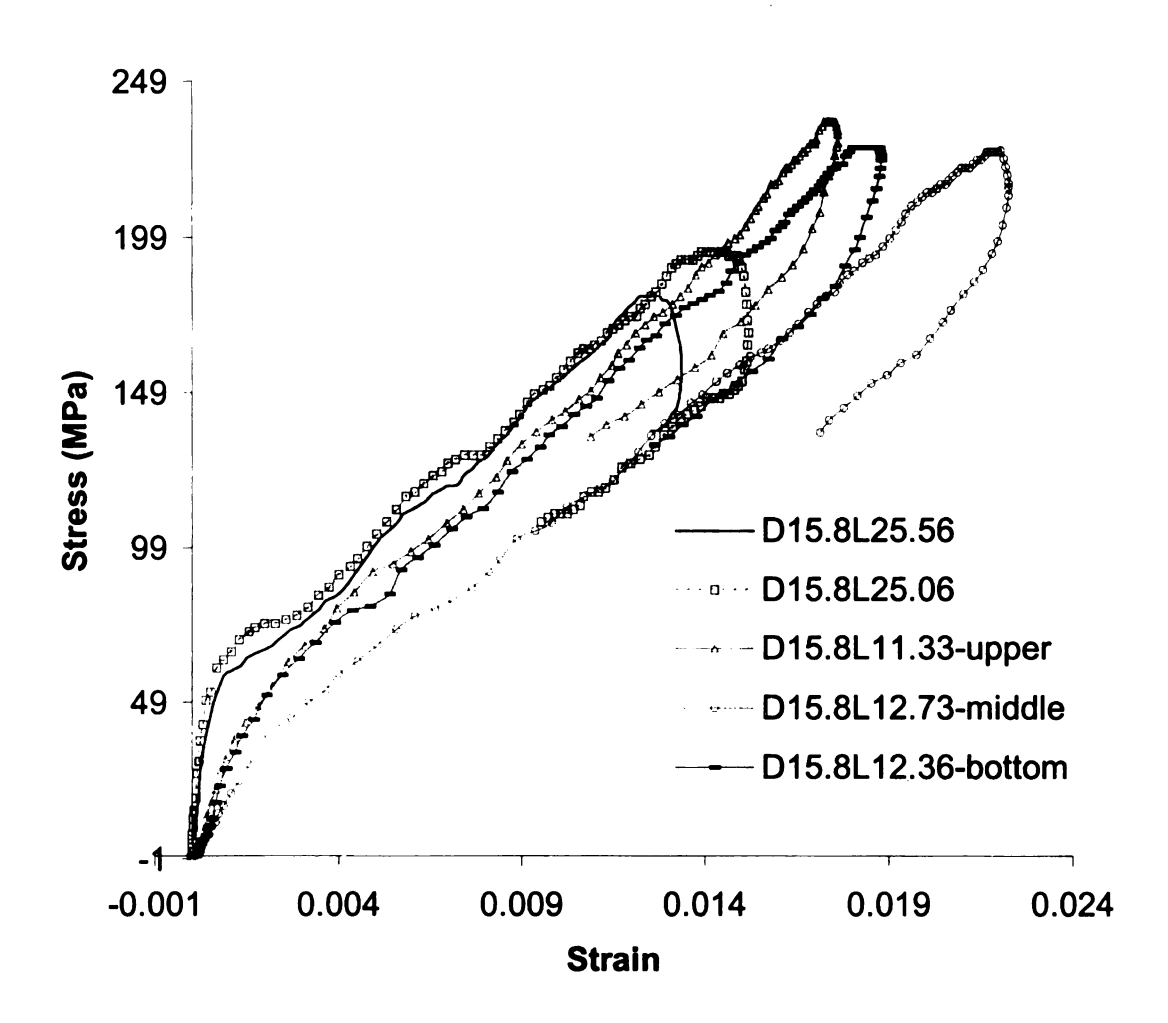


Figure A-2 Stress-strain curves of glass-epoxy composite specimens cutting from the same plate.

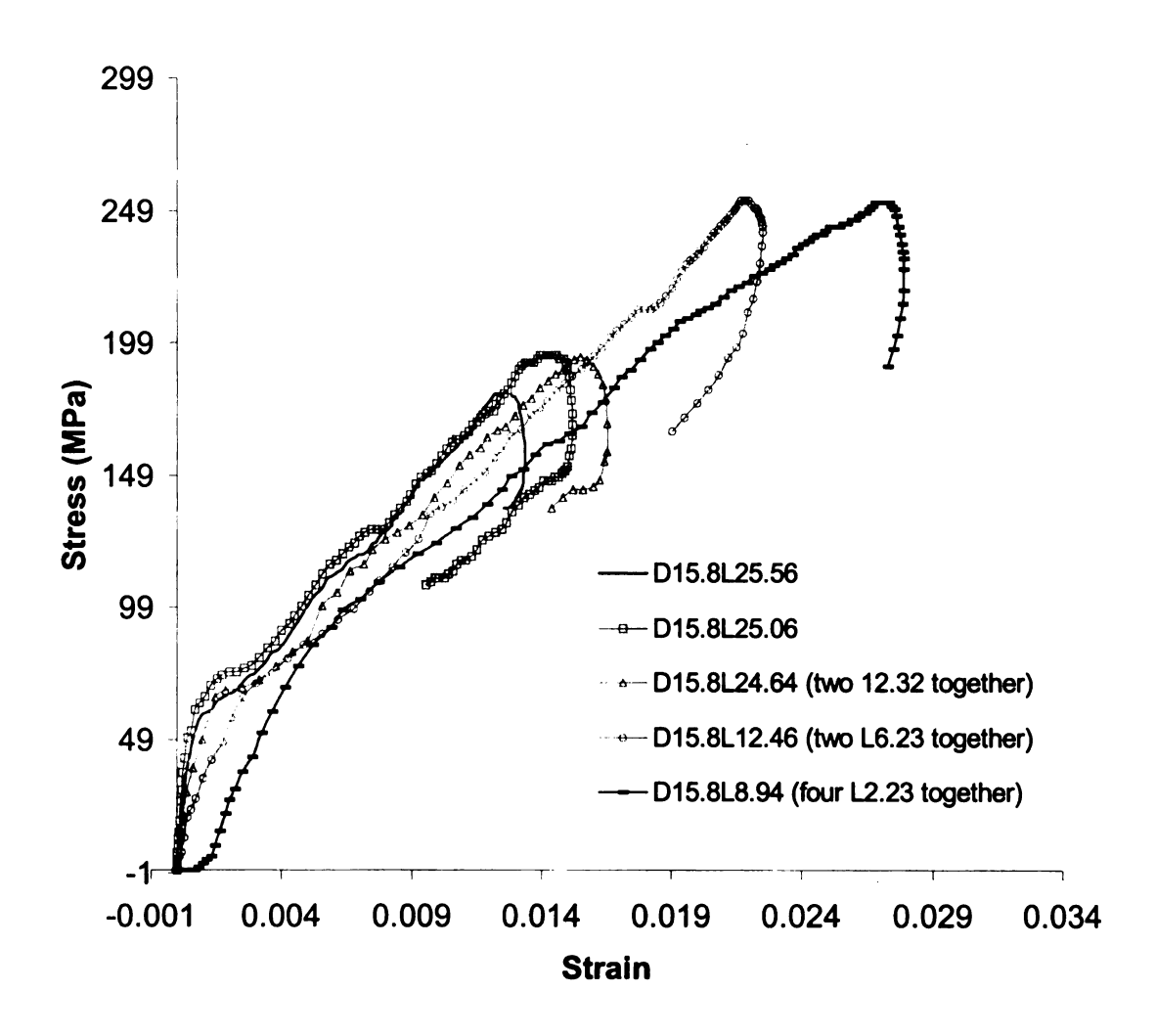


Figure A-3 Stress-strain curves of assembled glass-epoxy composite with different layers.

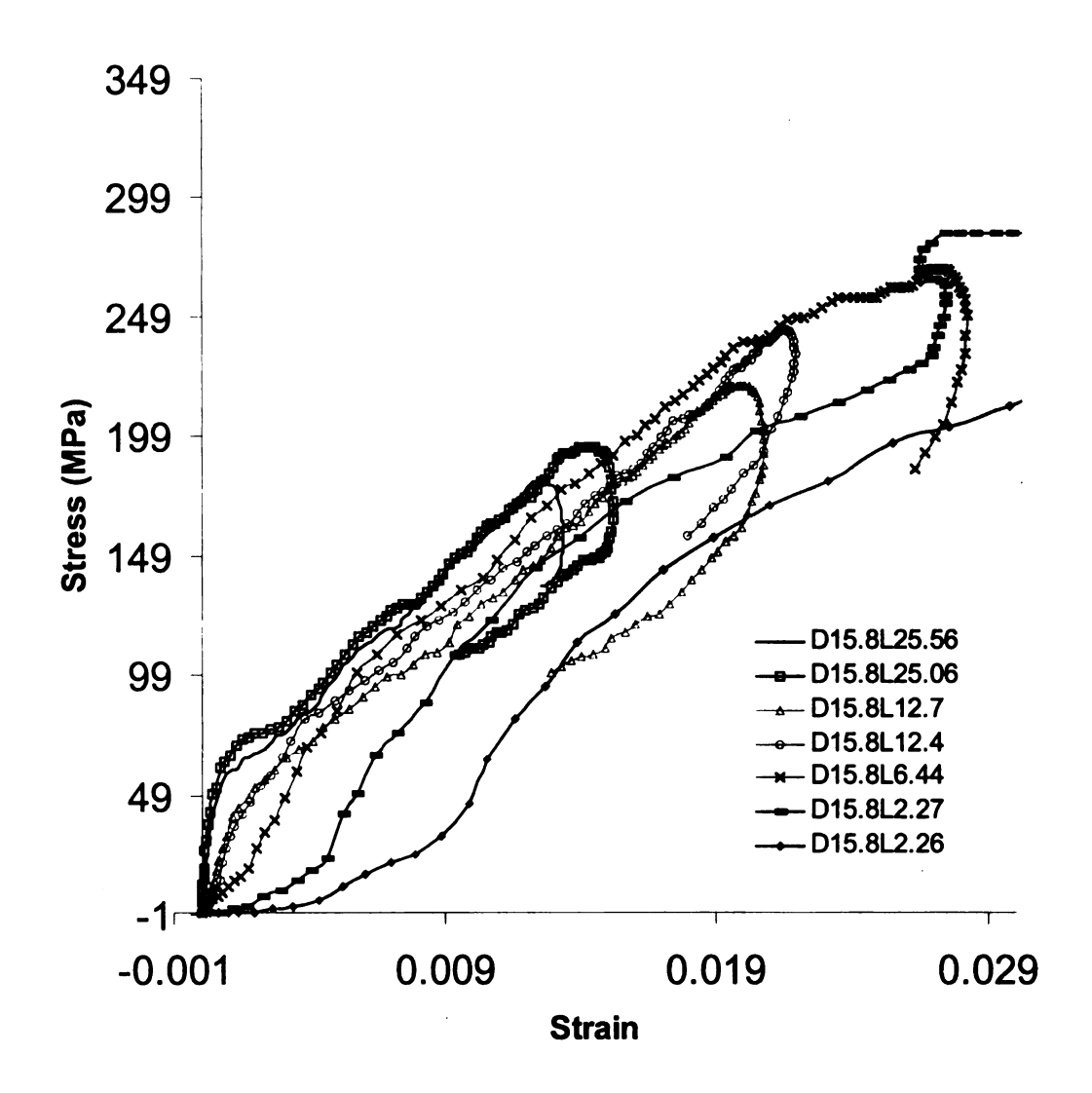
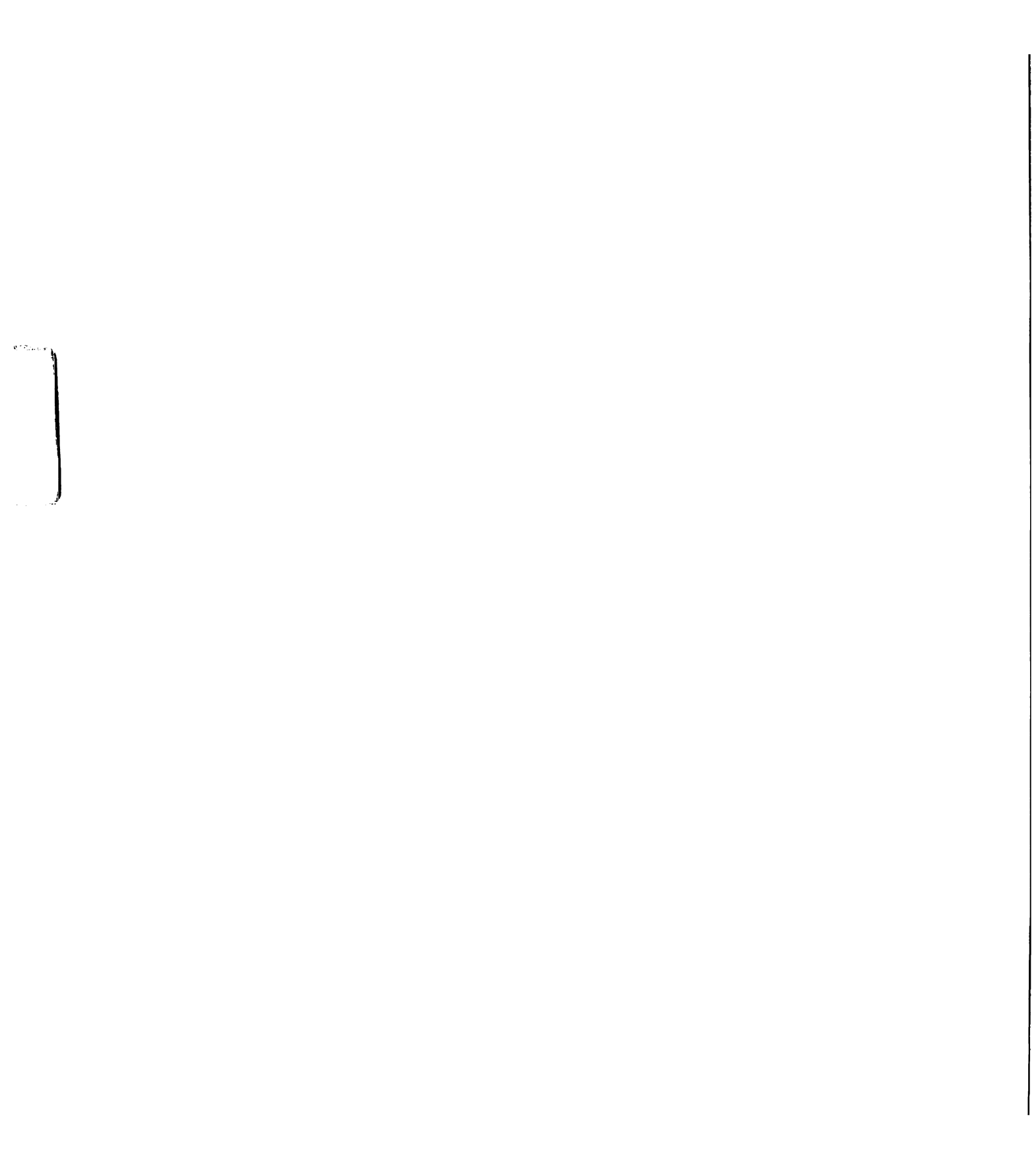


Figure A-4 Stress-strain curves of glass-epoxy composite with different L/D ratios.



The wave speed in the bars are calculated by:

$$\nu = 2\ell / T$$

 $\ell$  : the length of the bar.

T: the period of the waves, calculated by the way showed below.

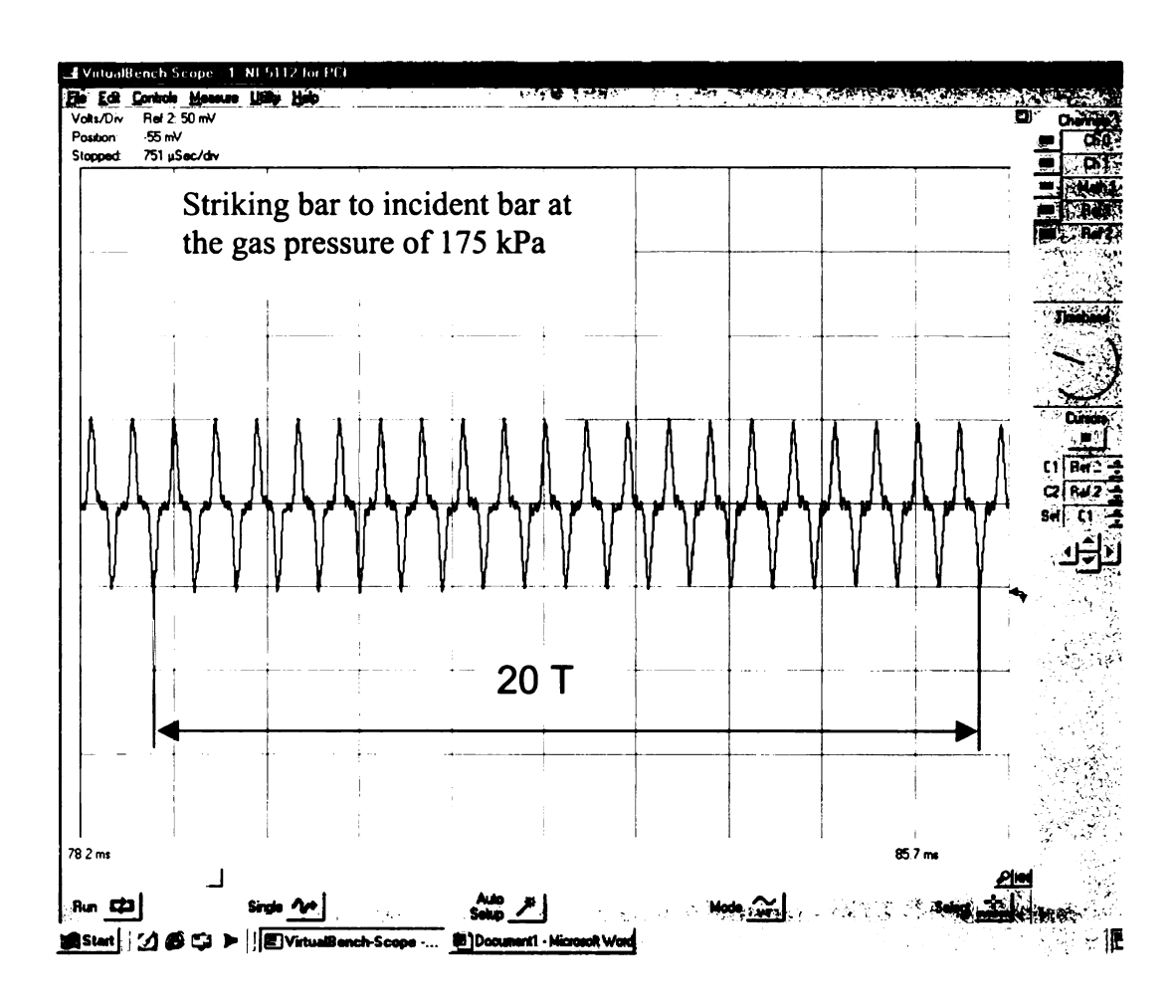
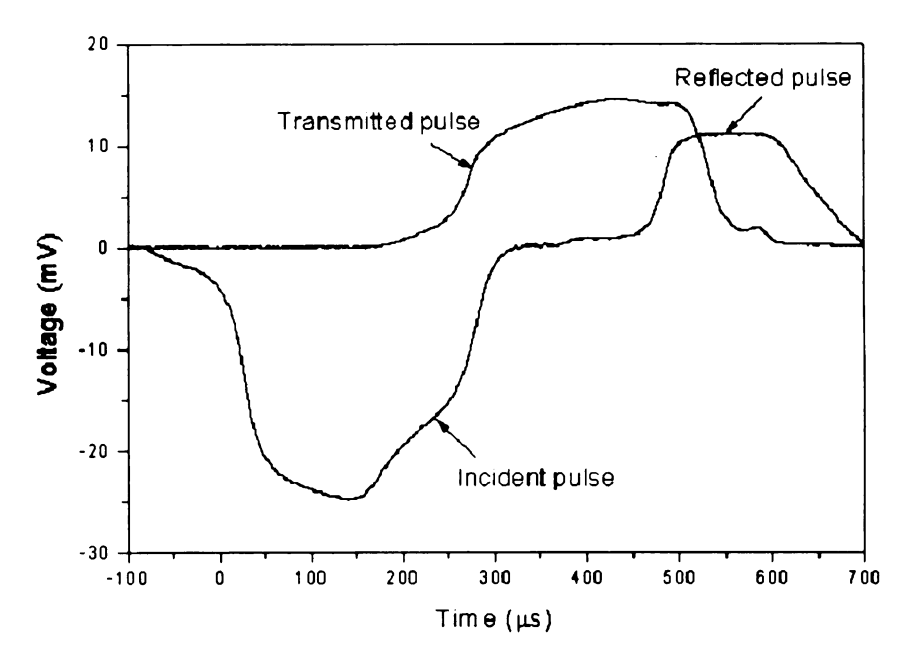
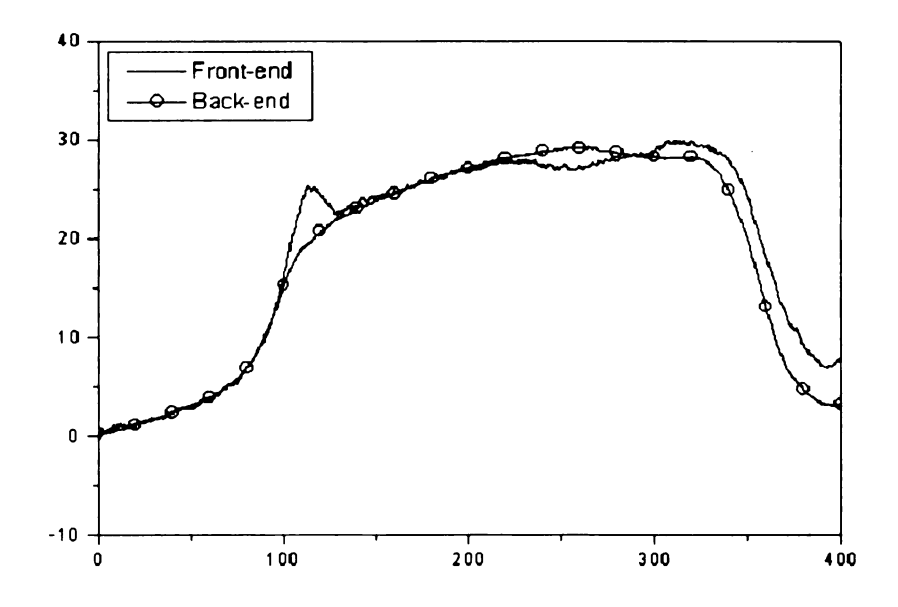


Figure A-5 Calculation of wave speed in bars.



Incident pulse, reflected pulse and transmitted pulse for Aluminum 6061-T6.



Comparison of force at front-end and back-end of Aluminum 6061-T6 specimen.

Figure A-6 Wave shapes and forces comparison of Aluminum 6061-Y6 with shaping technique. (from Dr. W. Chen [5]).

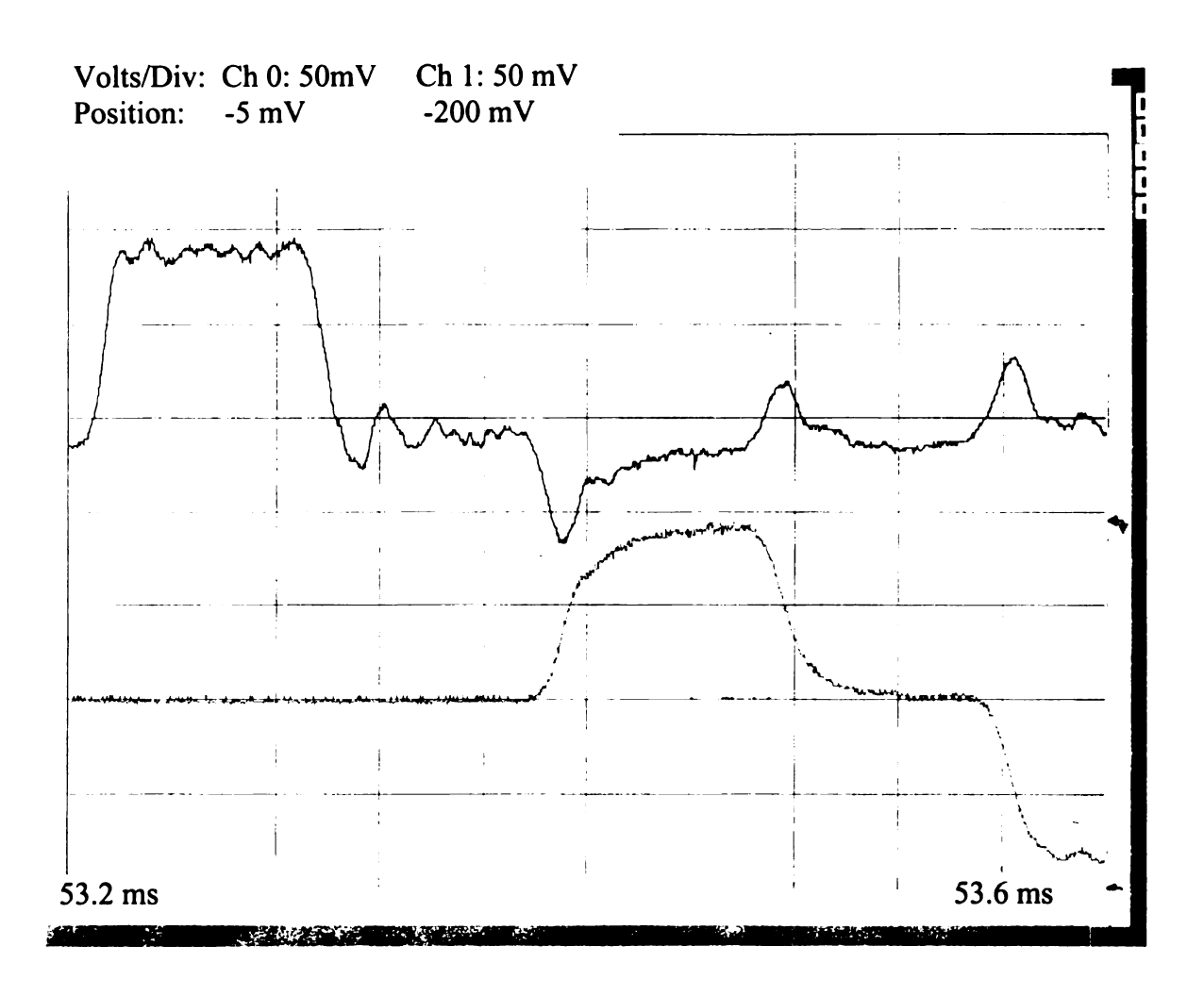
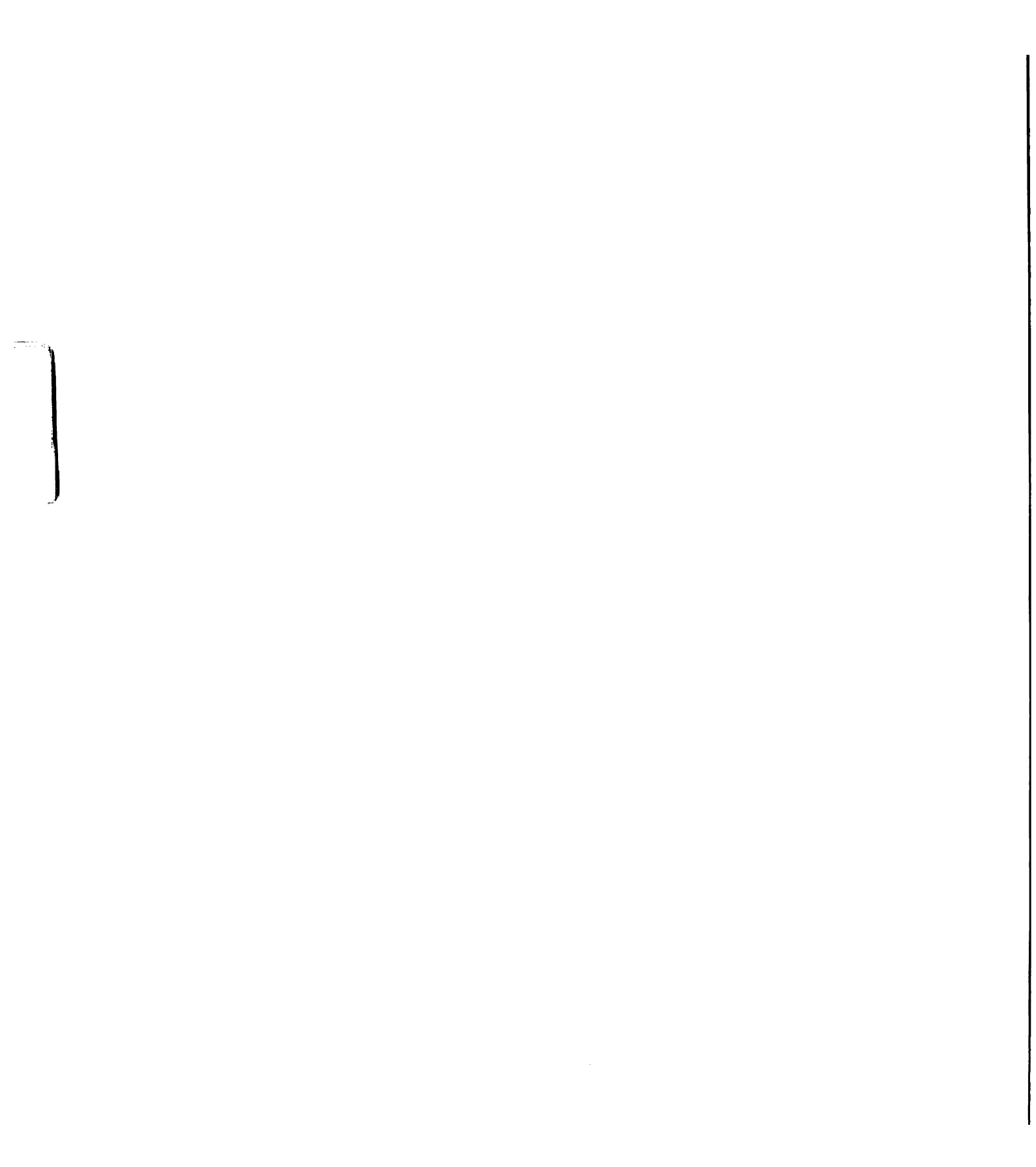


Figure A-7 Incident, reflected and transmitted waves for the aluminum 6061-T6 specimen with D15.88 L12.86.



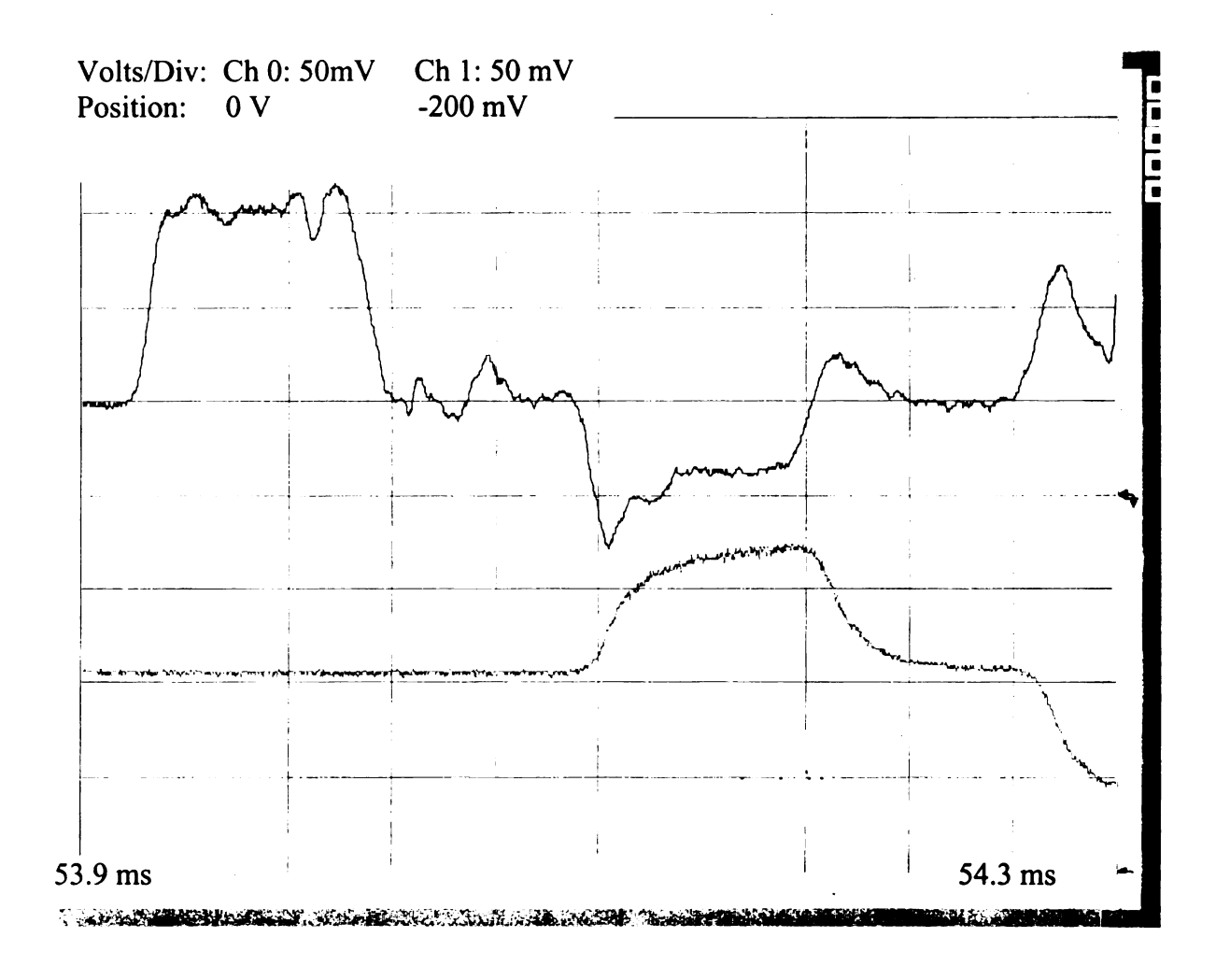


Figure A-8 Incident, reflected and transmitted waves for the aluminum 6061-T6 specimen with D12.8 L13.3.

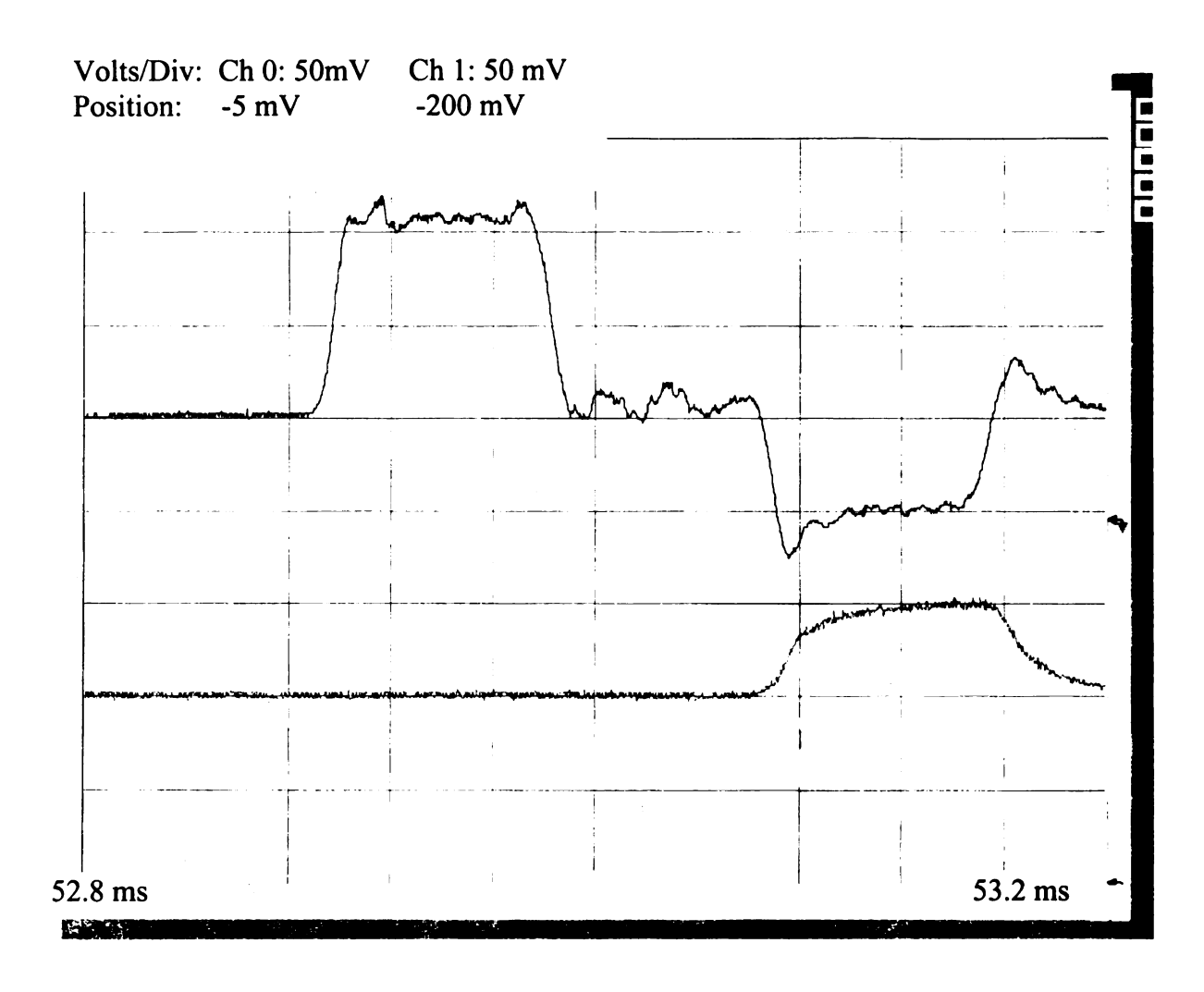


Figure A-9 Incident, reflected and transmitted waves for the aluminum 6061-T6 specimen with D10.68 L10.4.

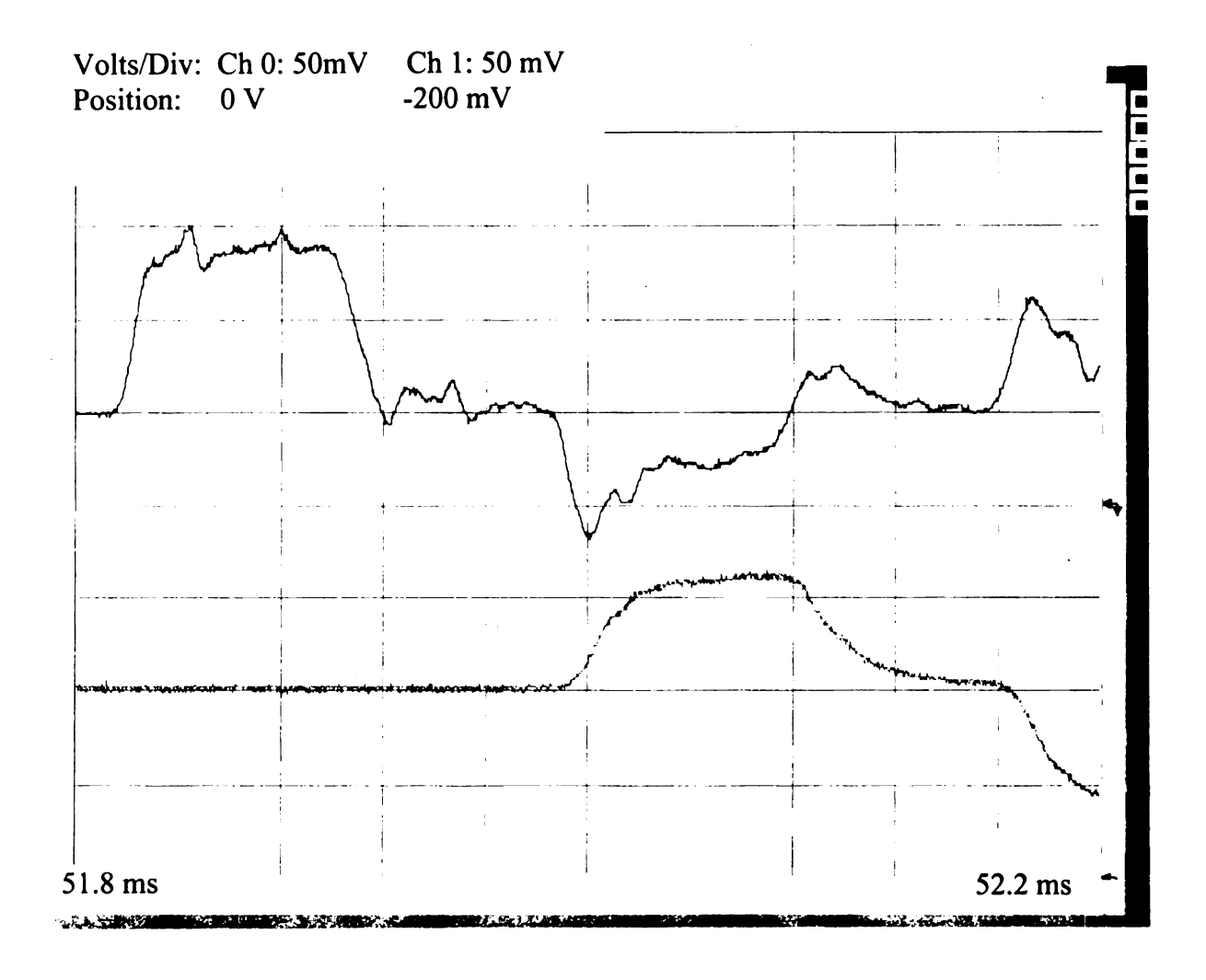


Figure A-10 Incident, reflected and transmitted waves for the aluminum 6061-T6 specimen with D12.44 L19.12.

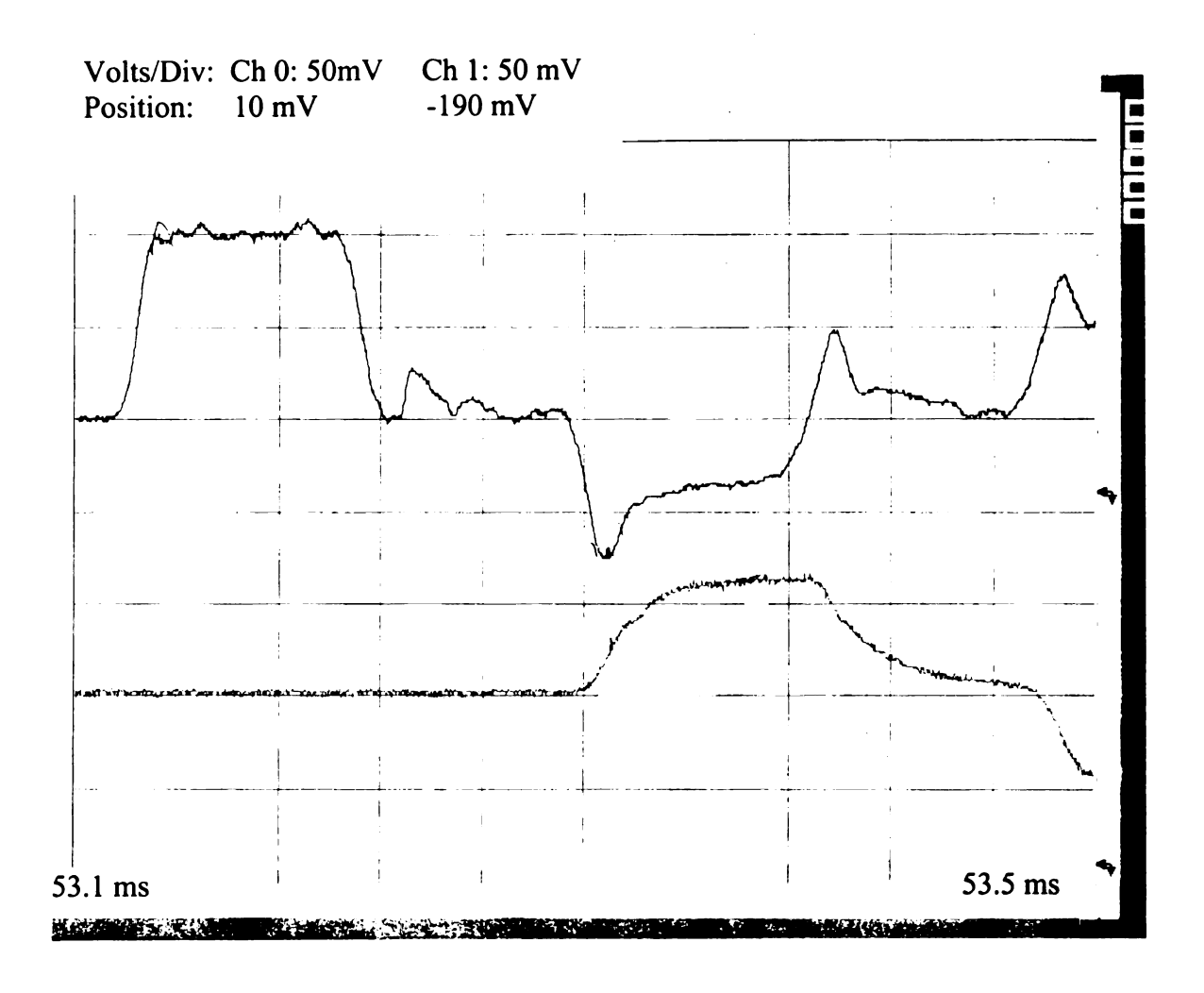


Figure A-11 Incident, reflected and transmitted waves for the aluminum 6061-T6 specimen with D12.6 L25.38.

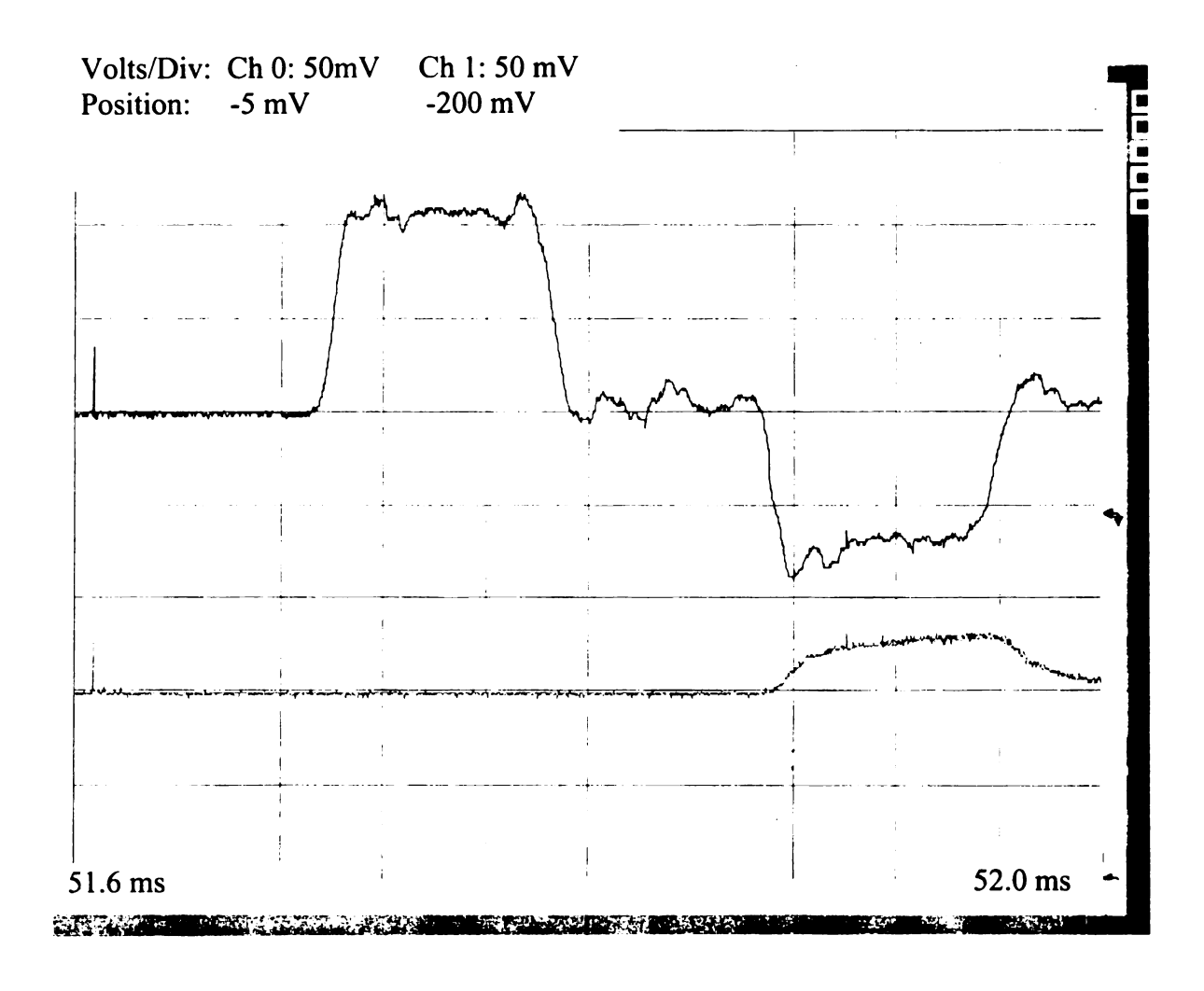


Figure A-12 Incident, reflected and transmitted waves for the aluminum 6061-T6 specimen with D8.08 L8.04.

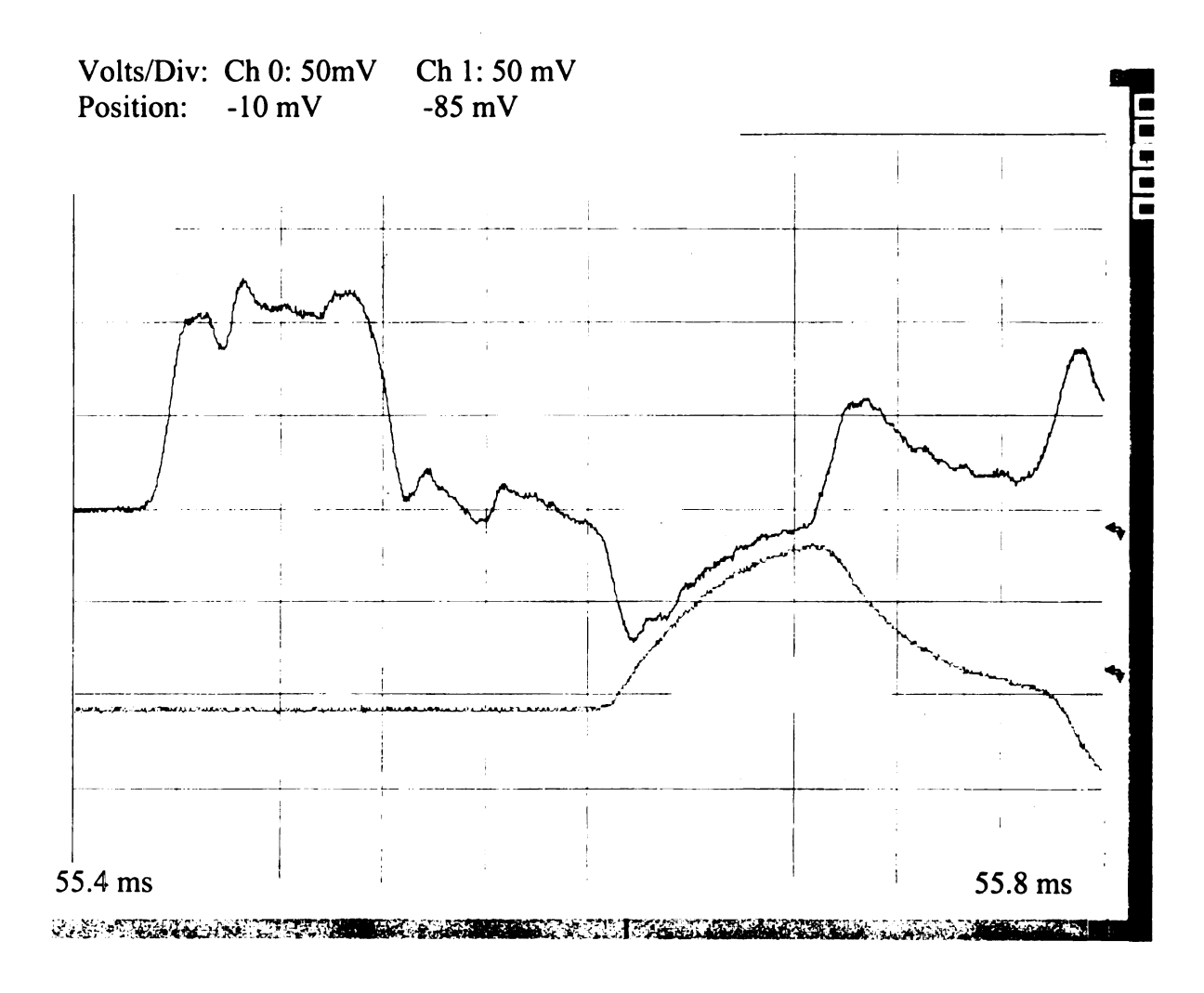


Figure A-13 Incident, reflected and transmitted waves for the glass-epoxy composite specimen with D15.8 L12.4.

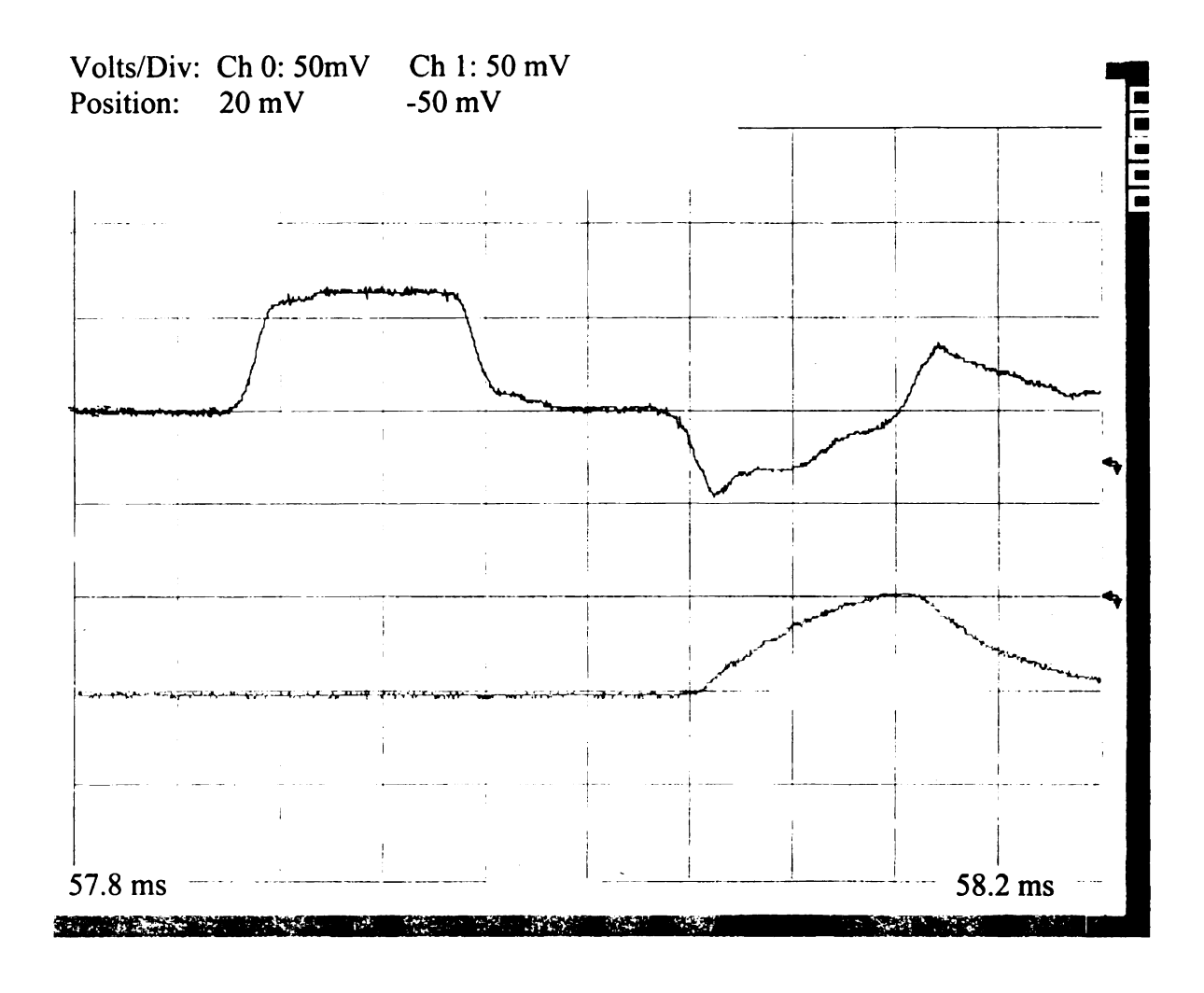


Figure A-14 Incident, reflected and transmitted waves for the glass-epoxy composite specimen with D15.8 L12.96-edge.

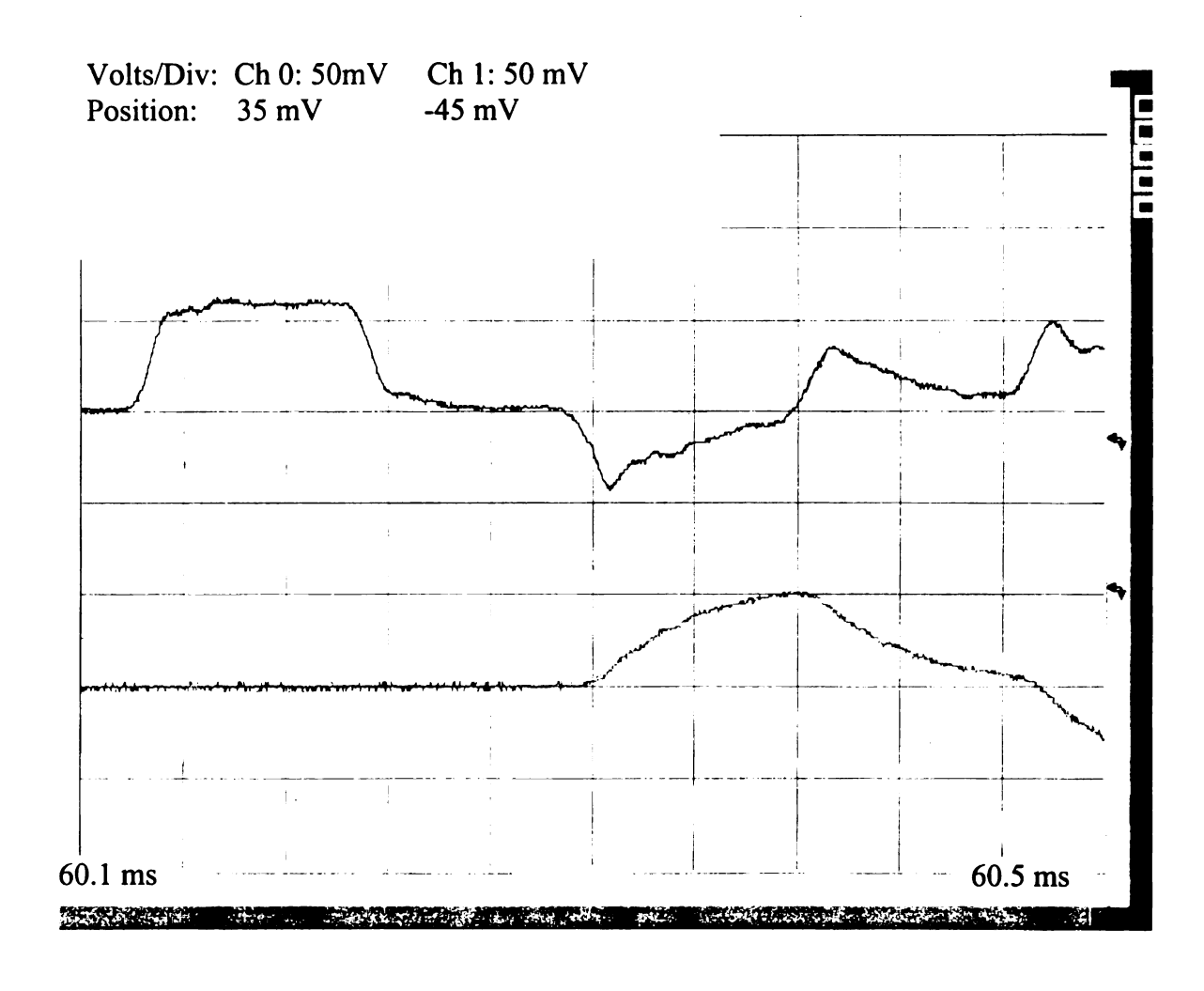


Figure A-15 Incident, reflected and transmitted waves for the glass-epoxy composite specimen with D15.8 L12.94-edge.

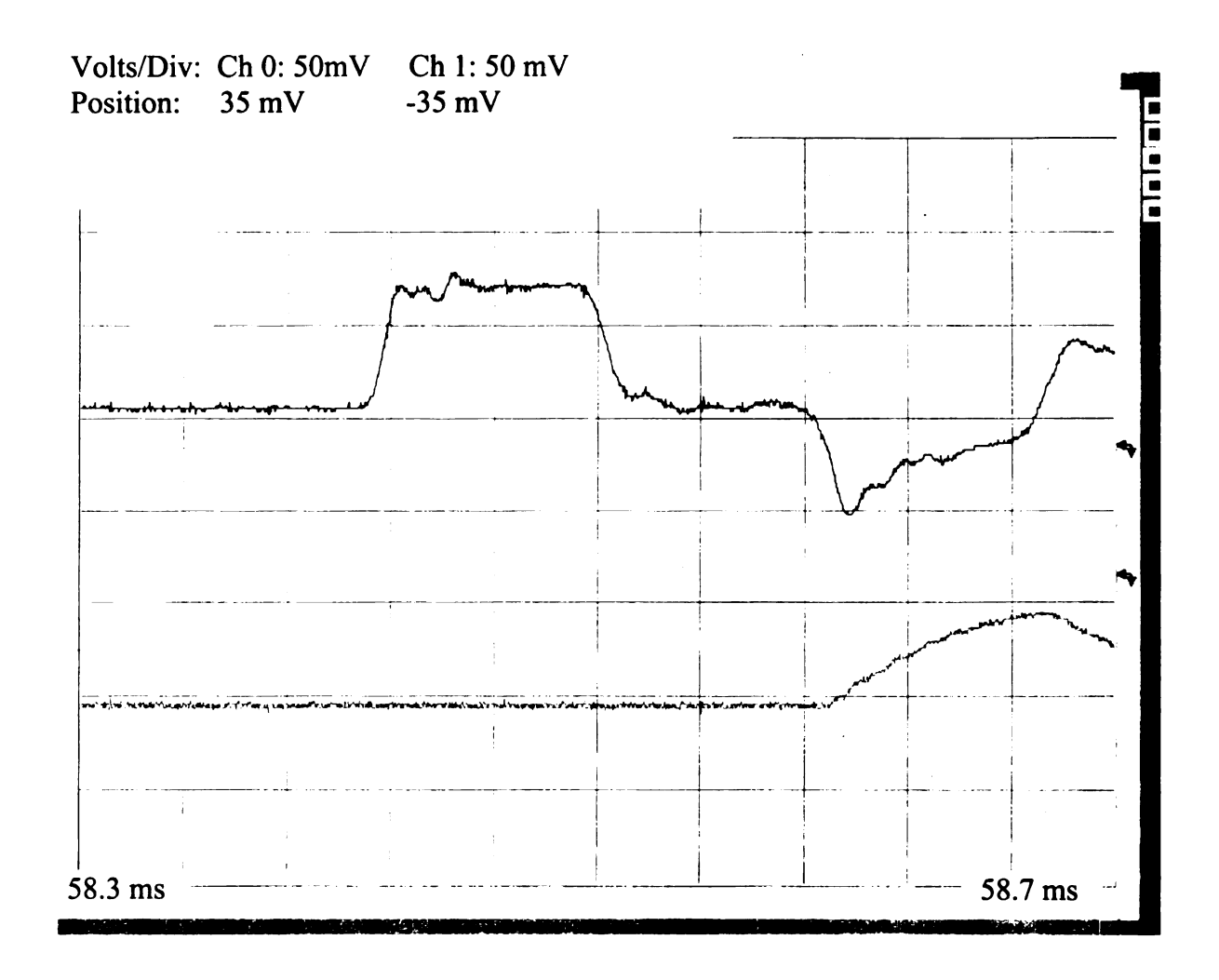


Figure A-16 Incident, reflected and transmitted waves for the glass-epoxy composite specimen with D12.3 L12.76.

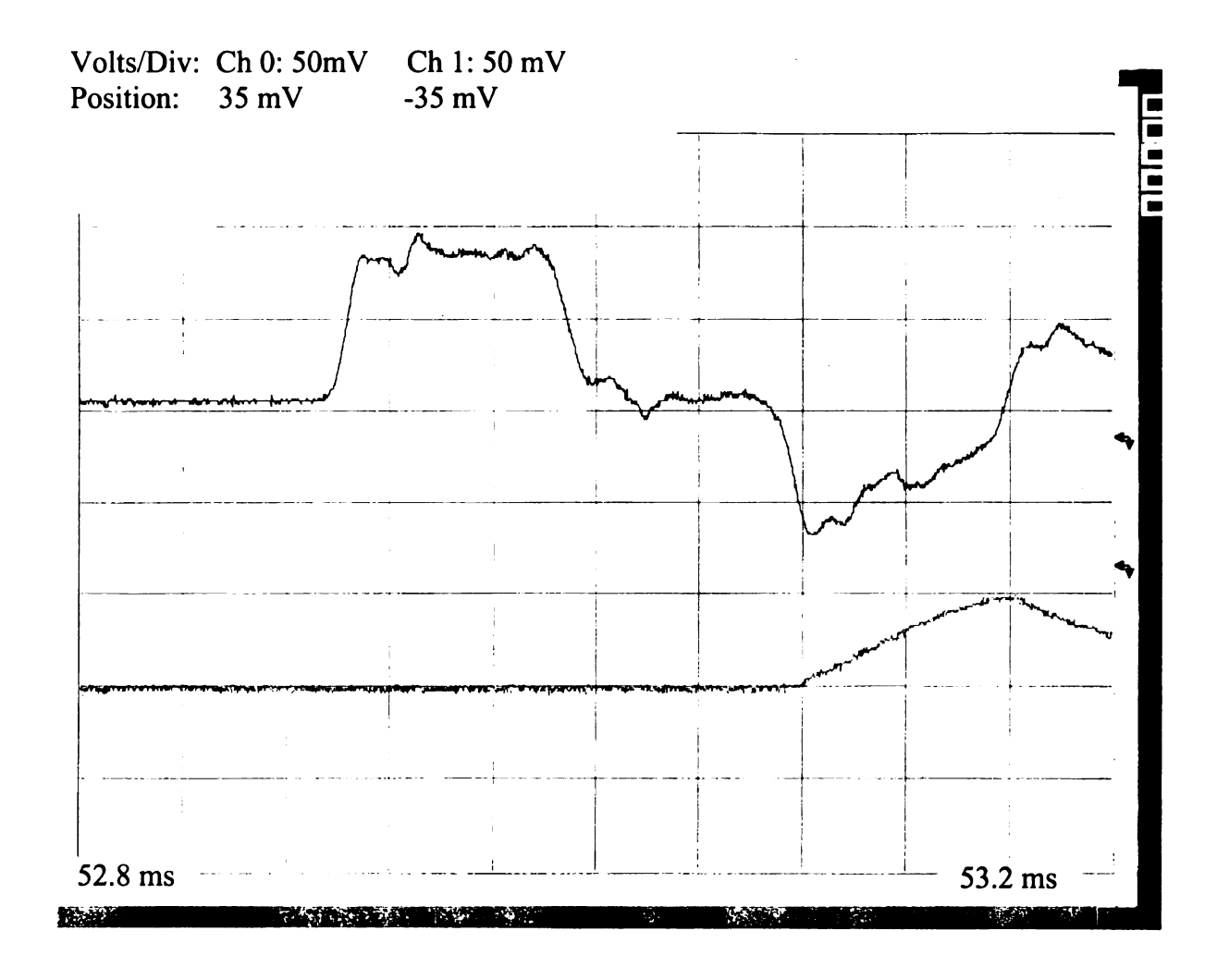


Figure A-17 Incident, reflected and transmitted waves for the glass-epoxy composite specimen with D10.84 L12.14.

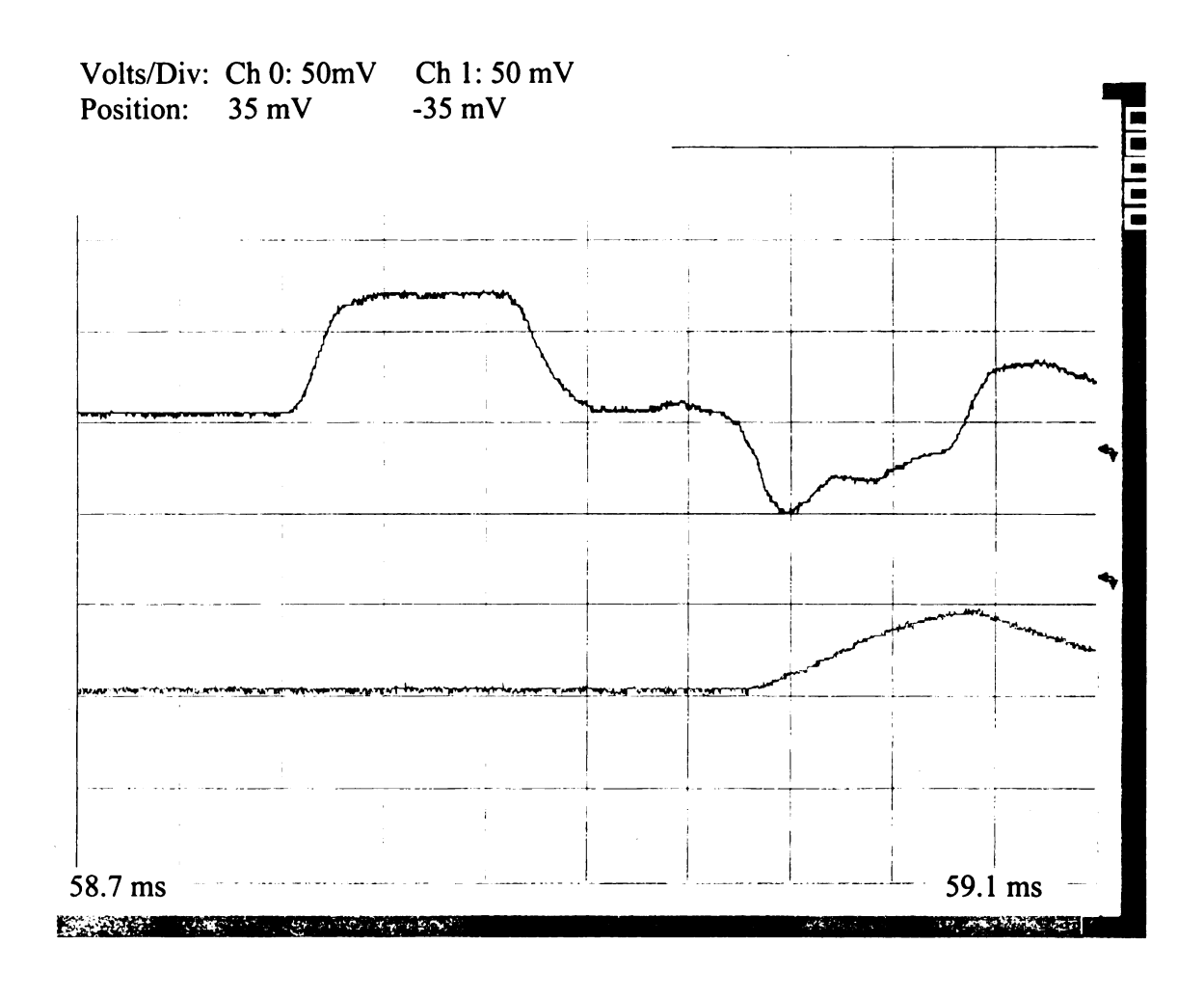


Figure A-18 Incident, reflected and transmitted waves for the glass-epoxy composite specimen with D10.84 L11.28.

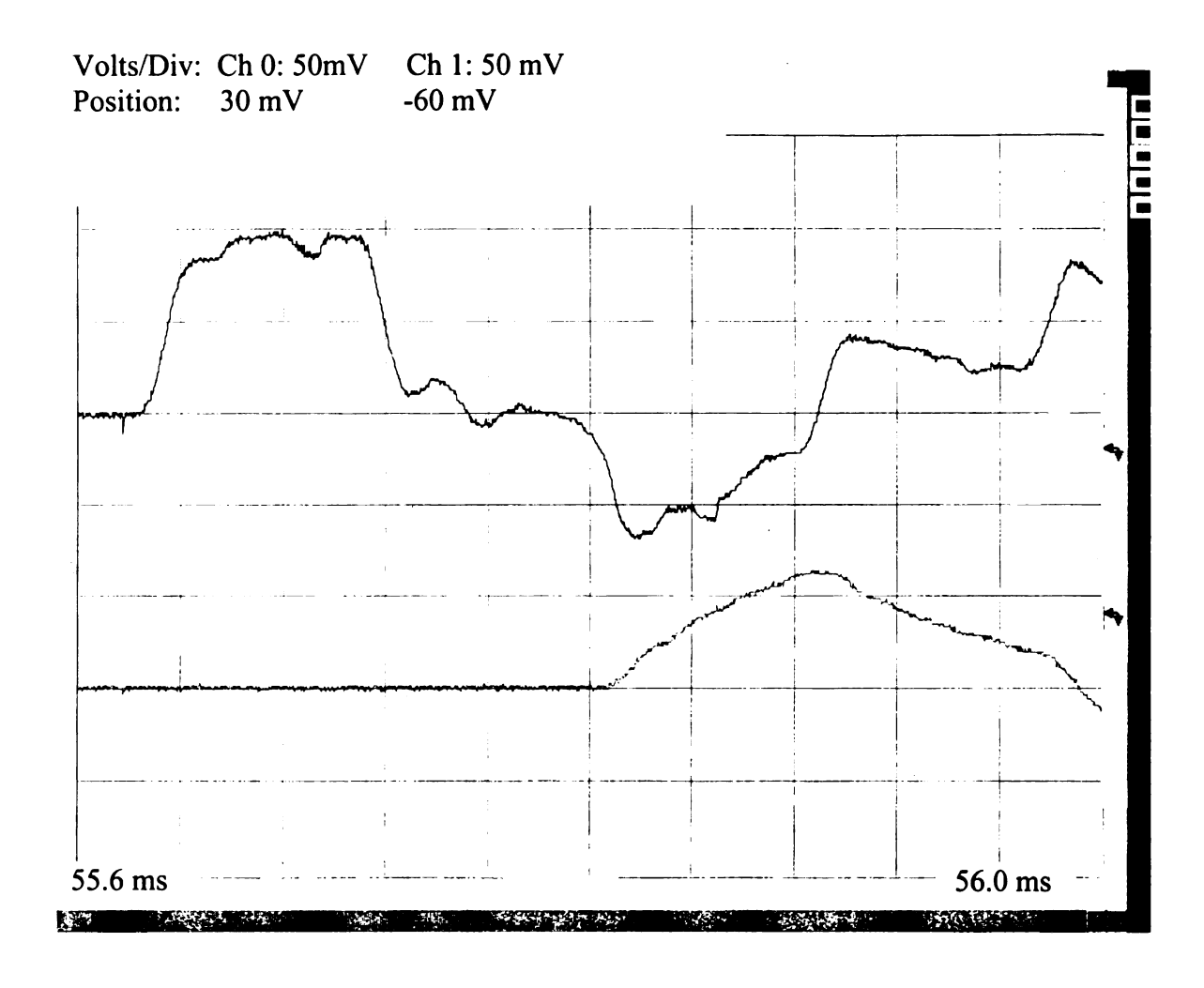


Figure A-19 Incident, reflected and transmitted waves for the glass-epoxy composite specimen with D15.8 L25.6.

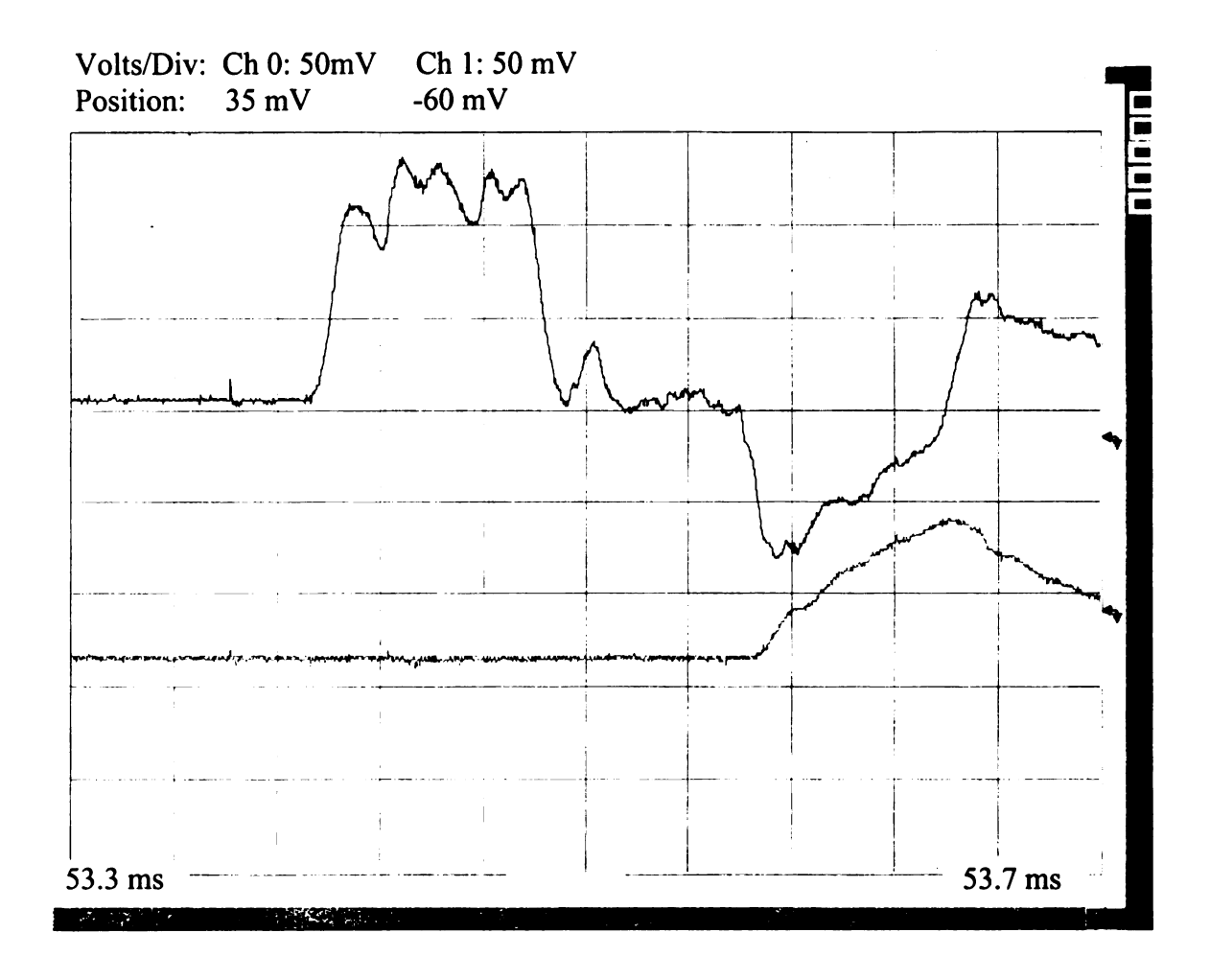


Figure A-20 Incident, reflected and transmitted waves for the glass-epoxy composite specimen with D15.8 L25.54.

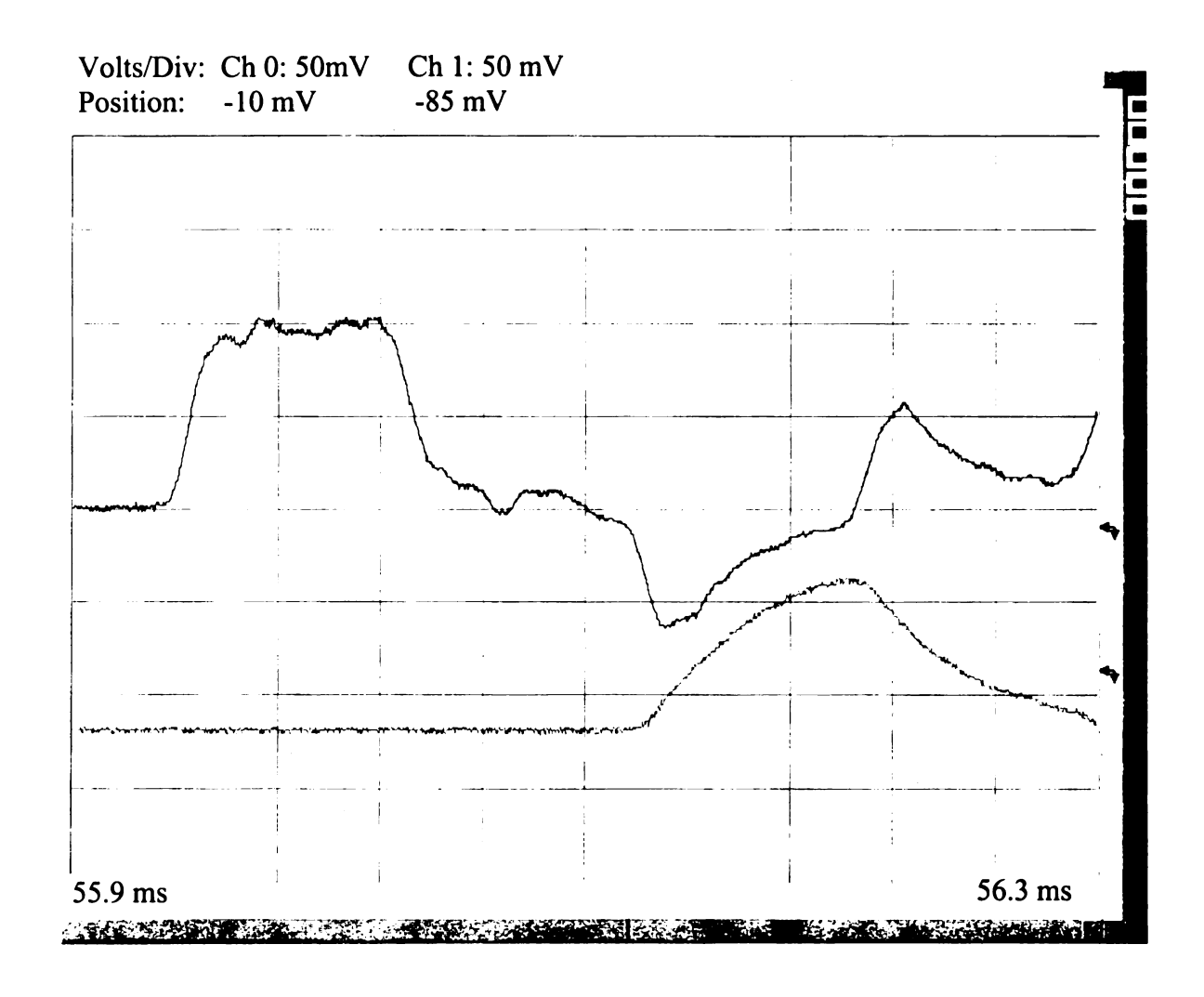


Figure A-21 Incident, reflected and transmitted waves for the glass-epoxy composite specimen with D15.8 L12.7.

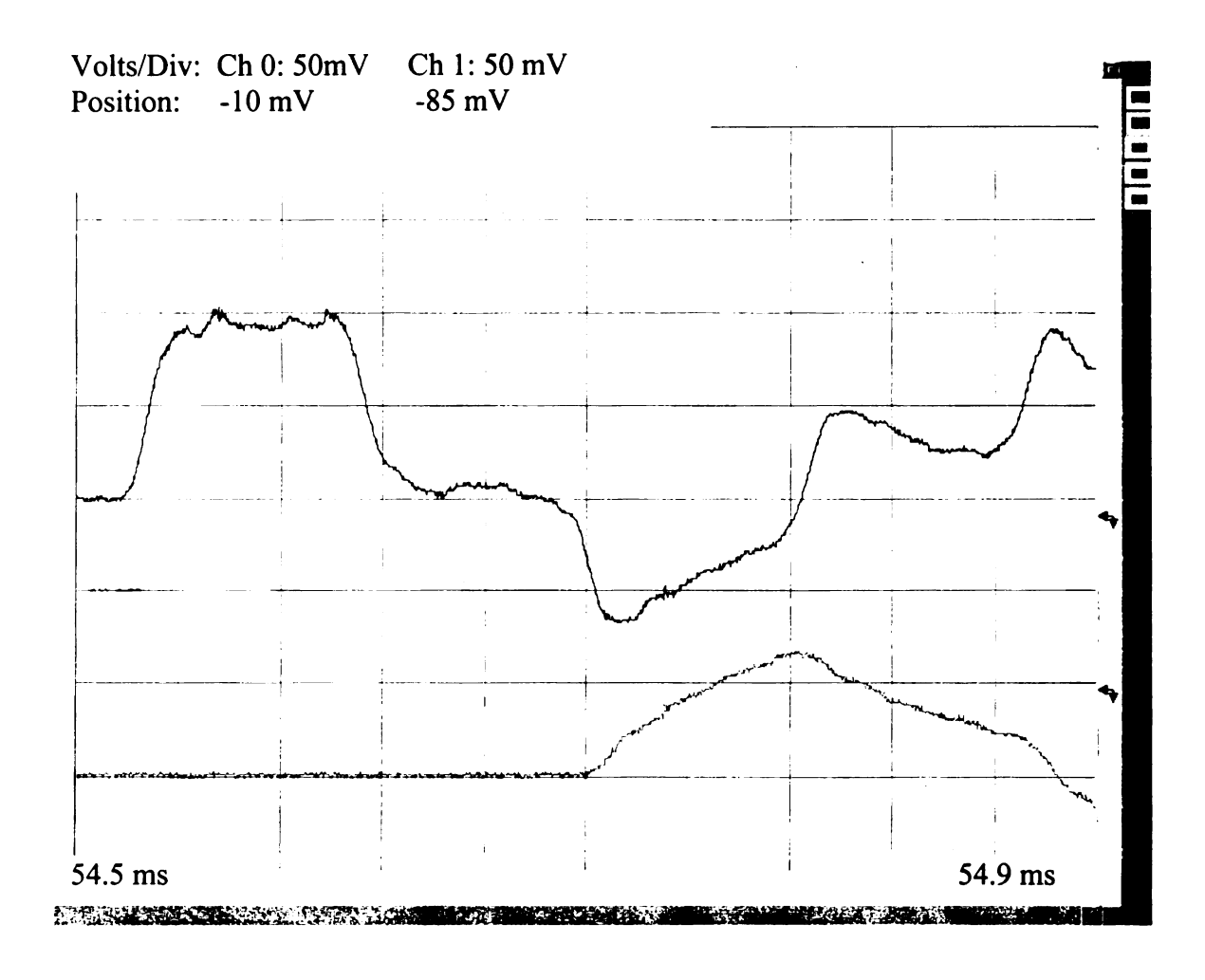


Figure A-22 Incident, reflected and transmitted waves for the glass-epoxy composite specimen with D15.8 L25.56.

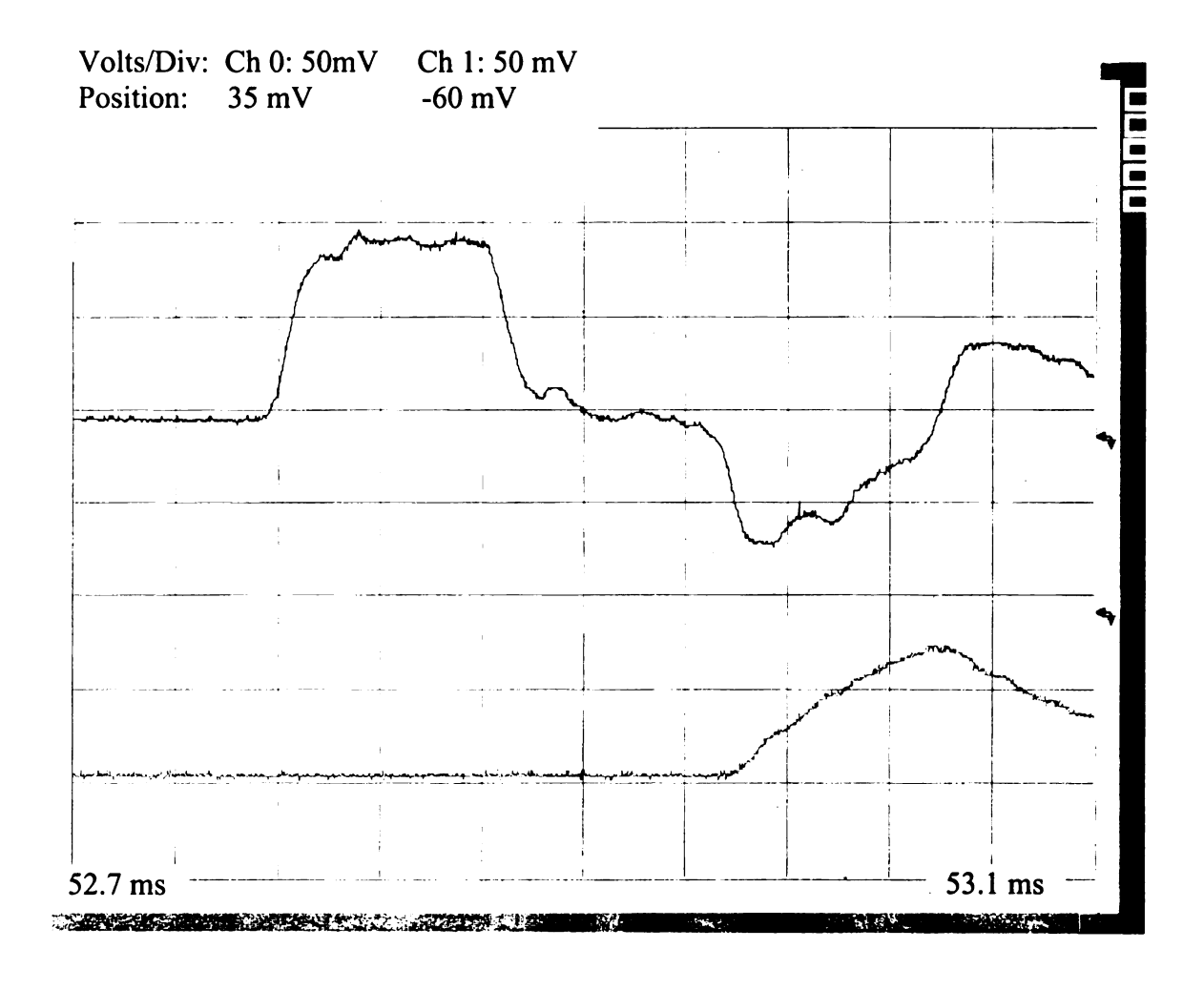


Figure A-23 Incident, reflected and transmitted waves for the glass-epoxy composite specimen with D15.8 L12.55x2.

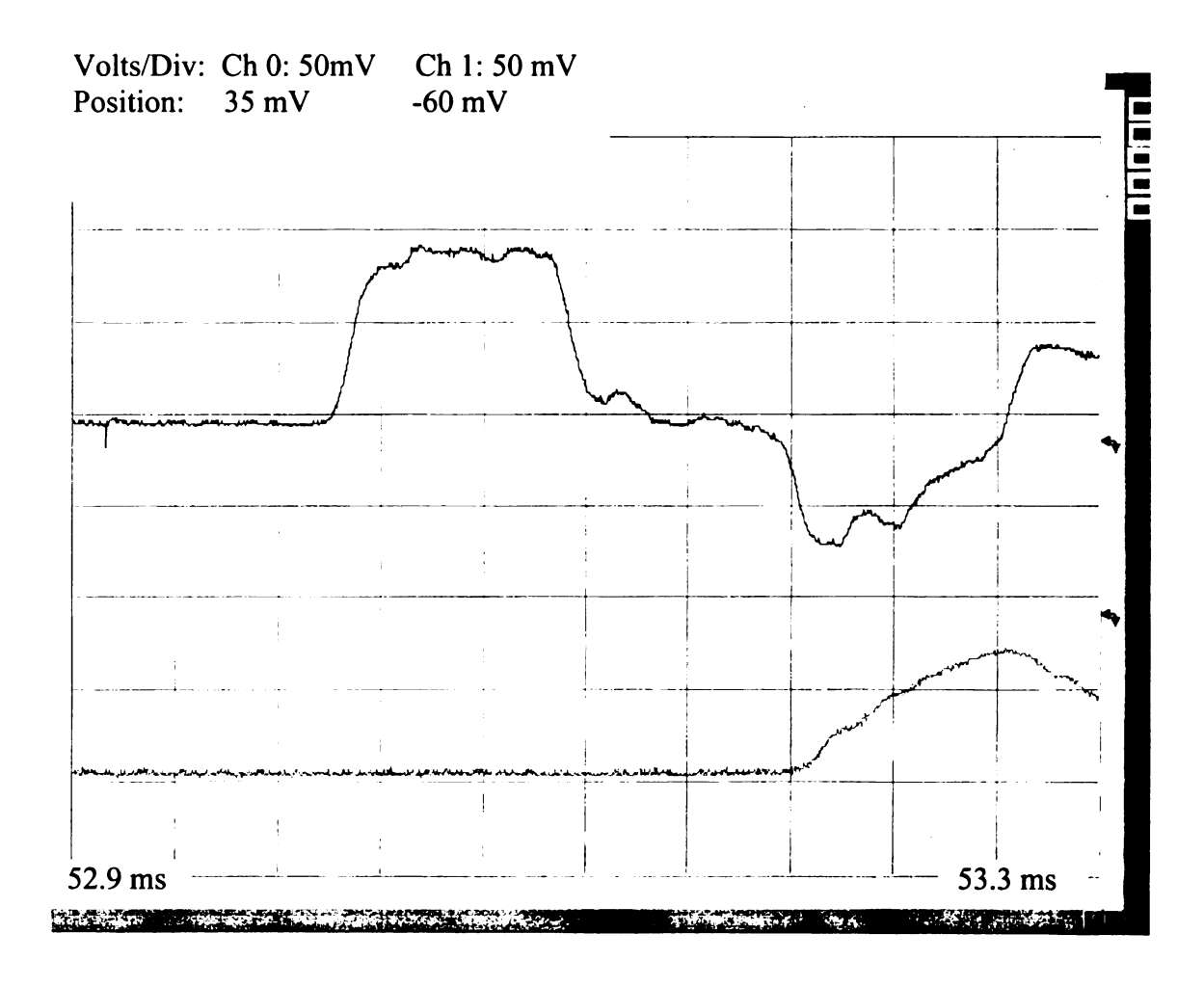


Figure A-24 Incident, reflected and transmitted waves for the glass-epoxy composite specimen with D15.8 L12.42x2.

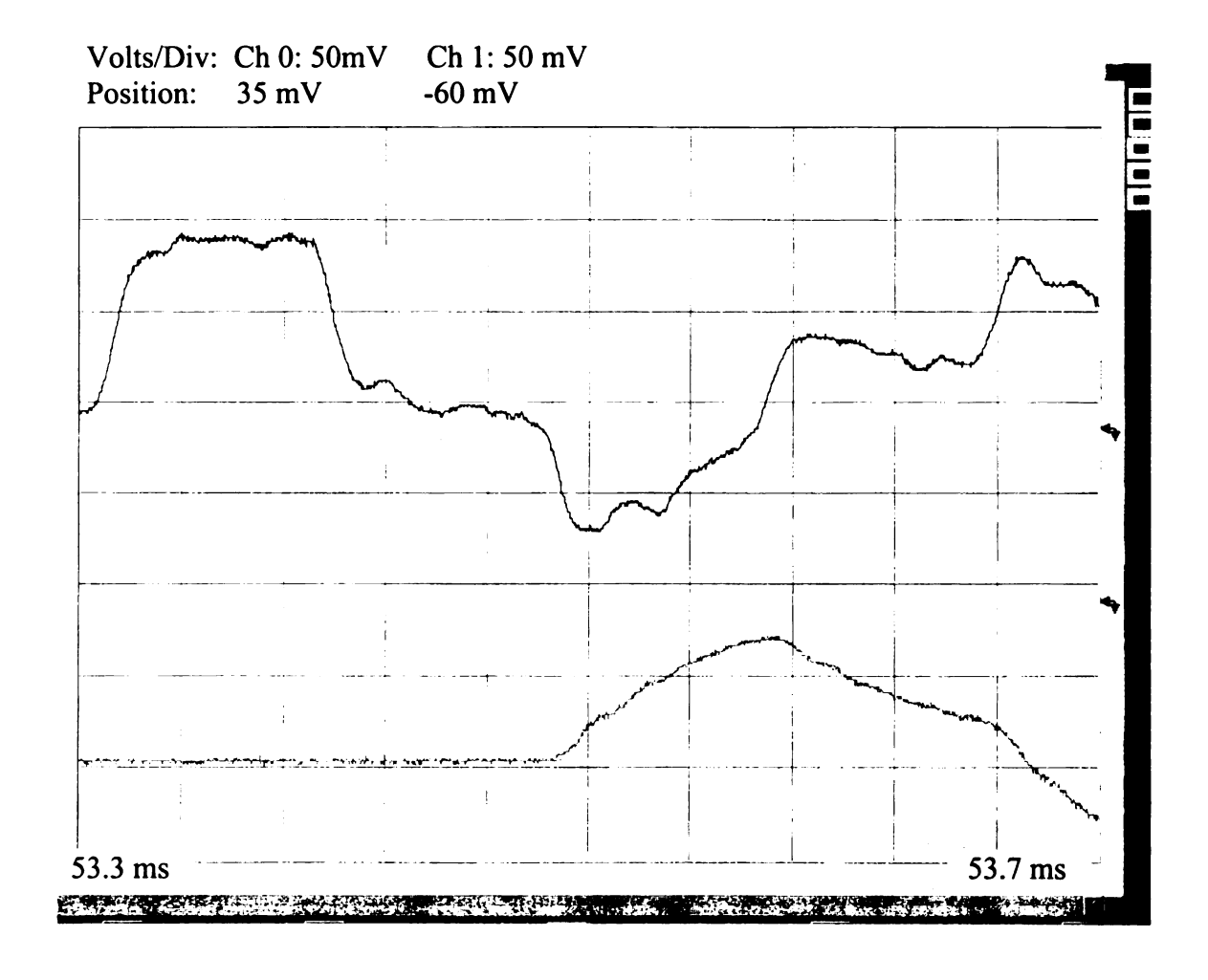


Figure A-25 Incident, reflected and transmitted waves for the glass-epoxy composite specimen with D15.7 L25.46.

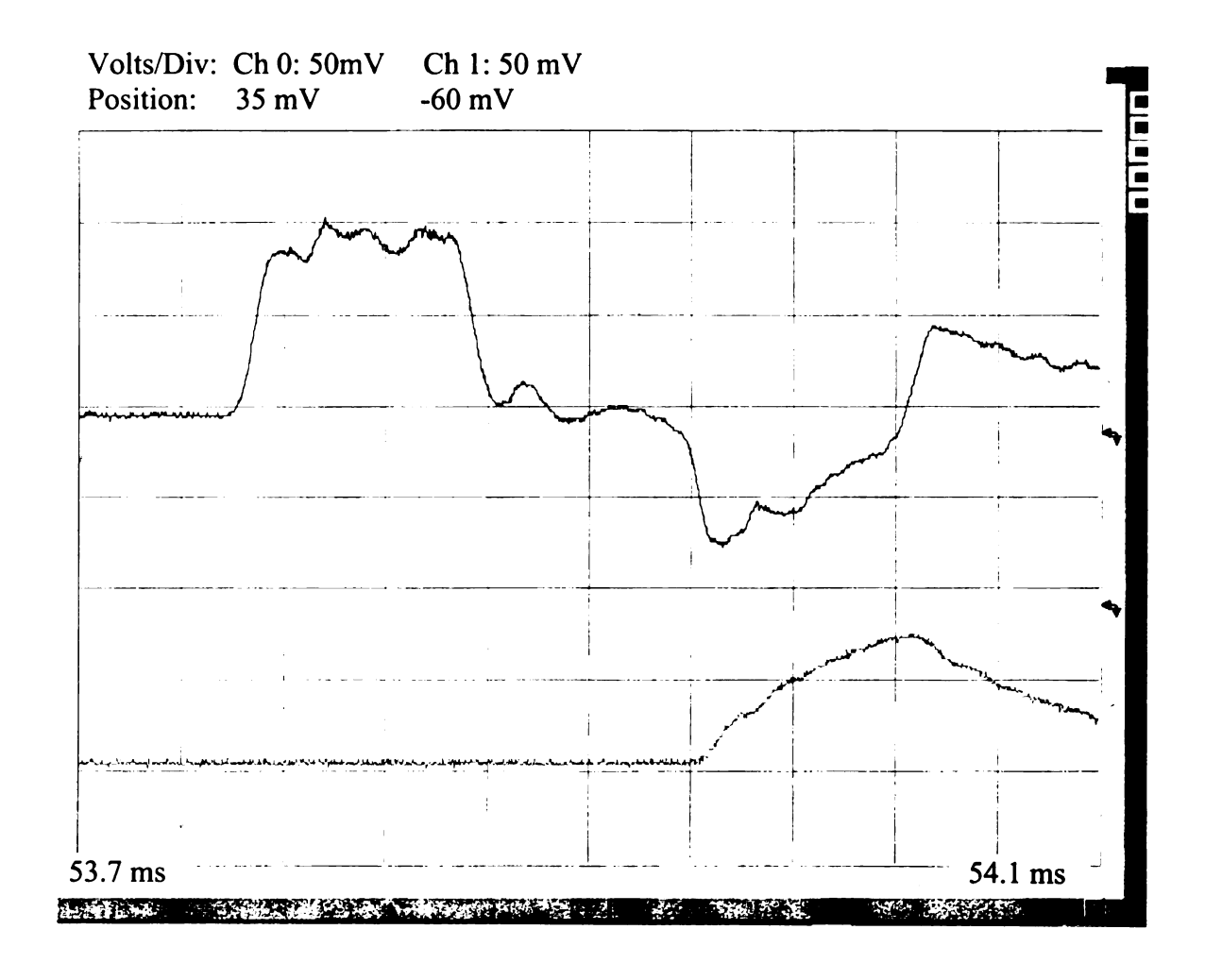
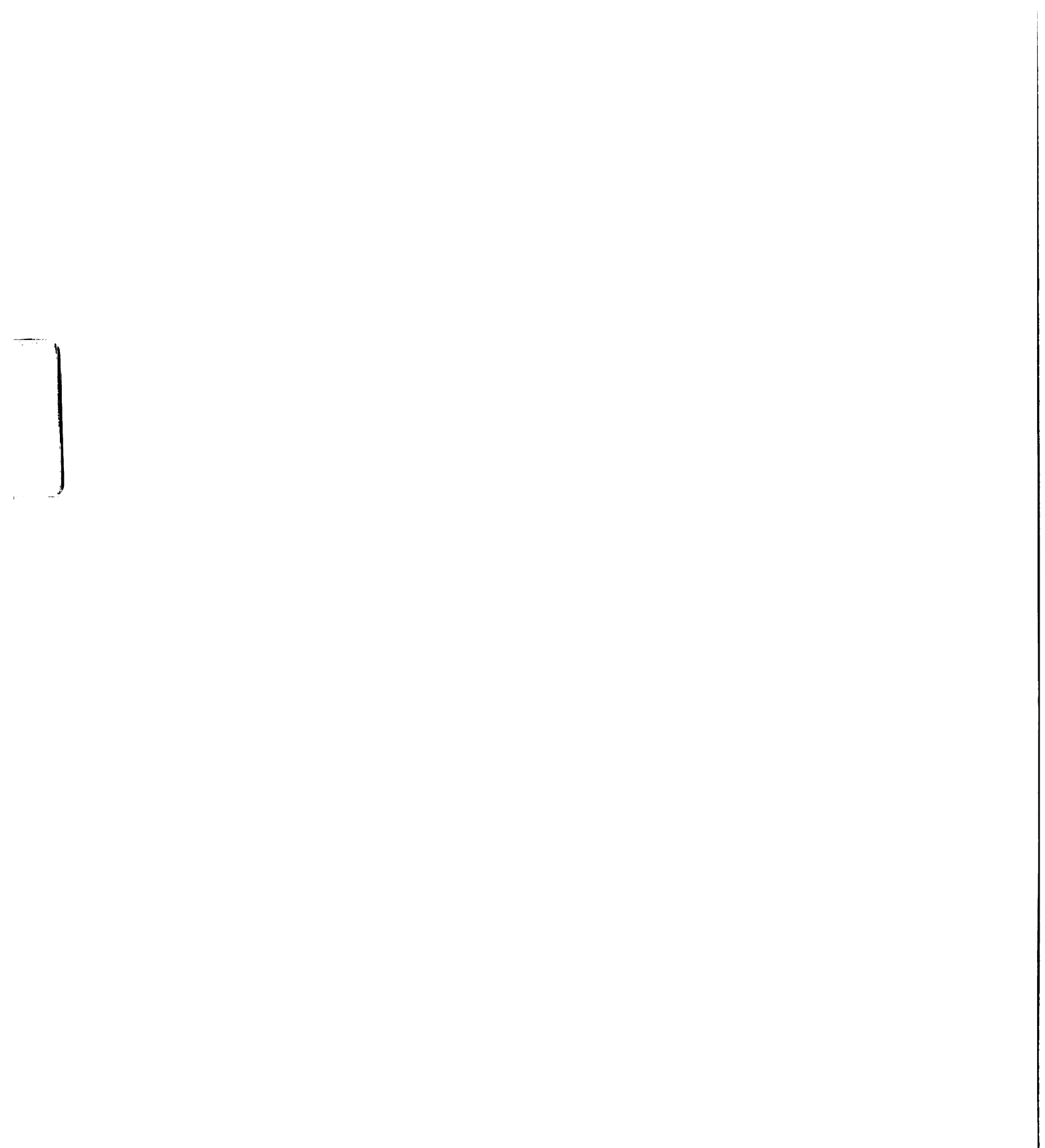


Figure A-26 Incident, reflected and transmitted waves for the glass-epoxy composite specimen with D15.7 L25.18.



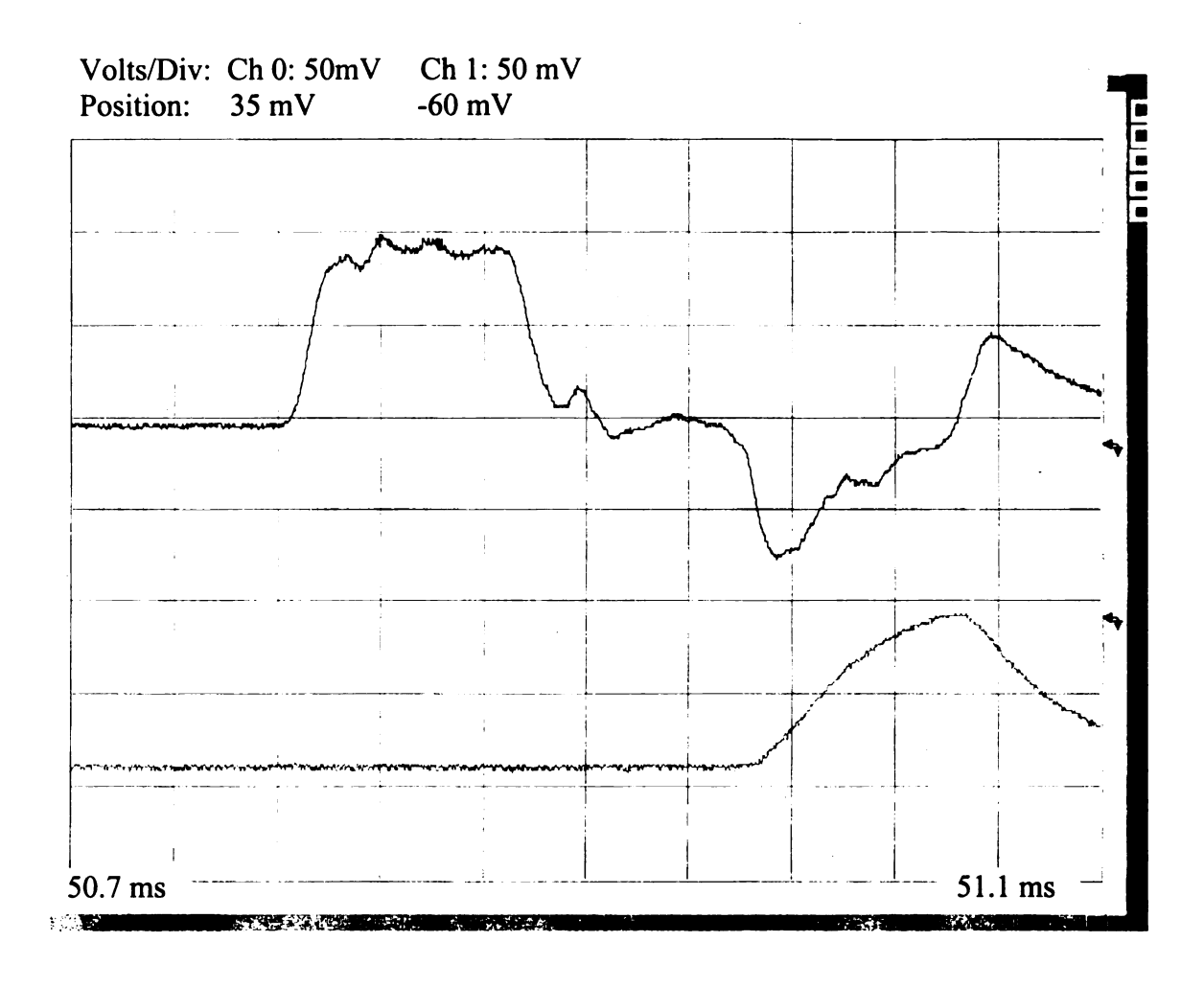


Figure A-27 Incident, reflected and transmitted waves for the glass-epoxy composite specimen with D15.8 L12.5-middle.

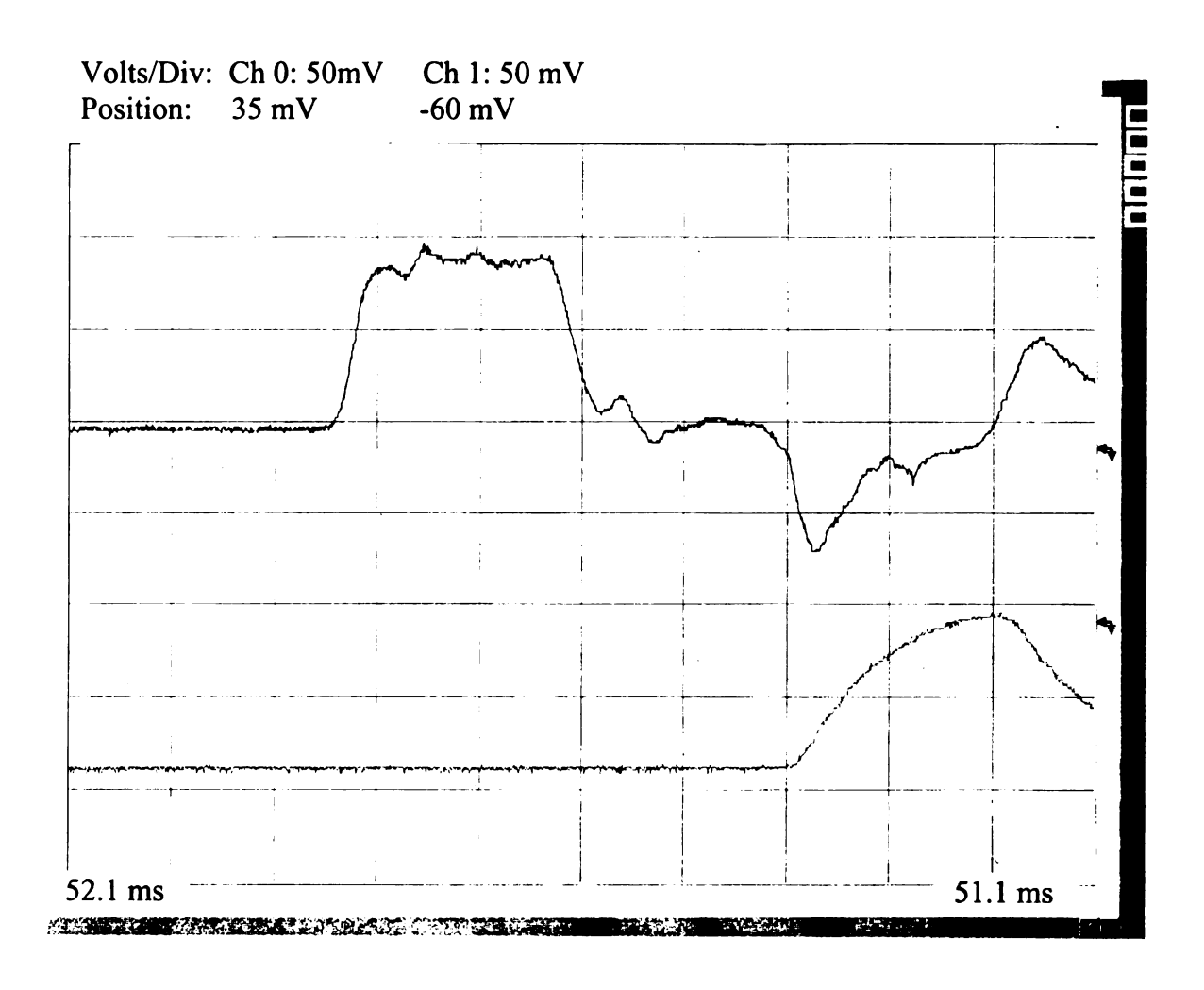
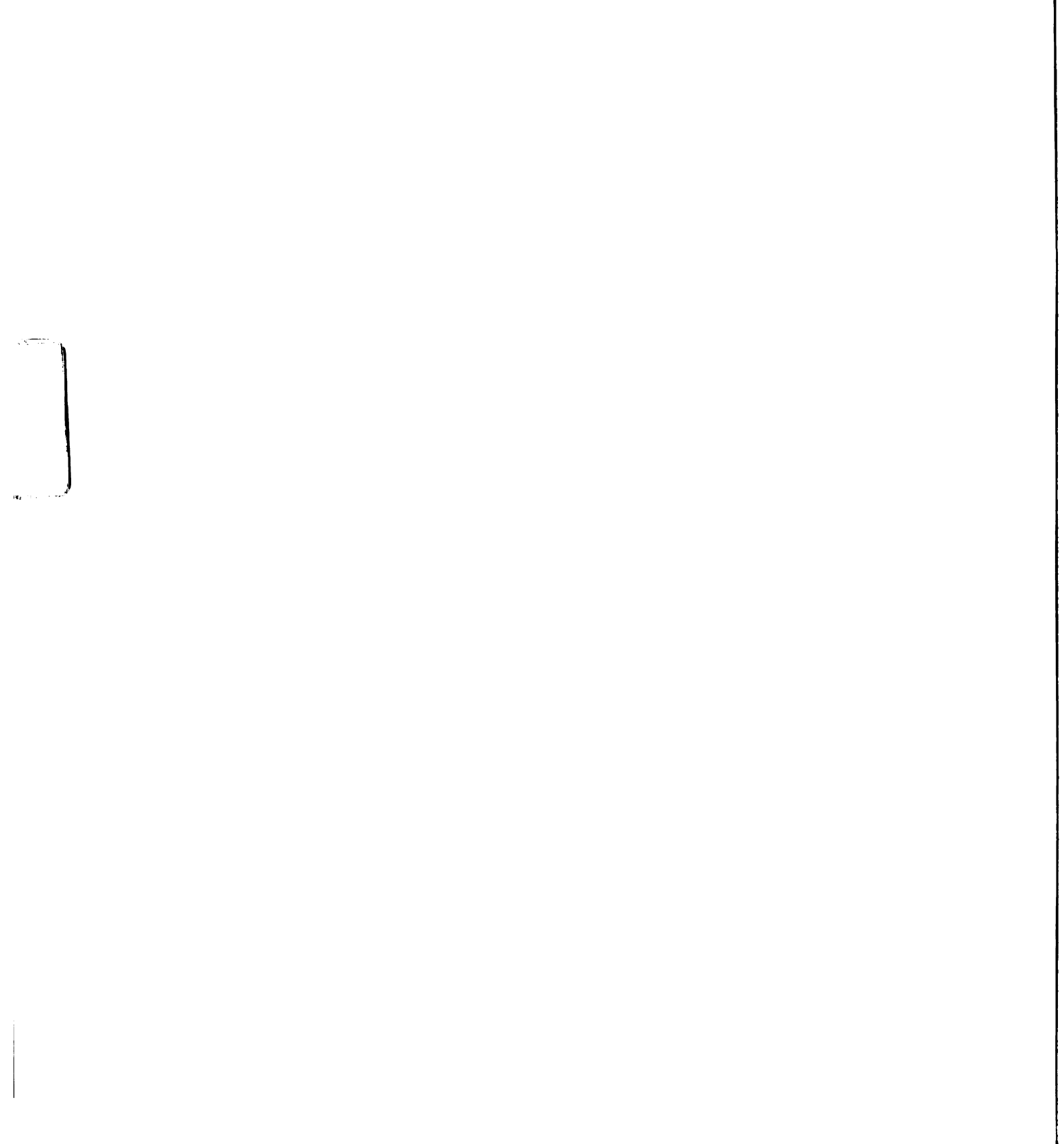


Figure A-28 Incident, reflected and transmitted waves for the glass-epoxy composite specimen with D15.8 L11.44-edge.



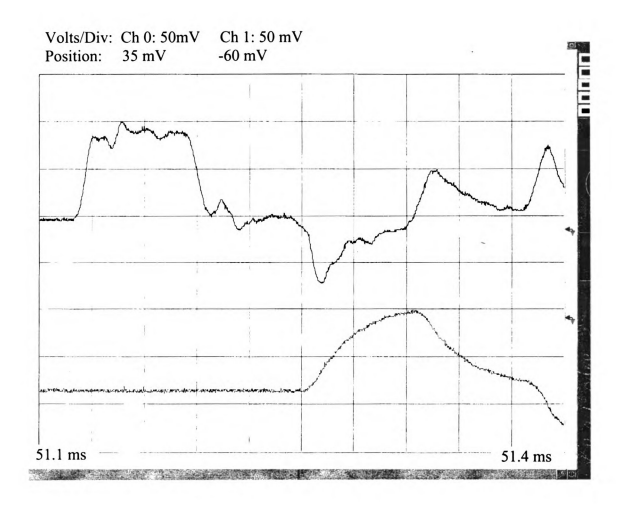


Figure A-29 Incident, reflected and transmitted waves for the glass-epoxy composite specimen with D15.8 L11.9-edge.

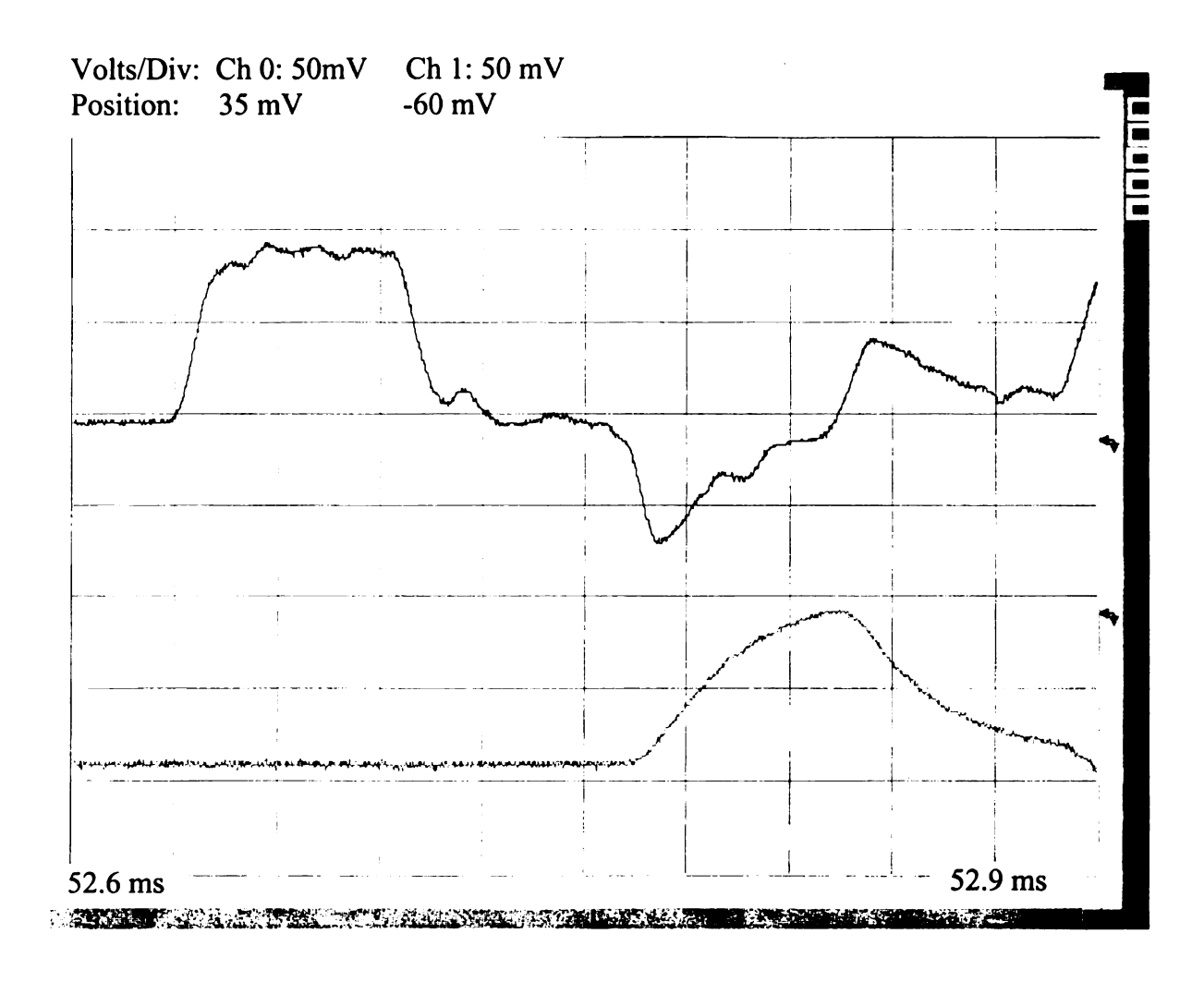


Figure A-30 Incident, reflected and transmitted waves for the glass-epoxy composite specimen with D15.8 L11.4-middle.

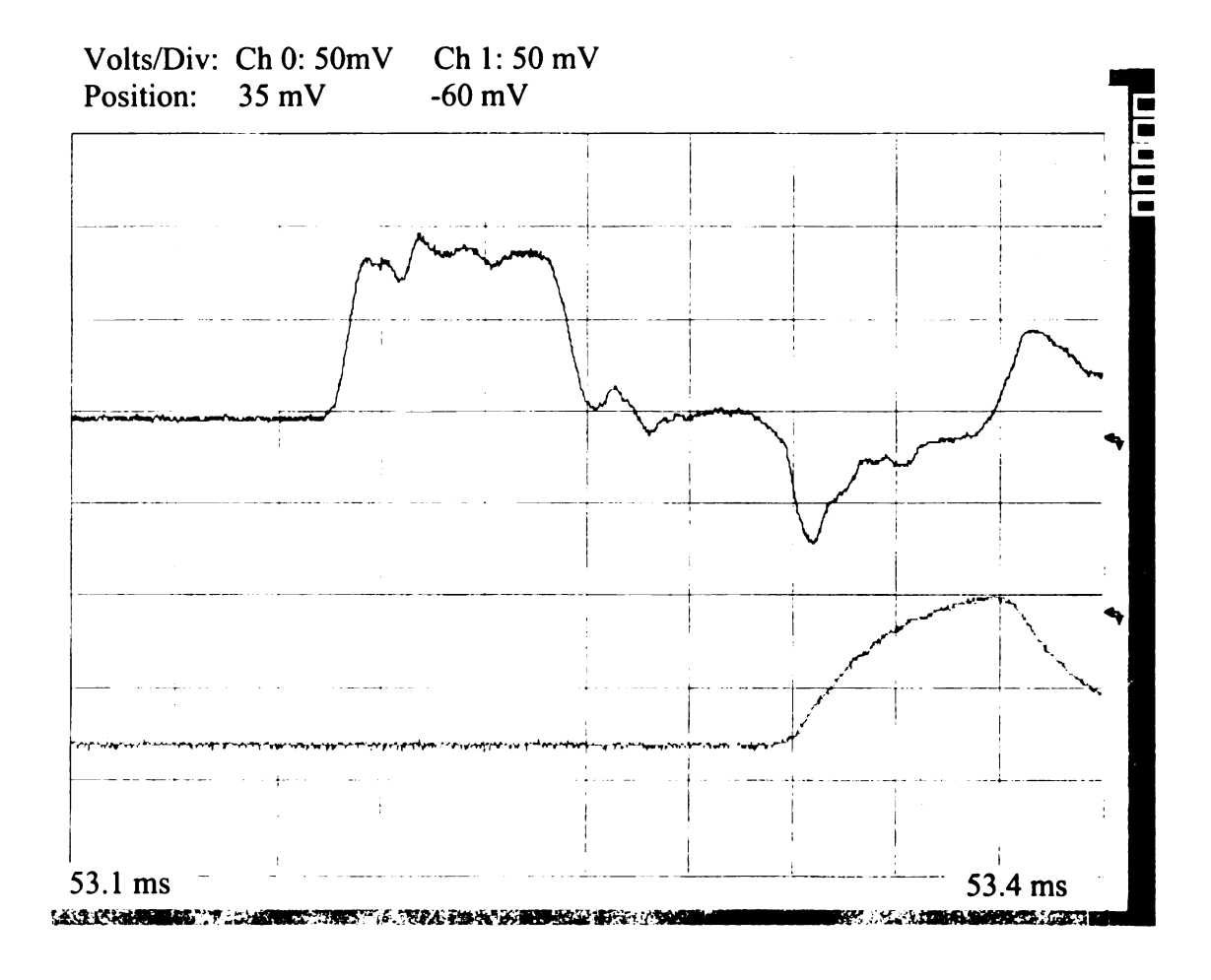


Figure A-31 Incident, reflected and transmitted waves for the glass-epoxy composite specimen with D15.8 L11.64-edge.

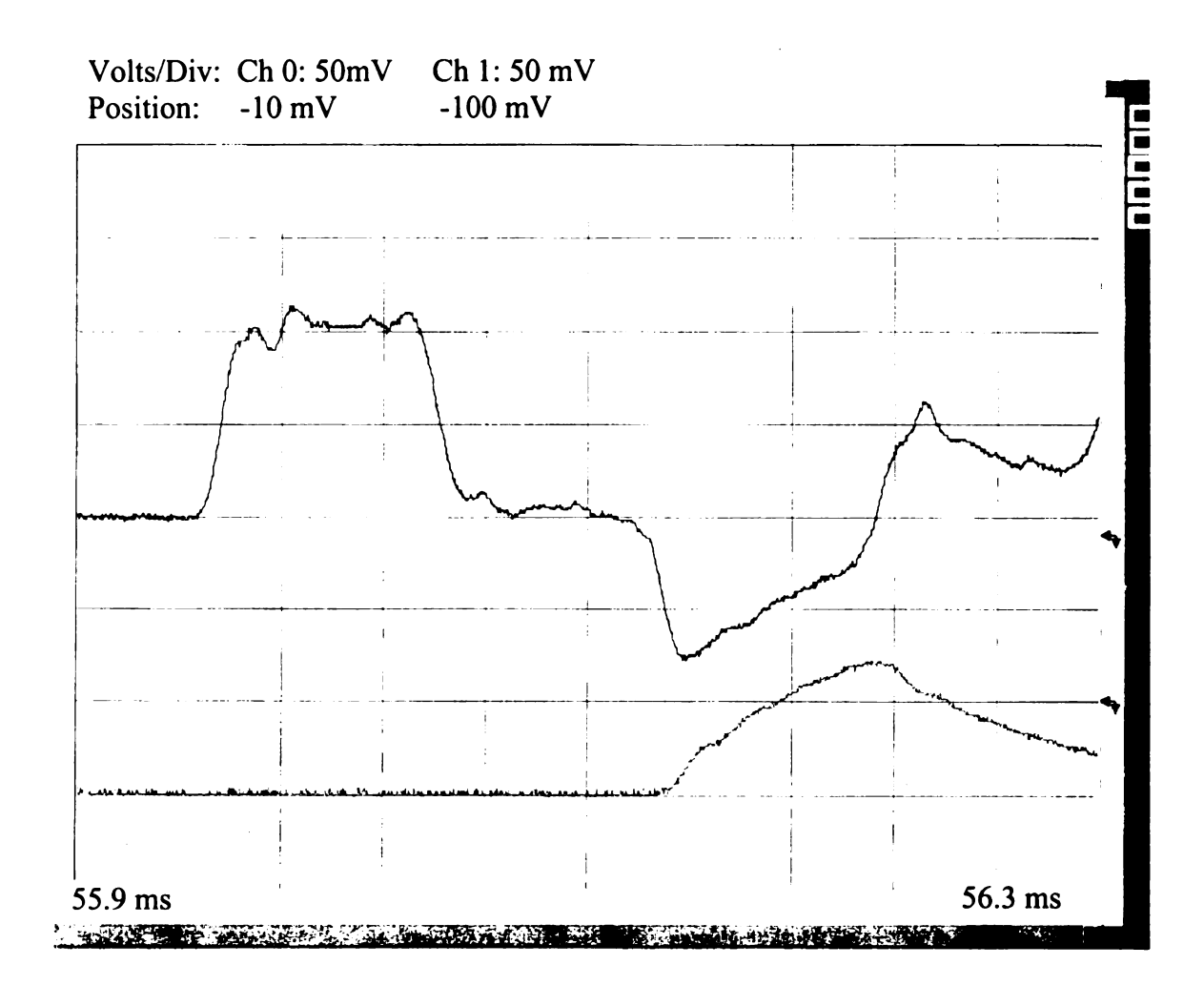


Figure A-32 Incident, reflected and transmitted waves for the glass-epoxy composite specimen with D15.8 L25.06.

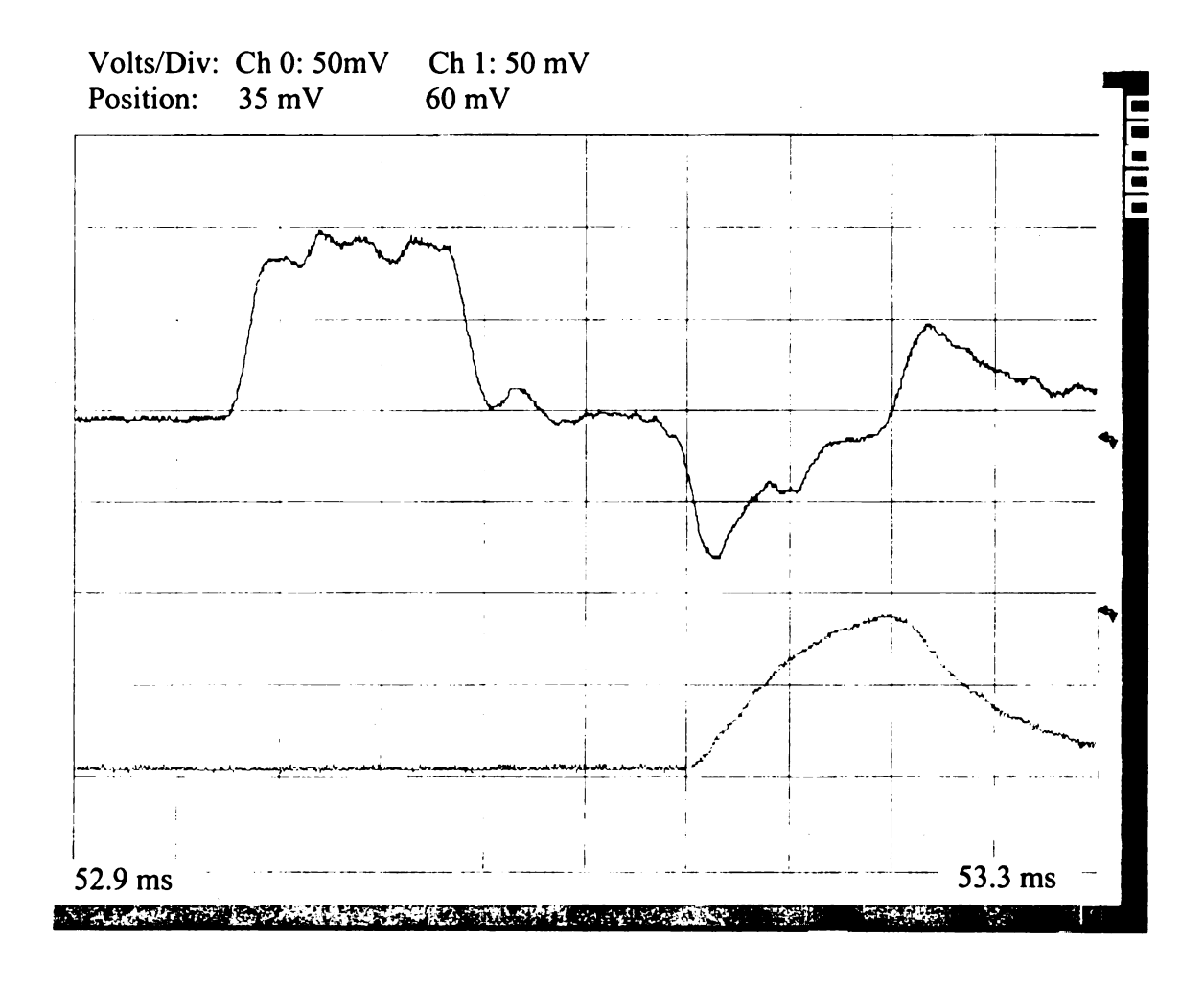


Figure A-33 Incident, reflected and transmitted waves for the glass-epoxy composite specimen with D15.8 L12.6.

### **APPENDIX B**

### SPLIT HOPKINSON PRESSURE BAR THEORY

## a. Strain and Strain Rate Equations

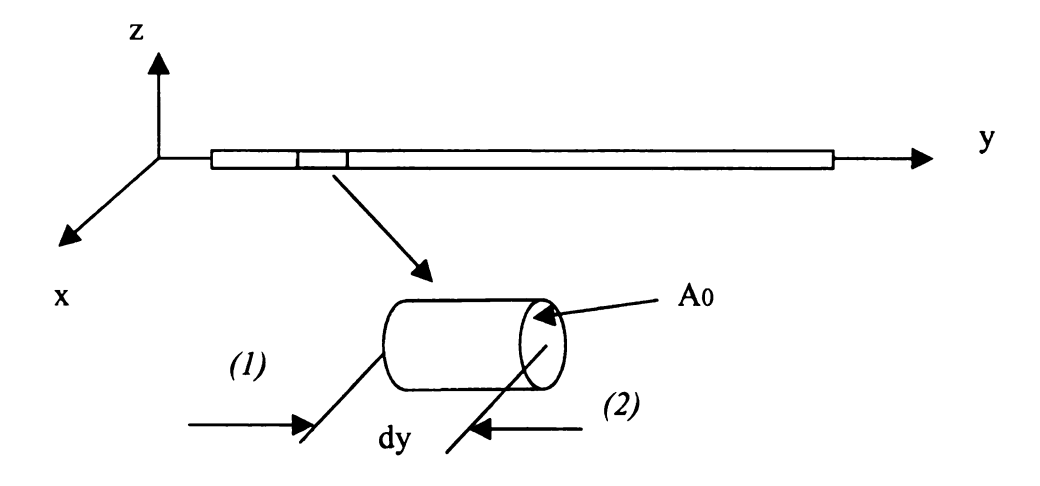


Figure A-34 Pressure bar shown with differential element.

The figure above shows a differential element with length *dy* and cross sectional area *Ao* in a pressure bar. After impact, the following equation can describe the motion of the pressure pulses.

$$A0E\frac{\partial u_1}{\partial y} - A0E\frac{\partial u_2}{\partial y} = A0dy \rho \frac{\partial^2 u_1}{\partial t^2}$$
(A-1)

where E is Young's Modulus of the bar material,  $u_1$  and  $u_2$  are the displacements of the differential element in both ends,  $\rho$  is the density of the bar material. As the wave velocity,  $C_0$ , can be calculated from

$$C = \sqrt{\frac{E}{\rho}}$$
 (A-2)

the equation A-1 can be simplified for the bar's equation of motion.

$$C0^{2} \left[ \frac{\partial u_{1}}{\partial y} - \frac{\partial u_{2}}{\partial y} \right] = \frac{\partial^{2} u_{1}}{\partial t^{2}} dy$$
 (A-3)

If the rates of change of displacement of the two sides of the element are equal, the equation of motion can be written as

$$u2 = u1 + \frac{\partial u1}{\partial y} dy \tag{A-4}$$

Upon differentiation, equation A-4 becomes

$$\frac{\partial u \, 2}{\partial y} = \frac{\partial u \, 1}{\partial y} + \frac{\partial^2 u \, 1}{\partial y^2} \, dy \tag{A-5}$$

By substituting equation A-5 into equation A-3, the equation of motion for the bar becomes

$$-C 0^2 \frac{\partial^2 u}{\partial v^2} = \frac{\partial^2 u}{\partial t^2}$$
 (A-6)

For harmonic waves,

$$E\frac{\partial}{\partial y}\left(\frac{\partial u_1}{\partial y}\right) = \frac{\partial \sigma}{\partial y} \tag{A-7}$$

where  $\sigma$  is the stress across the cross section.

So the equation of motion can be rewritten in terms of the pressure and velocity across the bar cross section as

$$-\frac{\partial \sigma(y,t)}{\partial y} = \rho \frac{\partial v}{\partial t}$$
 (A-8)

For a uniaxial state of stress, the pressure is equal to the stress over the pressure bar cross section, that is  $.p(y,t) = \sigma(y,t)$ . If we assume a positive traveling harmonic wave of the form

$$p(y,t) = Pe^{i(wt - ky)}$$
 (A-9)

where P is the amplitude of the pressure, w is the frequency, t is the time, k is the wave number and is defined as  $k=\frac{w}{C_0}$ . Taking the first derivative of equation A-9 with respect to y,

$$\frac{\partial \sigma(y,t)}{\partial y} = -ikPe^{i(wt-ky)} \tag{A-10}$$

Substituting this derivative into equation A-8,

$$\rho \frac{\partial v}{\partial t} = ikPe^{-i(wt - ky)}$$
 (A-11)

so the particle velocity can be given by equation A-12

$$v(y,t) = \frac{k}{\rho w} P e^{i(wt - ky)} = \frac{k}{\rho w} \sigma(y,t) = \frac{1}{\rho C_0} \sigma(y,t)$$
 (A-12)

As  $\sigma(y,t)=\varepsilon(y,t)E$  , the particle velocity in terms of the bar strain can be express as

$$v(y,t) = C \, 0 \, \varepsilon(y,t) \tag{A-13}$$

For a negative traveling wave the particle velocity is:

$$v(y,t) = -C \, 0 \, \varepsilon(y,t) \tag{A-14}$$

with above equations, specimen strain rate can be calculated easily.

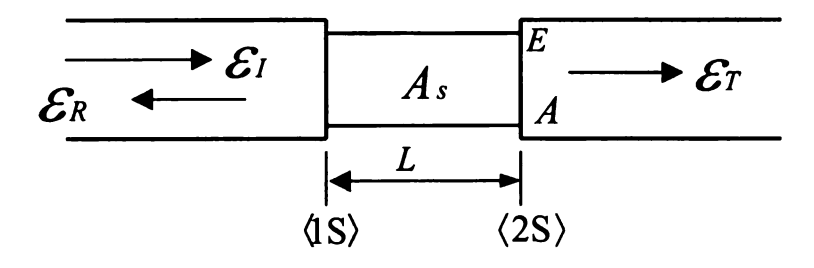
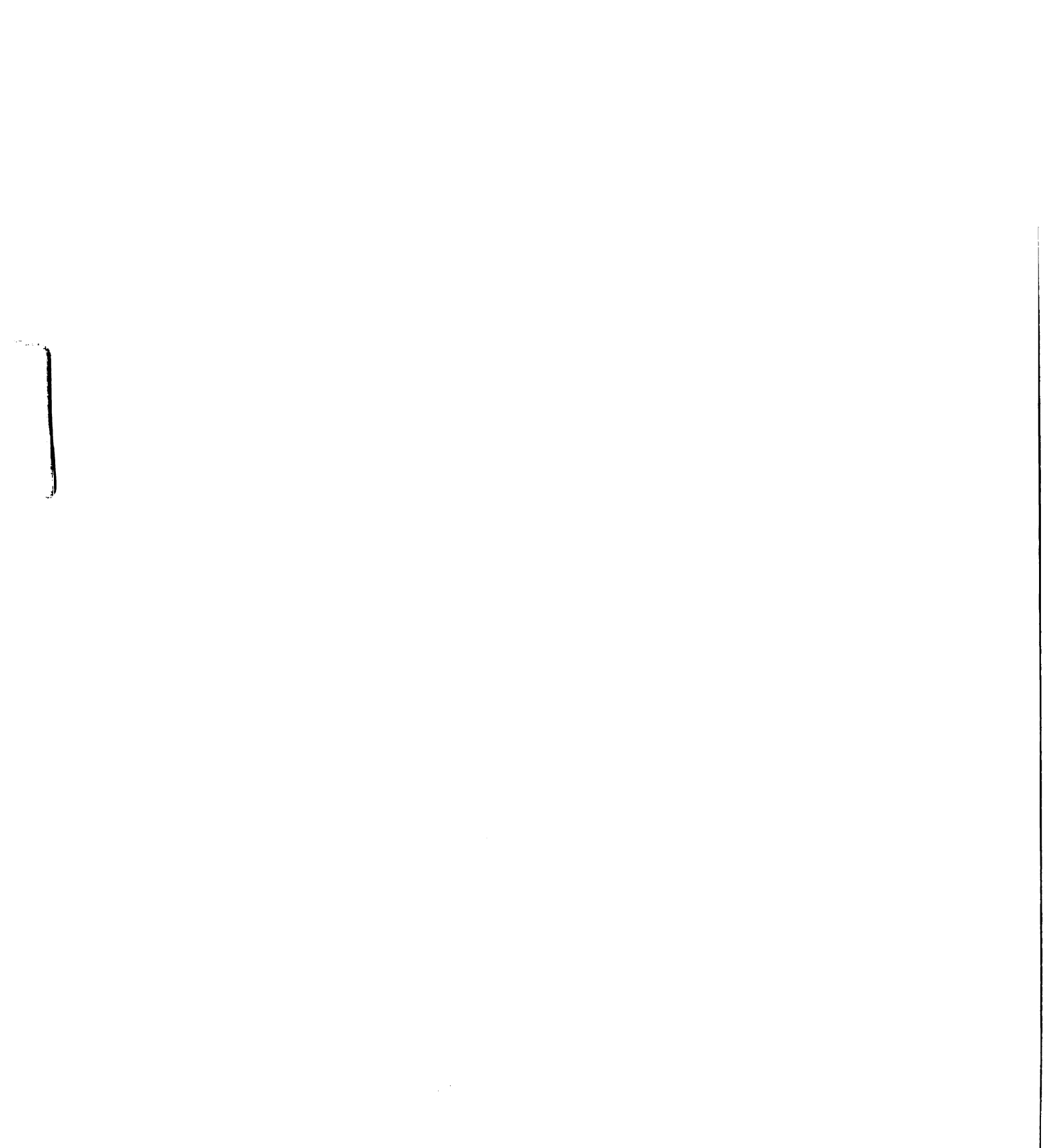


Figure A-35 Parameters of cylindrical specimen and bars



For the specimen shown in Figure A-2, The average strain at any time is given by

$$\mathcal{E} s = \frac{u_{1}s - u_{2}s}{L} \tag{A-15}$$

the average strain rate is:

$$\frac{d \varepsilon s}{dt} = \frac{\upsilon \, {}_{1}s - \upsilon \, {}_{2}s}{L} \tag{A-16}$$

the velocity at interface 1S is comprised of the incident (positive traveling wave) and the reflected (negative traveling wave) as

$$\upsilon_{1S} = C \circ \varepsilon_{I} - C \circ \varepsilon_{R} \tag{A-17}$$

the velocity of interface 2S is a positive quantity as

$$\upsilon zs = C \circ \varepsilon \tau \tag{A-18}$$

so the specimen strain rate in terms of the bar strains as

$$\frac{d\,\varepsilon_s}{dt} = -\frac{C\,0(\,\varepsilon_T - \,\varepsilon_I + \,\varepsilon_R\,)}{L} \tag{A-19}$$

If the specimen deforms uniformly, such that

$$\mathcal{E}_I + \mathcal{E}_R = \mathcal{E}_T \tag{A-20}$$

the equation for the specimen strain rate can be reduced to

$$\frac{d \varepsilon_s}{dt} = -\frac{2 C 0}{L} \varepsilon_R \tag{A-21}$$

which can be integrated to get the specimen strain

$$\varepsilon s(t) = -\frac{2C0}{L} \int_{0}^{t} \varepsilon_{R}(t) dt$$
 (A-22)

# **b. Stress Equation**

The average force on the specimen is given by

$$Pav = \frac{P1s + P2s}{2} \tag{A-23}$$

the forces at the ends of the specimen can be expressed in terms of the incident and reflected bar strains as

$$P \circ S = EA (\varepsilon_I + \varepsilon_R)$$
 (A-24)

$$P \circ S = EA \circ \varepsilon \tau \tag{A-25}$$

So the average force on the specimen in terms of the bar strains can be given as

$$P \, av = \frac{EA}{2} (\varepsilon_I + \varepsilon_R + \varepsilon_T) \tag{A-26}$$

with the equation A-20, and the equation followed,

$$\sigma s = \frac{P \, av}{A \, s} \tag{A-27}$$

the expression for the average specimen stress is:

$$\sigma s(t) = E \frac{A}{A s} \varepsilon \tau(t)$$
 (A-28)

**REFERENCES** 

### REFERENCES

- [1] Michael Adam Kaiser, Advancements in the split Hopkinson bar test, Master's thesis, Blacksburg, Virginia, 1998.
- [2] Paul S. Follansbee, Los Alamos National Laboratory. "High strain rate testing—the Hopkinson bar".
- [3] H. Zhao, G. Gary and J. R. Klepaczko, "On the use of a viscoelastic split Hopkinson pressure bar", International Journal of Impact Engineering, 19 (4), 319-330, 1997.
- [4] Lal Ninan, J. Tsai and C.T. Sun, "Use of split Hopkinsin pressure bar for testing off-axis composites", International Journal of Impact Engineering, 25, 291-313, 2001.
- [5] W. Chen, 'the testing result of 6061-T6 aluminum with shaping technique', sent by email, 2002.
- [6] D. J. Frew, M. J. Forrestal and W. Chen. "Pulse shaping techniques for testing brittle materials with a split Hopkinson pressure bar", Experimental Mechanics, 42 (1), 93-106, 2002.
- [7] D. J. Frew, M. J. Forrestal and W. Chen, "A split Hopkinson pressure bar technique to determine compressive stress-strain data for rock materials", Experimental Mechanics, 41 (1), 44-46, 2001.
- [8] W. Chen and F. Lu, "Dynamic compression testing of soft materials", ASME Journal of Applied Mechanics, 69, 214-223, 2002.
- [9] H. M. Hsiao, I. M. Daniel and R. D. Cordes, "Dynamic compressive behavior of thick composite materials, Experimental Mechanics, 38, 172-180, 1998.
- [10] O. Sawas, N. S. Brar and R. A. Brockman, "Dynamic characterization of compliant materials using an All-polymeric split Hopkinson bar", Experimental Mechanics, 38, 204-210, 1998.
- [11] Christophe Bacon and Arnaud Brun, "Methodology for a Hopkinson test with a non-uniform viscoelastic bar", International Journal of Impact Engineering, 24, 219-230, 2000.

- [12] Frank E. Hauser, "Techniques for measuring stress-strain relations at high strain rates", Experimental Mechanics, 395-402, 1966.
- [13] J. F. Bell, "An experimental diffraction grating study of the quasi-static hypothesis of the split Hopkinson bar experiment", J. Mech. Phys. Solids, 14, 309-327,1966.
- [14] Robert L. Sierakowski and Shive K. Chaturvedi, "Dynamic loading and characterization of fiber-reinforced composites", John wiley&sons, inc. New York, 41-77, 1997.
- [15] Jonas A. Zukas, Theodore Nicholas and Hallock. F. Swift, Impact Dynamics, John Wiley & sons Inc. 287-308, 1982.
- [16] Karl F. Graff, Wave Motion in Elastic Solids, Ohio State University, 75-134, 1975.
- [17] D. R. Veazie, S. W. Park and Min Zhou,"Post-impact behavior of polymeric composites and the effects of salt water aging on tensile properties", 1999.
- [18] Christophe Bacon, "Separation of waves propagation in an elastic or viscoelastic Hopkinson pressure bar with three-dimensional effects", International Journal of Impact Engineering, 22, 55-69, 1999.
- [19] David E. Lambert and C. Allen Ross, "Strain rate effects on dynamic fracture and strength", International Journal of Impact Engineering, 24, 985-998, 2000.
- [20] C. Bacon, "Numerical prediction of the propagation of elastic waves in longitudinally impacted rods: application to Hopkinson testing", International Journal of Impact Engineering, 13 (4), 527-539, 1993.

